EFFECT OF PRE-STRAIN AND CARBON CONTENT ON THE PERFORMANCE OF STRUCTURAL STEELS

BY

CONGLING ZHOU

ME (Mechanical Design and Theory),
Tianjin University of Science and Technology, China, 2002
BE (Mechanical and Electrical Engineering),
Tianjin University of Light Industry, China, 1999

A dissertation submitted in partial fulfillment of the requirements
for the Doctor of Philosophy degree in Department of
Engineering Systems and Technology,
Graduate School of Science and Engineering,
Saga University

September 2005

Supervisor: PROFESSOR SHIN-ICHI NISHIDA

ABSTRACT

Structural carbon steels are most widely used as structural materials in engineering, even in nowadays that many new materials have been developed and some are in developing, because of their good mechanical properties and low cost. They are formed as various kinds of products, such as pipes and tubes, sheets and plates, wires, rods, rails and other structural components. In engineering, more than 90% of failure cases are caused by fatigue, and torsional fatigue is one of the most basic fatigue types. On the other hand, many of the products are deformed before in use, that is, they are pre-strained before the components, and tensile pre-strain is one of the most common types in engineering. The previous studies are mostly focused on the bending fatigue properties, and the torsional properties are almost calculated from the bending ones based on certain relationship. To use the materials more safely and economically, it is necessary and important to obtain a comprehensive understanding of the torsional fatigue properties.

In this thesis, the torsional fatigue properties of structural carbon steels are studied. The main content includes three parts: relationship between tensile strain ratio and the surface deformation, effect of tensile pre-strain on the torsional fatigue properties and the carbon content influences on the torsional fatigue properties.

Tensile test was carried out to investigate the relation between tensile strain ratio and the surface deformation of structural carbon steels. Tensile properties were tested and the microstructural behaviors were observed by taking replica samples by certain interval until fracture. The results indicated that with the influence of carbon content, the stress-strain curves were divided into two groups, low carbon group and medium carbon group, though the yielding strength was much nearer to the lower group for S35C. There was no obvious deformation observed during the elastic and yielding period, then slip lines initiated in the ferrite grains or near the grain boundaries and concentrated for some while before translate to short cracks before the fracture. And the translating ratio became lower with the increasing of carbon content.

Torsional fatigue test were studied by performing on plain specimens with and without tensile pre-strain, to research the effect of tensile pre-strain on the torsional fatigue properties. At the same time, fatigue crack initiation and propagation behaviors and the non-propagating micro crack behaviors were investigated by successively taken replica samples on the specimen surface. The study results indicated that tensile pre-strain had significant impact on the torsional fatigue properties. Fatigue strength was improved after tensile pre-strain, and the torsional fatigue limits increased with the increasing of tensile pre-strain from 2% to 8%. The fatigue cracks initiated from torsional slip lines in ferrite grains, independent on the tensile pre-strain, while the initiation life was retarded by tensile pre-strain. At the same time, crack growth rate became slower with the increasing of tensile pre-strain ratio. Non-propagating cracks were observed in the surface of specimens. For tensile pre-strained ones, the crack length became shorter with the increasing of tensile pre-strain ratio from 2% to 8%. The different systems of tensile slip and torsional slip, work hardening and density of slip lines were considered as the main reasons for the tensile pre-strain effect to the torsional fatigue properties. Compared to bending fatigue limits, the fatigue limits ratio increased after tensile pre-strain, because tensile pre-strain increased the fatigue strength of torsional fatigue, however many of the bending fatigue limits of tensile pre-strained specimens were lower than that of the non-pre-strained ones though they also increased with the increasing of tensile pre-strain ratio.

Since the test materials were heat treated before test to get the same grain size of materials, and carbon is the mainly hardening element for structural carbon steels, it is necessary to investigate the effect of carbon content on the torsional fatigue properties of structural carbons steels. The fatigue test results showed that fatigue strength increased with the increasing of carbon content. For specimens with the same tensile pre-strain ratio, there was no obvious different in crack initiation and propagation behaviors. And the growth rate could be considered as the same for different specimens with the same tensile pre-strain ratio. Non-propagating micro crack length became shorter with the increasing of carbon content for specimens with the same tensile pre-strain ratio.

APPROVAL

Graduate School of Science and Engineering
Saga University
1- Honjomachi, Saga 840-8502, Japan
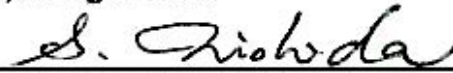
CERTIFICATE OF APPROVAL

Ph. D. Dissertation

This is to certify that the Ph. D. Dissertation of
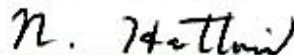
CONGLING ZHOU

ME (Mechanical Design and Theory),
Tianjin University of Science and Technology, China, 2002
BE (Mechanical and Electrical Engineering),
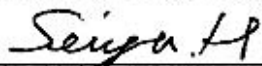Tianjin University of Light Industry, China, 1999

has been approved by the Examining Committee for the dissertation requirement for the Doctor of Philosophy degree in Engineering Systems and Technology at the September, 2005 graduation

Dissertation committee: _____

Supervisor, PROF. SHIN-ICHI NISHIDA
Dept. of Mechanical Engineering

_____

Member, PROF. NOBUYOSHI OHNO
Dept. of Mechanical Engineering

_____

Member, ASSOC. PROF. NOBUSUKE HATTORI
Dept. of Mechanical Engineering

_____

Member, ASSOC. PROF. SEIYA HAGIHARA
Dept. of Mechanical Engineering

ACKNOWLEDGEMENTS

CONTENT

LIST OF FIGURES

LIST OF TABLES

CHAPTER 1

Introduction

1.1 Failure and Fatigue

Failure

A part of assembly is considered to have failed under one of the following three conditions [1]. From the viewpoint of fracture mechanics, failure may be classified as fatigue, wear, fretting, creep, corrosion and others.

(a) When it becomes completely inoperable.

(b) When it is till operable but is no longer able to perform its intended function satisfactorily.

(c) When serious deterioration has made it unreliable or unsafe for continued use, thus necessitating its immediate removal from service for repair or replacement.

Fatigue

Fatigue refers the permanent structural change that occurs in a material subjected to fluctuating stress and strain. However, in the case of glass, fatigue is determined by long-term static testing and is analogous to stress rupture in other materials. In other word, fatigue is "the process of progressive localized permanent structural change occurring in a material subjected to conditions which produce fluctuating stresses and strains at some points or points which may culminate in cracks or complete fracture after sufficient number of fluctuation" [1]. In general, fatigue failure can occur with stress levels below the elastic limit.

According to a systematic study on the cause of engineering failure, more than 90% of total 242 failure cases are directly or indirectly caused by fatigue. Figure 1.1 shows the statistic data of the 242 cases by S. Nishida [2], in which 87% of failure cases were caused by fatigue (including simple fatigue, corrosion fatigue, thermal fatigue, etc.), and the other 13% cases consisted of "pure static fracture

(3%)" and "indirectly fatigue (10%)". Indirect fatigue means that static fracture incidentally occurred due to the advanced fatigue fracture, stress corrosion cracks and delayed cracks (5%), corrosion damage and others (5%) [2, 3]. Concerning the components subjected to failures, the greatest number of failures is observed in welds, and failures other than welds decrease in the following order: shafts, bolts, pulleys or rolls, gears, wire ropes, etc. The general aspects for various failures mechanism and the safe level in sense of the possibility to cause a catastrophic failure were listed in Table 1.1 [2]. It is clear that fatigue is the most dangerous type among the failures listed here.

Table1.1 Types of failure cases and macro features (After Nishida [2])

Type	Frequency of generation	Macroscopic phenomenon	Macroscopic growth	Safety level
Fatigue	1	Invisible	Rapid	Dangerous
Wear	2	Visible	Gradual	Safe
Corrosion	3	Visible	Gradual	Safe
Others*	4	Invisible	Rapid	Dangerous

Others includes impact load, overload, etc.
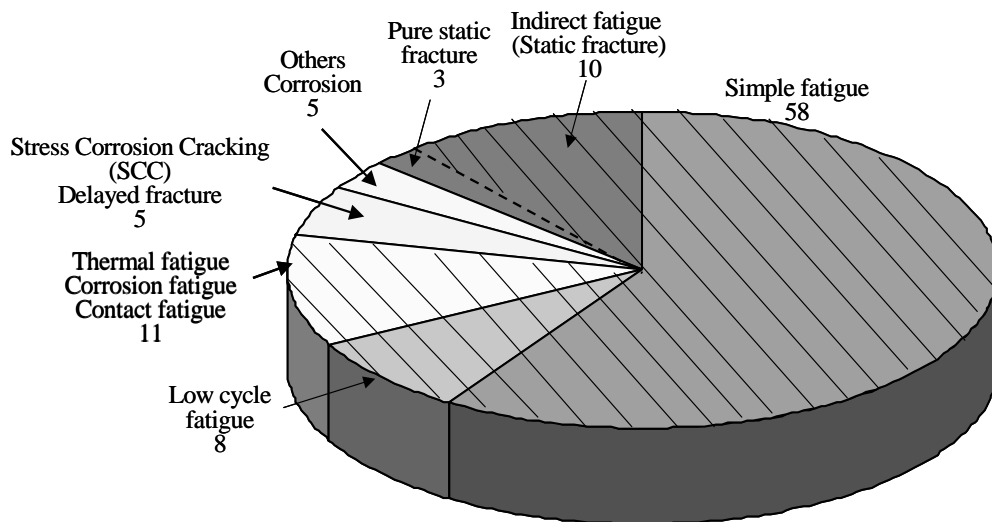
Total 242 cases, fatigue failure 87%.

Fig.1.1 Classification of failure cases according to cause (After Nishida [2])

1.2 Historical Background of Fatigue Studies

Innumerable accidents and failures have happened since the industry revolution in the 19th century, even in the modern industrial society, failures still often occur and accompanied with great human and economic loses. It is reported that among the various failures, fatigue failure is the most common failure patter in engineering [4]. Although the fatigue and failure studies have been researched for more than one and a half centuries since the first research in laboratories by August Wöhler, failures and fatigue cases are still very difficult to predict and prevent, and various conferences on fatigue of structures and materials are already planned for the forthcoming years implying that the fatigue problem is apparently not yet fully solved.

A number of train wrack and other accidents in the first half of the 19th century brought attention to the new failure model and some of the investigations concerning the mechanism of fatigue were initiated [5]. Poncelet (1839) used the term of "fatigue", who studied the failure of metals under the repeated load of tension and compression. It was claimed by McConnell (1849) that "a change from fibrous to crystalline character" occurred during fatigue, the material of the component that failed had "crystallized", as the material "tired". The so-called crystallized theory of fatigue was continuously explored mainly by railroad engineers [6].

Fatigue as a technique problem became evident around the middle of the 19th century. At that time, fatigue failures were frequently associated with steam engines, locomotives and pumps, systematic fatigue tests were done at a few laboratories, notably by August Wöhler, and one of the basic characteristic of metal fatigue—S-N curve, also called Wöhler's curve, representing the dependence of stress amplitude on the number of loading cycles to the final failure.

A fundamental step regarding fatigue as a material problem was made in the beginning of the 20th century by Ewing and Humfrey in 1903 [7]. They investigated the microscopic behavior which showed that fatigue crack nuclei start as micro cracks in slip bands. Palmgren (1924) [8] and then Miner (1945) [9] developed the "damage accumulation models" for the fatigue failure. Coffin (1954) [10] and Manson (1954) [11] proposed "plastic strain damage theory", which is called "Coffin-Manson relationship". Irwin (1957) [12] introduced the linear elastic fracture mechanics (LEFM) methods that models the quantitative relationship of fatigue crack growth rate. And the methods were developed by

Paris, Gomez and Anderson (1961) [13]. The concepts in fracture mechanics were introduced to the study of fatigue failures in 1960s, and some models explaining the propagation of fatigue cracks in material were purposed, such as by Larid and Smith in 1962, McClintock in 1963, Rice in 1967, Meumann and Pelloux in 1969 [14-18], *et. al*   Then the concept of crack closure was introduced in 1980 [19].

In the recent decades, more research interests have been concentrated on the fatigue properties of materials, such as Wang GS and Blom AF (1991) [20], Padmadinata UH and Schijve J (1994) [21], Dougherty DJ (1992) [22]. Some researchers, such as Radai D (1996) [23] and Schijve J (2003) [24] made good reviews of the fatigue studies in specific field of properties in the past. John Mann [25] published books with references to fatigue. Later he continued his work to arrive at about 100,000 references in the 20th century compared to less than 100 in the 19th century. The large number of publications and the various conferences on fatigue of structures and materials already planned for the forthcoming years implied that the fatigue problems is still apparently not yet fully solved.
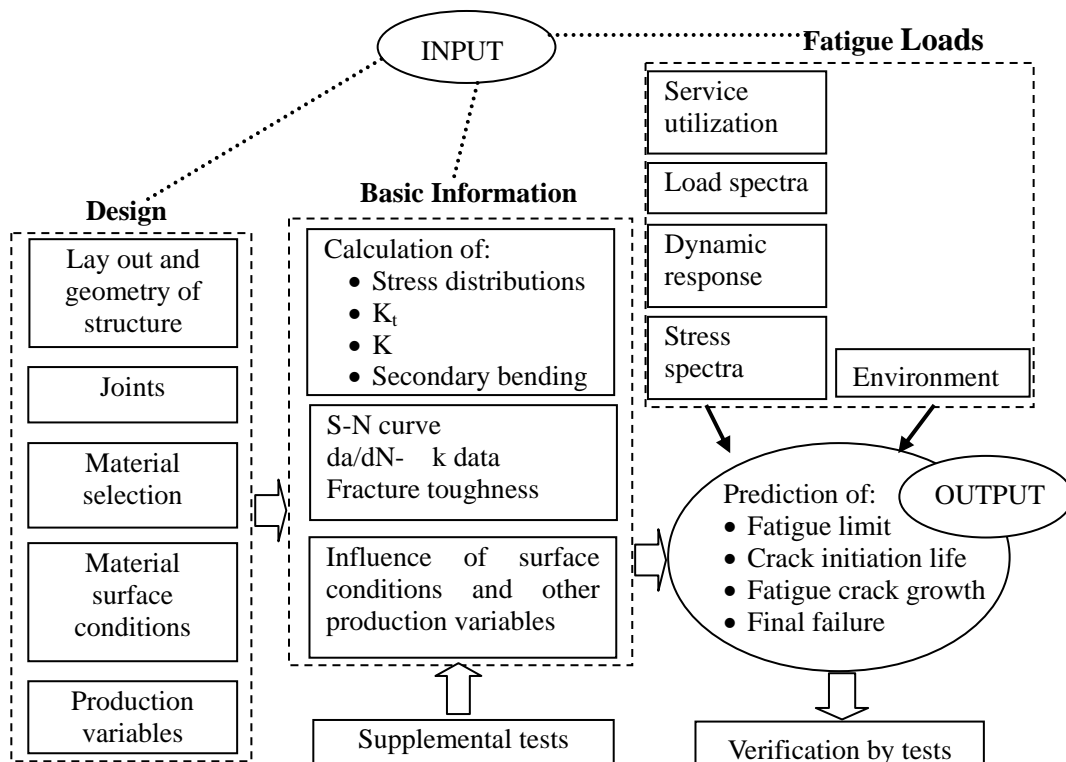
Fig.1.2 Survey of the various aspects of fatigue of structures
(After Schijve J. [26])

4

1.3 Factors Affect to the Fatigue Properties

Figure 1.2 was ever used to survey the prediction problems associated with fatigue properties [26]. The input problems occur in three categories: (i) design work; (ii) basic information used for the predictions; and (iii) fatigue load spectra to which the structure is subjected. Each of the categories contains a number of separate problems, which again can be subdivided into specific aspects. It is illustrates that the full problem can be very complex depending on the structural design, type of material, production variables, load spectra and environment.

Many parameters affect the fatigue performance of structural components, including the parameters related to stress (stress ratio, stress range, constant or variable loading, frequency or maximum stress, etc.), geometry and properties of the components (the stress or strain raisers, stress concentration level, material properties and heat treatment procedures, etc.), and external environment (temperature and aggressiveness of environment, etc.) [27].

1.3.1 Hardness and Grain Size

The microstructures of specimens are plastic deformed during the fatigue test. And it is shown that the bending fatigue limit σ_{w0}, yielding strength σ_Y, fatigue strength σ_B of the plain specimens increase with the increasing of the surface hardness value HV. For the structural carbon steel, the relationship between the rotating and bending fatigue limit σ_{w0} (MPa), fatigue strength σ_B (MPa) and the surface hardness value HV (kgf/mm^2), can be expressed as the following equations [28]:

$$\sigma_{w0}=0.50\ \sigma_B\ (\sigma_B<1479) \tag{1.1}$$

$$\sigma_{w0}=1.60\ HV\ (HV<400) \tag{1.2}$$

However, when fatigue strength is very high, the relationship between them will not necessarily be the same to the equations as shown above, because when strength is high, the material will be more sensitive to the contaminants. And the higher stress concentration around the contaminant will cause the decrease of fatigue limit and fatigue strength.

The fatigue limit σ_{w0} of plain specimen increases with the decrease of the grain size (equivalent diameter d), and the relationship between them can be expresses by the Hall – Petch equation:

$$\sigma_{wo} = \sigma_o + \frac{k_f}{\sqrt{d}} \qquad\qquad (1.3)$$

where, σ_{w0} is the fatigue limit of the test material, σ_0 and k_f are two constants of the material. Therefore, the grain size should be small to improve the fatigue strength of the test material. The relation between fatigue limit and the grain size of the structural carbon steels were also reported by some researches [29-31]. The research results show that the relation between the fatigue limit σ_{w0} and the mean diameter of grain size d is in agreement with the Hall-Petch relationship. At the same time, it is also proved that the refinement of grain does not only decrease the length of the non-propagating cracks, but also improves the fatigue limits by increasing the force against the crack propagation.

1.3.2 Stress Concentration Factor K_t and Fatigue Notch Factor K_f

Stress concentrations arise from any abrupt change in the geometry of a part under load. As a result, the stress distribution is not uniform throughout the cross-section. K_t is known as the stress concentration factor, it can be localized in a region with a diameter approximately equal to the diameter of the abrupt change area. Experiments have shown that the effect of small notches is less than that estimated from the traditional stress concentration factor, K_t. The fatigue notch factor, K_f, can be thought of as the effective stress concentration in fatigue. It depends on the size of the stress concentration and the material. Small stress concentrations are more effective in high strength materials. This effect is dealt with using a notch sensitivity factor, q, which is an empirically determined constant that depends on the notch radius and material strength.

$$K_f = 1 + (K_t - 1)\, q \qquad\qquad (1.4)$$

Figure 1.3 is a statistic result of 242 failure cases of the mechanical components. It shows that more than 90% of failures are initiated from the stress concentration parts of the structural components [2].
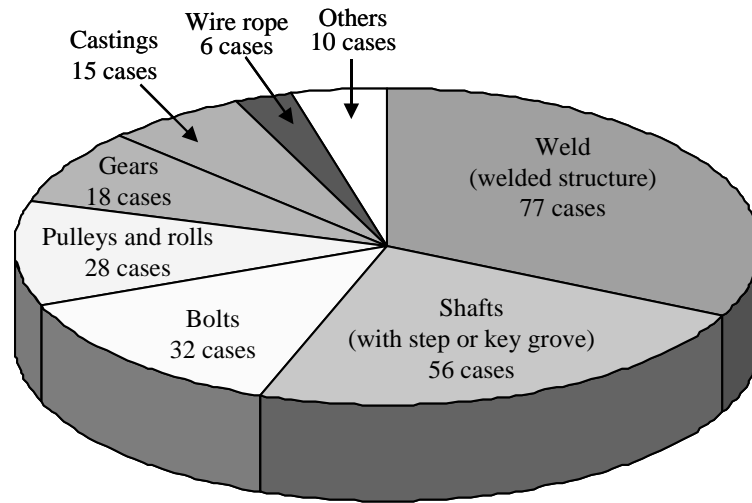
Total 242 cases, failure at stress concentration part: 90%.

Fig.1.3 Classification of failure cases according to failed

components (After S. Nishida [2])

1.3.3 Mean Stress and Residual Stress

As it is know that fatigue strength changes with the changing of mean stress, and the effect of mean stress on the fatigue limit σ_w can be expressed as [32]:

Direct line formula: $\qquad \sigma_a = \sigma_w (1 - \sigma_m / \sigma_T)$ $\qquad$ (1.5)

Gerber formula: $\qquad \sigma_a = \sigma_w [1 - (\sigma_m / \sigma_T)^2]$ $\qquad$ (1.6)

Modified Goodman formula: $\qquad \sigma_a = \sigma_w (1 - \sigma_m / \sigma_B)$ $\qquad$ (1.7)

Soderberg formula: $\qquad \sigma_a = \sigma_w (1 - \sigma_m / \sigma_S)$ $\qquad$ (1.8)

Where σ_a is the stress amplitude, σ_T is the true fracture stress and σ_B is the nominal tensile strength. For the tensile compressive fatigue test, tensile mean stress decreases the fatigue strength and compressive mean stress increases the fatigue strength. The mean stress effect on the rotating and bending fatigue test is smaller than that on the tensile-compressive fatigue test, and it is much smaller on the torsional fatigue test.

Many of the pre-process during the manufacture of the component will cause residual stress in the surface of components, such as mechanical machining, surface process, heat treatment, etc. Generally, the residual stress in surface of the component can be mechanically considered same effect as a mean stress loaded to

the component. However, the residual stress changes during the fatigue test, and it should be modified when the change is too large [33, 34].

1.3.4 Surface Modification

Surface modification is a very important and effective method to improve the fatigue strength of materials, it includes a wide field of technologies and the common among them is the formation of a modified surface layer in which the microstructure and/or the mechanical properties are different from the initial material. The techniques can be briefly divided into plastic deformation method, heat treatment and surface treatment, in which surface treatment can be further divided into two principle methods according to reaction occurred on the surface of substrate [35]. Table 1.2 lists some surface modifications and their effects [36]. The potential improvements in engineering materials characteristics may be expected include [37, 38]:

- Improved corrosion and erosion resistance
- Enhanced hardness and improved wear resistance
- Improved strength, toughness and fatigue properties

Table 1.2 Surface modification methods and the effect

Method		Wear resistance	Corrosion resistance	Heat treatment	Fatigue properties	
					Plane	Notched
Heat treatment	Quenching	Good	No effect	No effect	Excellent	Good
Chemical method	Nitriding	Excellent	No effect	Fine	Excellent	Bad
	Carburizing	Good	No effect	No effect	Excellent	Fine
	CVD	Excellent	Excellent	Excellent	Bad	Bad
Physical and electrical method	Laser treatment	Excellent	Excellent	Good	No effect	No effect
	PVD	Excellent	Excellent	Excellent	Bad	Bad
	Plating	Fine	Good	Fine	Bad	Bad
	Spraying	Excellent	Good	Good	Bad	Bad
Mechanical method	Shot peening	No effect	No effect	No effect	Excellent	Fine
	Rolling	No effect	No effect	No effect	Excellent	Excellent

1.4 Mechanisms of Fatigue

1.4.1 Fatigue Process Mechanism

It is now clear that there are many effect factors to the fatigue properties, and fatigue process is conditioned by cyclic plastic deformation. Plastic deformation plays an essential role in the initiation and propagation of fatigue cracks, without repeated plastic deformation, there would be no fatigue. In a fatigue condition, the multiple repetition of a very small plastic deformation can lead to cumulative damage and end in fracture [4].

Ewing and Humphrey [7] introduce the metallurgical microscope in making their observation. They noted that the slip bands initiated from the surface of the specimen and the fatigue cracks originated within these slip bands. On the basis of the changes caused by the cyclic plastic deformation, the whole fatigue process can be divided into the following three stages [4, 39]:

(1) Fatigue hardening and/or softening. This process mainly depends on the original state of the material and the stress or strain amplitude. Fatigue hardening manifests itself by an increase in the stress amplitude necessary to achieve a given strain amplitude. Fatigue softening is typical for hardened materials, and takes place when the obstacles are either removed or at least weakened during cycling.

(2) Microcrack nucleation. This process takes place in a small part of the total volume, the surface layer namely. A common denominator of all types of nucleation is the stress concentration in the surface layer. Direct slip observation of the surface show that there are three types of nucleation site: fatigue slip bands, grain boundaries, and surface inclusions [40]. For the case of fatigue slip band, its nature is slip concentration within the grains. At all plastic strain amplitude slips and cracks are generally the most frequent crack nuclei. However their damaging potential is small due to their low tendency to propagate. Their main contribution to the cracking process is to accelerate quickly growing crack types by being linked up into their crack paths. Nucleation at grain boundaries is typical for high strain fatigue, especially at higher temperature. Grain boundary cracks appear to play the most important role at all amplitudes, and because of their high stress tendency to propagate, their damaging potential is very high. Surface inclusion nucleation is only typical for some commercial alloy containing large enough particles.

(3) Crack propagation ending in final failure. The controlling factor of crack

propagation is the highly concentrate cyclic plastic deformation within the plastic zone at the crack tip [4].

1.4.2 Fatigue Propagation Mechanisms

When a crack is considered small, local stress gradients due to geometry are negligible. However, as a crack extends beyond the small crack regime, stress gradients are constraint caused by geometry cannot be ignored. The stresses that a crack feels decay from the local stresses to the nominal applied stresses. A fracture mechanics treatment of these cracks must be able to integrate LEFM (Linear Elastic Fracture Mechanics), EPFM (Elastic Plastic Fracture Mechanics) and MFM (Micro Fracture Mechanics) seamlessly.

Linear Elastic Fracture Mechanics (LEFM)

Fatigue crack life is generally divided into three stages: Stage I, Stage II and Stage III [27, 39]. Figure 1.5 is a schematic illustration of a crack growth rate curve with the characteristics of the curve taken from [41].

Stage I covers the crack initiation and the early crack growth state, which includes cyclic plastic deformation prior to crack initiation of one or more microscopic cracks and coalescence of these micro-cracks to form an initial macro-crack. Stage II is characterized by stable crack growth, while at the last stage the crack growth accelerates due to interaction between fatigue and fracture mechanisms. The duration of the third period (Stage III) is usually quite short and it can be neglected in the fatigue life estimation.

The lifetime of structures with initial cracks is very closely related to the
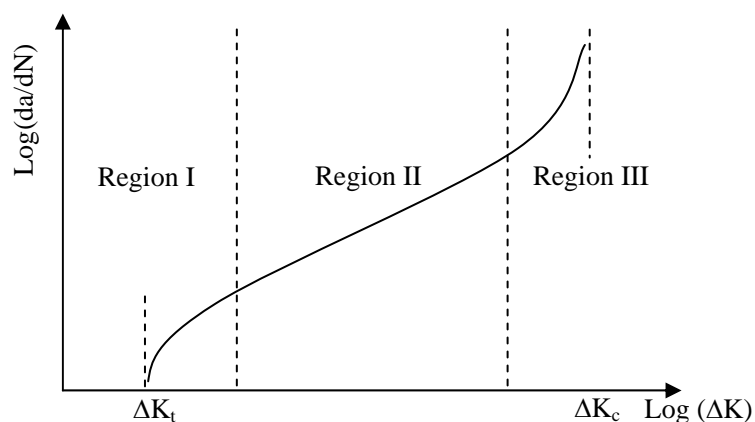
Fig.1.4 Variation of crack propagation rate

crack propagation period, since the initiation time is essentially short. Current experimental and theoretical linear elastic approaches try to describe the stable and unstable crack growth by a crack propagation rate da/dN, which is defined as a function of the stress intensity factor range ΔK during a load cycle that can be expressed by:

$$da / dN = f(\Delta K, K_{max}(or R), v, environment, wave form \cdots) \qquad (1.9)$$

where R is the ratio of minimum to maximum applied loads and v is the frequency. The crack behavior in Stage I exhibits low values of ΔK and da/dN. An important factor of this region is fatigue threshold ΔK_{th}, below which cracks do not propagate under cyclic stress fluctuations. Stage II represents the fatigue crack propagation behavior above ΔK_{th}, which can be represented by:

$$da/dN = C(\Delta K)^m \qquad (1.10)$$

$$\Delta K = K_{max} - K_{min} = F(\Delta\sigma)\sqrt{\pi a} \qquad (1.11)$$

here C and m are material constants. K_{max} and K_{min} are the maximum and minimum stress intensities at the crack tip. This equation, the famous Paris law [13] is applicable in linear elastic condition and it is the most widely used form of characterizing crack growth rate for a vast spectrum of material and conditions.

Elastic Plastic Fracture Mechanics (EPFM)

Under the elastic plastic conditions, EPFM can be employed to characterize fatigue crack growth.

Rice [42] proposed the J-integral to provide a loading parameter for the characterization of monotonic, nonlinear fracture in rate-dependent materials. And a power law [43] was proposed for the characterization of fatigue crack advance under the elastic plastic conditions based on the cyclic J-integral, ΔJ (or J^c):

$$da / dN \propto \partial(\Delta J)^m \qquad (1.12)$$

where m is an exponent analogous to the m in equation (1.12).

Considering a crack body subjected to monotonic load, assuming that the tractions T are independent of crack size and that the crack faces are tractions free, the line integral J along any contour Γ which encircles the crack tip is given by:

$$J = \int_{\Gamma} \left\{ wdy - T(\partial\mu/\partial x)ds \right\} \qquad (1.13)$$

where μ is the displacement vector, y is the distance along the direction normal to the plane of the crack, s is the arc length along the contour, T is the traction vector and w is the strain energy density of the material. The relationship between ΔK and ΔJ can be expressed as [43]:

$$\Delta J = (\Delta K)^2 / E \qquad (1.14)$$

Huntchinson pointed out that the use of J-integral for characterizing fracture in real ductile materials required ascertaining certain conditions [44]. Tomkins proposed the relationship between da/dN and the crack tip decohesion as [45]:

$$da/dN = B(\Delta\varepsilon_p \sqrt{\pi a})^n - D \qquad (1.15)$$

where D is the threshold condition, $\Delta\varepsilon_p$ is the strain amplitude and B is the scaling factor.

Micro Fracture Mechanics (MFM)

One of the more active areas of research in the field of fatigue in recent years has been the study of the fatigue crack growth behavior of small cracks. Small fatigue cracks can be divided to four classes [40], and usually the small crack studies are focused on the first three kinds.

- Mechanically small crack: crack length less than the plastic zone size;
- Microstructurally small crack: crack length less than a critical microstructural dimension such as grain size;
- Physically small crack: crack length less than that at which crack closure is fully developed, usually less than 1mm in length;
- Chemically small crack: crack length may be up to 10mm, depending upon the crack tip environment.

A small crack may grow hundreds of times faster than a long one under the same level of ΔK and may decelerate then arrest or then deceleration. Though LEFM approaches are quite successful to characterize stable long fatigue crack growth (associated to Stage II fatigue), it is inapplicable to characterize the growth of comparatively small cracks (associated to Stage I fatigue). To cover the so-called "anomalous behavior" of small cracks, MFM crack growth model proposed by Navarro and de los Rios [46] led to the laws of the form:
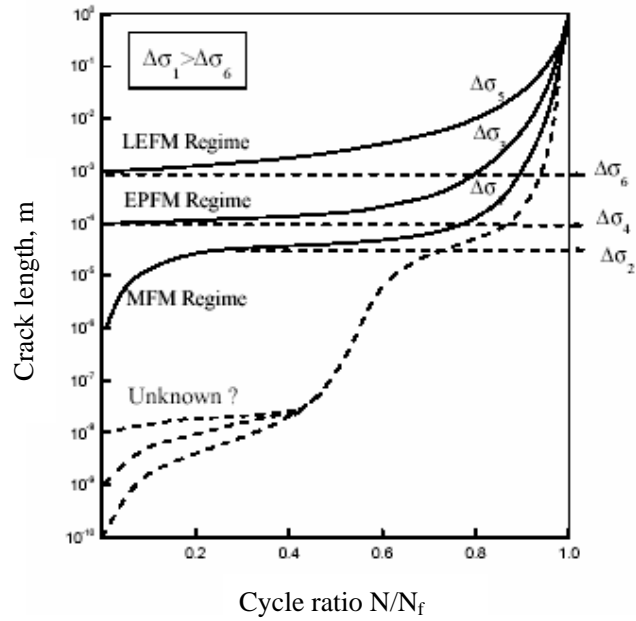
Fig.1.5 Effect of initial crack size and fundamental crack growth
behaviors in materials (after Miller [46])
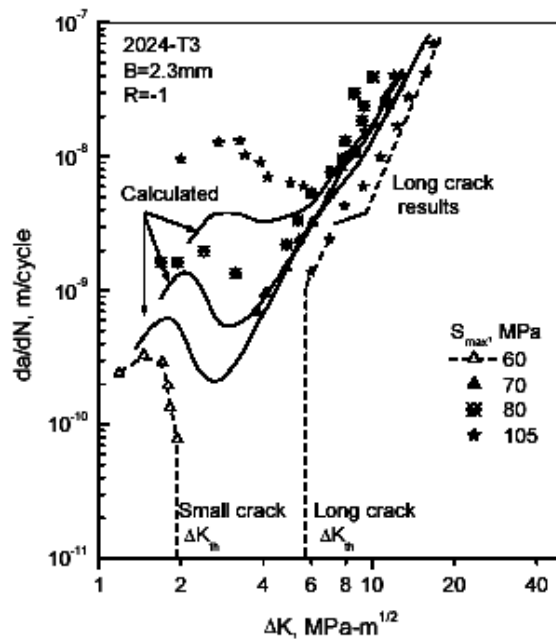
Fig.1.6 Experimental and predicted small fatigue crack growth rates
(after Miller [47])

$$da/dN = C_m \Delta\gamma^\beta (d - a) \qquad\qquad (1.16)$$

where $\Delta\gamma$ is the shear strain amplitude, d is a micro structural dimension (for instance, grain size), a is the crack depth, C_m and β are the scaling factors related to materials, loading conditions and temperature.

MFM indicates the case of crack growth when "a" approaches to the micro structural dimension. If the crack continues to grow, there should be an overlap between MFM and EPFM or between MFM and LEFM for the transition.

Figure 1.5 schematically describes the fatigue crack growth behaviors in different regimes, and Figure 1.6 illustrates the experimental and predicted small fatigue crack growth rate [47].

1.4.3 Intrinsic and Extrinsic Mechanisms of Crack

Ritchie systematically studied fatigue crack propagation in ductile and brittle materials [39, 48]. He considered the process of fatigue crack growth as a mutual competition between intrinsic mechanisms and extrinsic mechanisms of crack advance ahead of the crack tip. Intrinsic mechanisms (e.g. alternating crack tip blunting and re-sharpening) promote crack growth and extrinsic mechanisms (e.g.crack closure and bridging) impede the crack growth. Take metallic materials as an example, intrinsic damage mechanisms involve processes which create micro cracks or voids in the highly stressed region ahead of the tip, leading to classical failure by cleavage, intergranular cracking or micro void coalescence; comparable mechanisms under cyclic loads involve the repetitive blunting and re-sharpening of the crack tip. Extrinsic shielding mechanisms result from the creation of inelastic zones surrounding the crack wake or from physical contact between the crack surfaces via wedging, bridging, sliding or combination thereof. These mechanisms are shown in Fig.1.7 briefly.

The intrinsic mechanisms are an inherent property of the material, and thus are active irrespective of the length of the crack or geometry of the test specimen; in other words, theses mechanisms relative to initiation of crack. Conversely, extrinsic mechanisms act in the crack wake and are thus critically dependent on crack size and geometry. These mechanisms can have no effect on crack initiation (since there is no crack wake), and relative to continued crack growth.
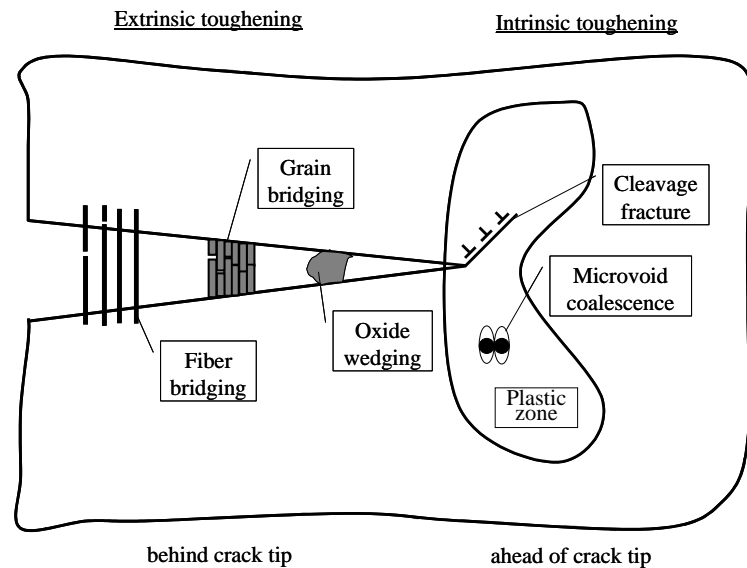
Fig.1.7 Schematic illustration of mutual competition between intrinsic mechanisms of damage/crack advance and extrinsic mechanisms of crack tip shielding involved in crack growth (after Ritchie [48])

1.5 Objectives and Scope of the Present Study

Structural carbon steels are widely used in many fields as castings and forgings, pipes and tubes, sheets and plates, wires, rods, rails and other structural components, because of their good mechanical properties and low cost. It is reported that more than 90% of failure cases are caused by fatigue failure, and most of the mechanical components have been plastically worked before in service. Moreover, most of the fatigue studies since the beginning of the fatigue research have been focused on the rotating and bending fatigue properties. Therefore, it is very important and necessary to study the torsional fatigue properties of structural carbon steels which is pre-strained with tensile stress.

The objectives of the present study are to evaluate the effects of tensile pre-strain and carbon content on the torsional fatigue properties of structural carbon steels, and to investigate the relationship between tensile pre-strain ratios and the surface plastic deformation.

Chapter 1 reviews the general history of fatigue study, introduces the basic mechanisms of fatigue crack initiation and propagation. Chapter 2 is concentrated to introduce the test materials and the experimental procedure. In Chapter 3, the

relationship between tensile strain ratio and the surface plastic deformation is investigated and discussed. Chapter 4 and Chapter 5 are focused on the effects of tensile pre-strain and carbon content to the torsional fatigue properties of structural carbon steels, respectively. The influence on the fatigue strength, fatigue crack initiation and propagation behaviors are investigated, observed and discussed in detail. Finally Chapter 6 is a general summary of the present study and some recommendations for the future research are provided.

References

[1]. Metals Handbook 8th Edition, Vol. 10, Failure analysis and prevention, American Society for Metals, 1975, p. 1.

[2]. S. Nishida, Failure analysis in engineering application, Butterworth Heinemann Ltd., 1992, p. 1-5.

[3]. Kenneth G. Budinski, Michael K. Budinski, Engineering materials - properties and selection, Sixth Edition, Prentice Hall International, Inc., 1999, New Jersey, USA.

[4]. M. Klesnil and P. Lukas, Fracture of Metallic Materials, United States: Elsevier Science Publishing Company, 1980.

[5]. R. A. Smith, The Versailles railway accident on 1842 and the first research into metal fatigue, in Fatigue 90 (Eds. H. Kitagawa and Tanaka), Birmingham: Materials and Component Engineering Publications, Vol.4, p. 2033-2041.

[6]. A. J. McEvily, Metal failures: mechanisms, analysis, prevention. Willey Interscience Publication, U.S.A.

[7]. J. A. Ewing, J. C. W. Humfrey, The fracture of metals under repeated alternations of stress. Phil Trans Roy Soc 1903, A200, p. 241-250.

[8]. A. Palmgren, Die Lebendauer von Kugellagern, Zeitschrift des Vereins Deutscher Enginieure, 68, 1924, p. 339-341.

[9]. M. A. Miner, Cumulative damage in fatigue, Journal of Applied Mechanics, No.12, 1945, p. 159-164.

[10]. L. F. Coffin, A study of the effect of cyclic thermal stresses on a ductile metal, Transactions of the American Society of Mechanical Engineering, 1954, 76, p. 931-950.

[11]. S. S. Manson, Behavior of materials under conditions of thermal stress, National Advisory Commission on Aernautics, Cleveland: Lewis Flight Propulsion Lab, Report 1170, 1954.

[12]. G. R. Irwin, Analysis of stress and strains near the end of a crack traversing plate, Journal of Applied Mechanics, 1957, 24, p. 361-364.

[13]. P. C. Paris, M. P. Gomez and W. P. Anderson, A rational analytic theory of fatigue, The Trend in Engineering, 1961, 13, p. 9-14.

[14]. C. Larid and G. C. Smith, Crack propagation in high stress fatigue, Philosophical Magnize, 8, p. 847-857.

[15]. F. A. McClintock, On the plasticity of the growth of fatigue cracks, Fracture

of Solids, Vol. 20, New York, Wiley, p. 65-102.

[16]. J. R. Rice, Mechanics of crack tip deformation and extension by fatigue, In fatigue crack propagation, Special Technical Publication, 415, Philadelphia: American Society for Testing and Materials, p. 247-309.

[17]. P. Newmann, Coarse slip model of fatigue, Acta Metallurgica, 17, p. 1219-1225.

[18]. R. M. N, Pelloux, Mechanism of formation of ductile fatigue striation, Transactions of the American Society for Metals, 62, p. 281-285.

[19]. R. O. Ritchie, S. Suresh and C. M. Moss, Near-threshold fatigue crack closure at near threshold stress intensities due to fracture surface morphology, Metallurgical Transactions, 13A, p. 293-299.

[20]. G. S. Wang, A. F. Blom, A strip model for fatigue crack growth predictions under general load conditions, Engng Fract Mech, Vol. 40, 1991, P467-471.

[21]. U. H. Padmadinata, J. Schijve, Prediction of fatigue crack growth under flight simulation loading with the modified CORPUS model. In: Harris C. E., editor, Advanced structural integrity methods for airframe durability and damage tolerance, NASA Conf Publ, 1994, p. 547-562.

[22]. D. J. Dougherty, De Koning A. U., B. M. Hillerry, Modeling high crack growth rates under variable amplitude loading. In ASTM STP 1122, Philadelphia, PA: American Society for Testing and Materials, 1992, p. 214-233.

[23]. D. Radai, Review of fatigue strength assessment of non-welded and welded structures based on local parameters, International Journal of Fatigue, 1996, 18, p. 153-170.

[24]. J. Schijve, Fatigue of structures and material in the 20th century and the state of the art, International Journal of Fatigue, Vol. 25, 2003, p. 679-702.

[25]. J. Y. Mann, Bibliography on the fatigue of materials, components and structures, Vol. 1-4, coving 1828-1969. Pergamon Press, 1970-1990.

[26]. J. Schijve, Fatigue of structures and materials. Dordrecht, Boston: Kluwer Academic Publ, 2001.

[27]. J. M. Barsom and S. T. Rolfe, Fracture and Fatigue Control in Structures, United States, Prentice-Hall, Inc, 1987.

[28]. I. Nakazawa, Fatigue strength of metals. Yokendo Ltd., 1982, p. 23.

[29]. Masaru Tamura, Kunihiro Yamada, Masao Shimizu and Takeshi Kunio, Study on the endurance and non-propagating crack behaviors of structural carbon steel, JSME (A), Vol. 49, 1983, p. 1378-1387.

[30]. Isamu Yamada, Kunihiro Yamada and Takeshi Kunio, Effect of grain size on threshold behavior of small crack in plain carbon steel, JSME (A), Vol.52, 1986, p. 412-416.

[31]. Shunichi Tachibana, Shunichi Kawachi, Kunihiro Yamada and Takeshi Kunio, Effect of grain refinement on the endurance limit of plain carbon steels at various strength levels, JSME (A), Vol. 54, 1988, p. 1956-1961.

[32]. Materials Science Society of Japan, Strength and fracture of materials, 2001, p. 104-106.

[33]. S. W. Wang, S. Nishida, N. Hattori, H. Tamasaki and N. Nakamura, Effect of Plastic Deformation by Roller-working on Fatigue Strength of Notched Specimen, JSME Int. J, Vol.43, 2000, p. 425-422.

[34]. S. W. Wang, S. Nishida, N. Hattori, H. Tamasaki, Improvement of Fatigue strength of notched specimen by roller working, JSME (A), Vol. 64, 1998, p. 3038-3043.

[35]. Materials Science Society of Japan, Handbook of Fatigue Design, Tokyo, Yokendo, 1995.

[36]. S. W. Wang, Improvement of fatigue strength of notched structural steel components by surface plastic working, Ph. D thesis, Saga University, 1999.

[37]. Materials Science Society of Japan, Surface Treatment in Materials, Tokyo, Shokabo, 1996.

[38]. X. D. Peng, A. Kharlov, V. Bystritski, E. Garate and E. J. Lavernia, Characteristics of Material Surface Modified Using Plasma-Enhanced Ion Beams, Mater. Sci. Eng., A251, 1998, p. 142-149.

[39]. R. O. Rithcie, Mechanisms of Fatigue Crack Propagation in Ductile and Brittle Solids, International Journal of Fatigue, 100, 1999, p. 55-83.

[40]. Arthur J. McEvily, The Growth of Short Fatigue Cracks: a review, Material Science Research International, Vol.4, 1998, p. 3-11.

[41]. R. O. Ritchie, Influence of microstructure on near-threshold fatigue crack propagation in ultra-high strength steel, Metal Science, 1977.

[42]. J. Rice, A path independent integral and approximate analysis of strain concentration by notches and cracks, Journal of Applied Mechanics, 35, 1968, p. 379-386.

[43]. N. Dowling and J. A. Beley, In Mechanics of crack growth, ASTM STP 590, 1976, p. 82-103.

[44]. J. W. Hutchinson, Fundamental of the phenomenological theory of non-linear fracture mechanics, Journal of Applied Physics, 50, 1983, p.

1042-1051.

[45]. B. Tomkins, Philosophical Magazine, 155, 1968, p. 1041-1066.

[46]. K. J. Miller, A historical perspective of the important parameters of metal fatigue and problems for the next century, Proceeding of Fatigue'99, Beijing, 1999, p. 15-39.

[47]. J. C. Newman Jr., M. H. Swain and E. P. Phillips, Small fatigue cracks, The metallurgical Society, AIME, Warrendale, 1986, p. 427.

[48]. R. O. Ritchie, C. J. Gilbert and J. M. McNaney, Mechanics and mechanisms of fatigue damage and crack growth in advanced materials, Inter. J. Soli. Struc., Vol. 37, 2000, p. 311-329.

CHAPTER 2

Materials and Experimental Procedure

2.1 Introduction

Carbon steels are simply alloys of iron and carbon, with carbon as the major strengthening agent [1]. The handbook of the U.S. steel industry, the Steel Product Manual, published by the Iron and Steel Society more rigorously describes carbon steels as steels with up to 2% carbon and only residual amounts of other elements except those added for deoxidation (for example, aluminum), with silicon limited to 0.6%, copper to 0.6%, and manganese to 1.65%. In other words, carbon steels are alloys of iron and carbon with carbon limits between approximately 0.06% and 2%. When iron-carbon alloys have less than 0.005% carbon present at room temperature, they are considered as pure iron. On the other end of carbon content scale, iron-carbon alloys with more than approximately 2% by weight of carbon are considered to be cast iron. Usually, carbon steels are grouped into 5 classes, all

Table 2.1 Classes of carbon steels

Type of carbon steel	Percentage of carbon content
High carbon steel	Above 0.5%
Medium carbon steel	0.2-0.49%
Low carbon steel	0.05-0.19%
Extra low carbon steel	0.015-0.05%
Ultra low carbon steel	Below 0.015%

with different percentages of carbon content, as listed in Table 2.1 [2]. Other terms applied to this class of steels are plain carbon steels, mild steels, low-carbon steels, and straight-carbon steels. These steels make up the largest fraction of steel production. They are available in almost all product forms: sheet, strip, bar, plates,

tube, pipe, wire. They are used for high-production items such as automobiles and appliances, but they also play a major role in machine design for base plates, housings, chutes, structural members, and literally hundreds of different parts.

2.2 Test Materials

The materials used in the torsional fatigue study are four kinds of traditional low and medium structural carbon steels, JIS S15C, S25C, S35C and S45C, that carbon content is about 0.15% to 0.45%, their chemical positions are listed in Table 2.2, Table 2.3 lists the main mechanical properties of the test materials.

Table 2.2 Chemical composition, mass%

	C	Si	Mn	P	S	Al
S15C	0.16	0.22	0.50	0.017	0.006	0.037
S25C	0.26	0.25	0.39	0.017	0.013	-
S35C	0.36	0.23	0.76	0.021	0.022	0.001
S45C	0.46	0.20	0.73	0.029	0.017	0.018

Table 2.3 Heat treatment conditions and mechanical properties

	Heat treatment condition	σ_Y, MPa	σ_B, MPa	ψ, %	Average grain size
S15C	900°C 2hrs A.C.	284	442	71.1	
S25C	895°C 2hrs A.C.	298	495	64.7	20µ
S35C	850°C 2hrs F. C.	327	544	49.8	
S45C	990°C 2hrs F. C. (2 times)	360	633	54.4	

σ_Y, Yield strength, σ_B, tensile strength, ψ, Reduction of area.

2.3 Pre-process

2.3.1 Heat Treatment

All specimens were firstly cut out from round bars (ϕ25). Some researches have shown that grain size affect the fatigue strength much, even though it was for the same material [3]. Therefore, all of the specimens were heat treated at specific

temperature respectively in order to get almost the same grain size for the entire test materials, the specific heat treatment temperature and conditions are listed in Table 2.3. Figure 2.1 shows their micro structure behaviors after heat treatment. After the heat treatment, the oxidized layer of the specimens was removed before the mechanical machining.

2.3.2. Mechanical Machining

After been heat treated, the short round bars were machined to the shapes shown in Fig.2.2 by two times of mechanical machining. At the first machining, the round bars were machined to the shape shown in solid lines, drilled the hole at

S15C   S25C

S35C   S45C

Axial direction

200 μm
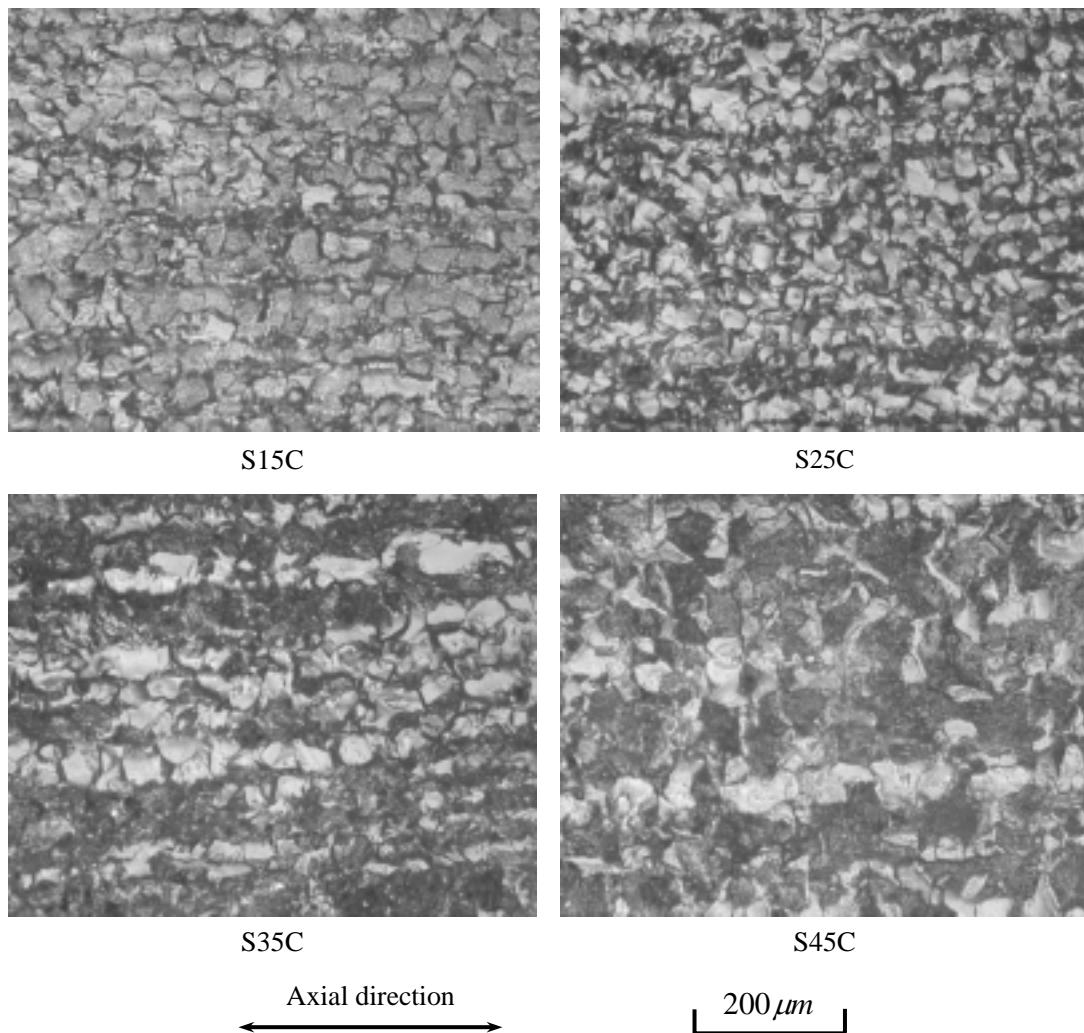
Fig.2.1 Micro structure of heat treated materials
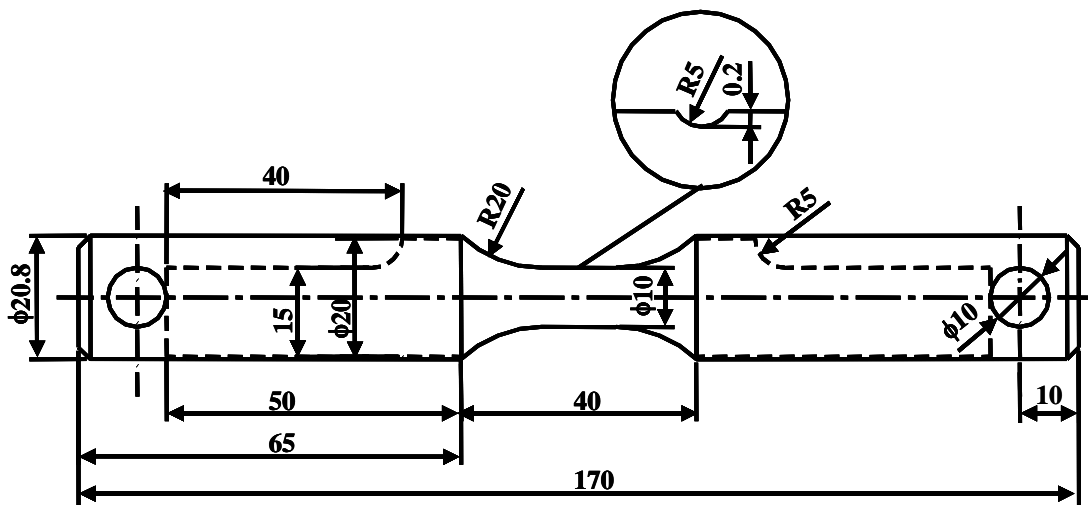
Fig.2.2 Shapes and dimensions of the specimen

the two ends and made the notch in the center part of the specimen. The shallow notch in the center part of the specimen is to ensure that the fatigue crack will initiate there. It has been considered that the notch actor of such a notch is about 1 and it does not affect the fatigue strength of the specimens [4-7]. The shape in solid lines shown in Fig.2.2 is for tensile pre-strain and the shape in dashed lines is for the torsional fatigue test. At the second time, the tensile pre-strained specimen was machined to the shape in dashed lines shown in the figure. During this machining, it was made sure not to make any deformation in the middle part of the specimen that had been electro-polished and tensile pre-strained.

2.3.3 Polishing Process

After the first time of mechanical machining, the specimens were paper polished by emery paper from 400# to 3000#, to relieve the machining scratches. Then they were annealed at 600°C for one hour in vacuum and then electro polished to the depth of more than 50μm in diameter to eliminate the residual stress introduced by mechanical machining and remove the work hardened layer. The electrolyte used in this study and the electro polishing condition are listed in Table 2.4 [8]. The setting of the specimen and the arrangement of equipments are shown in Fig.2.3. After been electro polished, specimens were dried completely and kept in dry environment to make sure the clean surface of the polished part.

Table 2.4 Electrolyte for electro polishing of structural carbon steels

Electrolyte	Current (A)	Time (Min)
Phosphoric acid (2000ml) Acid (40g) Gelatin (40g) Distilled water (200ml)	10+2	3×3+1
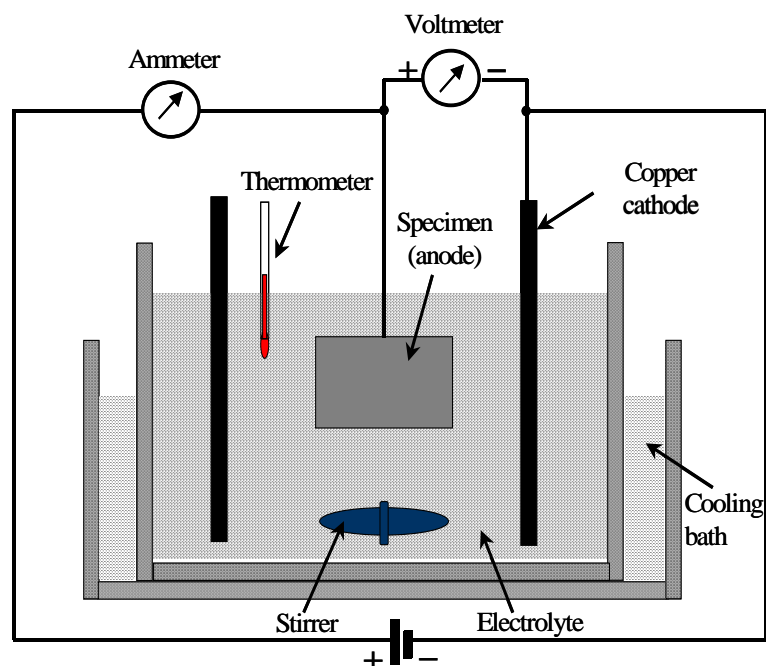
Fig.2.3 Electrical circuits and arrangement of
equipment for electro polishing

2.3.4 Tensile Test and Tensile Pre-strain

The ability of a metal to undergo plastic deformation is probably its most outstanding characteristic in comparison with other materials. All shaping operations such as stamping, pressing, spinning, rolling, forging, drawing, and extruding involve plastic deformation of metals. Various machining operations such as milling, turning, sawing, and punching also involve plastic deformation.

Tensile property is one of the most basic important mechanical properties of materials. Therefore, tensile test of four kinds of low and medium structural carbon steels (JIS S15C, S25C, S35C and S45C) were performed by a universal

test machine (Shimadzu AG-IS 100) with a loading speed of 20mm/min. Figure 2.4 shows the shape and dimensions of the specimens for tensile test.

Tensile pre-strain were applied to specimens by a universal testing machine (SHIMADZU EHF-10 type, Kyoto, Japan). The shape and dimensions of the specimen for tensile pre-straining are the same as those in solid lines shown in Fig.2.2. Three different pre-strain ratios 2%, 5% and 8% were applied to the specimens, which were called pre-strained specimens. And the specimens without tensile pre-strain were called non-pre-strained ones.
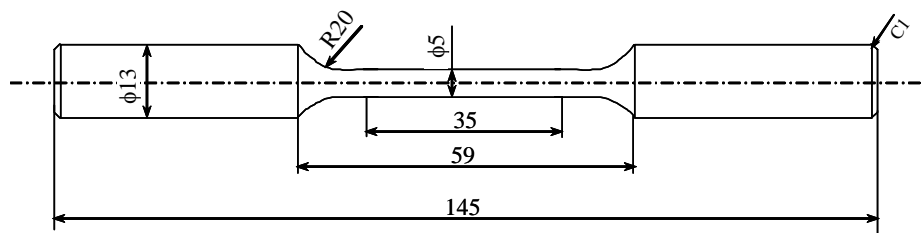
Fig. 2.4 Shape and dimensions of tensile specimen

2.3.5 Hardness

It is well known that after surface modification, one of the direct consequences is the formation of a strengthened surface layer with high hardness and high strength. On this reason, the surface hardness of specimens is an important index of materials after tensile pre-strain. The surface hardness was tested by a Vickers hardness tester (AKASHI MVK-G2 Vickers Hardness Test) with a load of 0.49 N and the load applying speed of 3 μm/sec, and the load holding time was 15 seconds on the surface of specimens.

2.3.6 Aging and Etching Process

Aging refers to the process that when the supersaturated solid solution is unstable and left alone, the excess will precipitate out of the phase. There are three types of aging: natural aging, artificial aging and abnormal aging [9, 10].

Natural Aging When the process occurs at room temperature, it is called natural aging.

Artificial Aging If the material that has been solution heat treated requires a heating to speed up the precipitation, the process is called artificial aging. It should be noted that freezing the solution heat treated material will retard the aging process.

Abnormal Aging In many instances aging will occur without precipitation. The particle may actually diffuse within the lattices and distort them. This type of aging is called abnormal aging.

After a period of time, the solute material precipitates and hardening develops. When the composition reaches its saturated normal state, the material reaches its maximum hardness. However, as the precipitate continues to grow, the fine precipitates disappear and they have grown larger. As a result the tensile strength of the material decreases. Figure 2.5 shows the hardness and tensile strength variations during aging and averaging.

The tensile pre-strained specimens were aging processed in vacuum at 250°C for 2 hours before torsional fatigue test, to make all the specimens are in the same strength condition which is different with the passing of time. Some of them were etched with a solution of 5% HNO_3 and 95% Ethanol to get clear microstructure and monitor the surface condition during fatigue test by replica method.
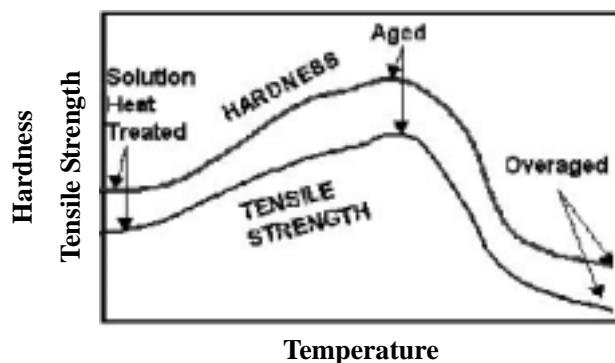
Fig.2.5 Relationship between hardness,
tensile strength and aging stages

2.4 Torsional Fatigue Test

Torsional fatigue tests were carried out at room temperature with a Shimadzu type bending and torsional testing machine (49Nm, 2000rpm). The moment model of the fatigue test machine is presented in Fig.2.6. And the torsional fatigue testing machine was driven as follows [11]:

J: Inertia moment of the vibrating portion (Load taker, grip implement at the loading side)

M: Dynamic moment of rotating eccentric weight

K: Spring constant of the torque bar

k: Spring constant of the specimen

θ: Vibration degree of the load taker

$$J \frac{d^2\theta}{dt^2} + K\theta + k\theta = M \sin \omega t \qquad (2.1)$$

Here, an assumption was put that $\theta = \theta_0 \sin \omega t$, then the moment loaded on the specimen will be:
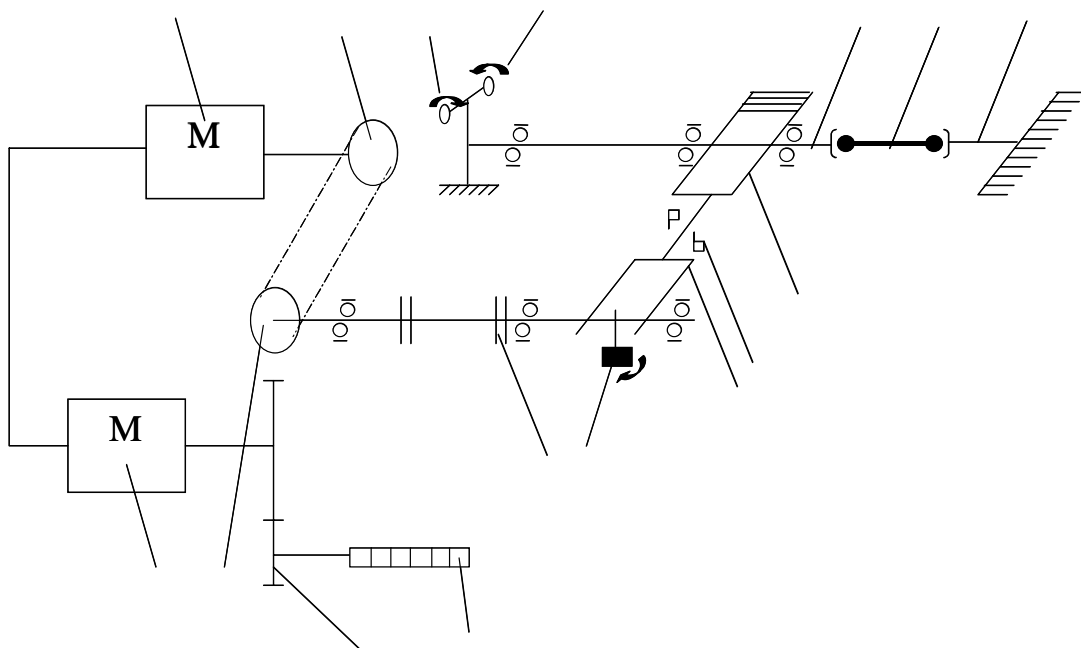
Grip tool on the fixed side	Belt pulley on the eccentric
Torsional specimen	weight
Grip tool on the loading side	riving gear of accouter
Support bolt	Accouter
Mean load bolt	Coupling
Belt pulley on the synchronous	Rotating eccentric weight
motor side	Loading taker
Synchronous motor	Limit switch
Same type synchronous motor	Torque bar

Fig.2.6 Mechanism model of torsional fatigue testing machine

$$k\theta_0 = J\theta_0\omega^2 + M - K\theta_0 \tag{2.2}$$

To this torsional fatigue testing machine, $J\omega^2 = K$. Therefore, there will be:

$$k\theta_0 = M \tag{2.3}$$

The moment loading on the specimen $k\theta_0$ is equal to the dynamic moment out put by the testing machine, which is based on that the spring constant of the specimen and the out put moment of the machine do not change during the fatigue test.

To the specific testing machine, the out put moment could be decided by getting the relationship between the situation of the rotating eccentric weight and the dial gauge. Firstly, the strain gauge was affixed on the surface of specimen, a strain amplifier (DPM-711B) and an oscillographic recorder (Kyowa RDM-2004A) were used to get the micro strain output ($\mu\varepsilon$).

When the static load (T) and dynamic load/dial gauge load moment (D) was put on, the electric signal output ($\mu\varepsilon$) will be out put on the strain amplifier, respectively. Based on the output of the amplifier, the gotten relationship between the micro strain ($\mu\varepsilon$) and the static moment (T) is shown in Fig.2.7, which can be fitted approximately as:

$$\mu\varepsilon = 65.335T \tag{2.4}$$
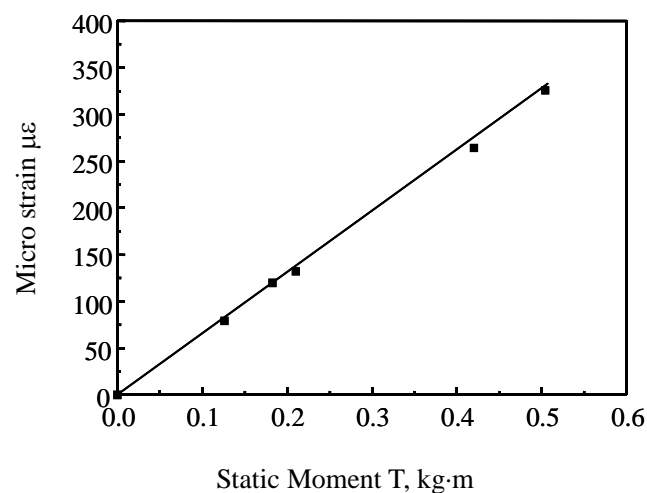
Fig.2.7 Relation between static moment T and micro strain $\mu\varepsilon$

With the same method, the relation between micro strain ($\mu\varepsilon$) and the dynamic load/dial gauge load moment (D) can also be gotten, as shown in Fig.2.8, and the fitted relationship is:

$$\mu\varepsilon = 662.22D \tag{2.5}$$

Therefore, the static load can be expressed by the dial gauge load D as:

$$T=10.136D \tag{2.6}$$

The maximum of torsional stress loaded on the specimen, τ_{max} can be calculated as [12]:

$$T = \frac{\pi d^3}{16}\tau_{max} \tag{2.7}$$

where, M is the maximum torsional stress, d is the minimum diameter of specimen. Since the calculated relationship between static load T and the dial gauge load moment D as shown in Eq.(2.6), the maximum torsional stress is:

$$\tau_{max} = \frac{51.62}{d^3} \times D \tag{2.8}$$
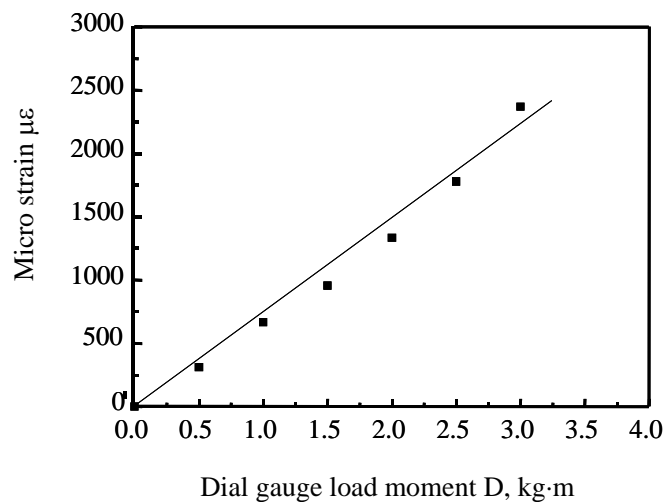
Fig.2.8 Relation between Dial gauge load moment
D and micro strain $\mu\varepsilon$

2.5 Microstructure Observation

During tensile pre-strain, plastic deformation is introduced to the surface layer of materials, consequently causing the change in microstructure of the surface layer. To investigate this change, an optical microscope (Olympus BHM Microscope) was used to observe the surface microstructure before and after tensile pre-strain.

On the other hand, the fatigue crack initiation, propagation and the non-propagating crack behaviors were also observed with successively taken replica samples, and the crack length was measured with an optical microscope equipped with a digital measurement system (Keyence VH-6300 digital microscope).

Reference

[1]. Kenneth G. Budinski, Michael K, Budinski. Engineering Materials, properties and Selection, sixth edition, Prentice Hall International Inc., 1999. New Jersey, USA.

[2]. Tuan Suhaimi Bin Salleh, Study on service performance of automobile steel sheets, Master Degree Thesis, Saga University, 2004.

[3]. N. Hasegawa, Y. Kato, and Masaki Nakajima, Effect of grain size on fatigue strength of low carbon steel at elevated temperature. JSME, Vol. 21, 1978, p. 181-188.

[4]. M. Goto, H. Nisitani, H. Miyagawa and A. Miura, Effect of pre-strain on the fatigue strength of a heat treated 0.45% C steel, JSME A, Vol. 57, 1991, p.1475-1480.

[5]. K. Fujimura, H. Nisitani and S. Fukuda, Changes in residual stress and successive observation by electron microscope in the fatigue test of pre-strained or shot peened carbon steel, JSME A, Vol. 59, 1993, p. 3006-3013.

[6]. H. Nisitani, S. Tanaka, S. Yamada and T. Teranishi, Relation between micro cracks and the coaxing effect of pre-strained low carbon steel, JSME A, Vol.54, 1988, p.190-195.

[7]. Y. Nagase and M. Izumisawa, Effect of small pre-strain on the fatigue strength of low carbon steel, JSME A, Vol.54, 1988, 1474 -1481.

[8]. H. Nisitani and Y. Murakami, Torsional fatigue and bending fatigue of electro polished low carbon steel specimens, JSME, Vol.13, 1970, p. 325-333.

[9]. S. Timoshenko and D. H. Young, Strength of Materials, Fifth Edition, D. Van Nostrand Company, Inc., Princeton, New Jersey.

[10]. William F. Smith, Foundations of Material Science and Engineering, Second Edition, McGraw-Hill Inc., Singapore.

[11]. Manual of the Shimadzu torsional fatigue testing machine, Shimadzu Seisakusho Ltd, Kyoto, Japan.

[12]. S. Timoshenko and D. H. Young, Strength of materials, fifth edition, Japanese translation. Charles E. Tuttle Company, Inc., Tokyo, 1972, p. 77.

CHAPTER 3

Tensile Strain Ratio and Surface Deformation

3.1 Introduction

The ability of a metal to undergo plastic deformation is probably its most outstanding characteristic in comparison with other materials. All shaping operations such as stamping, pressing, spinning, rolling, forging, drawing, and extruding involve plastic deformation of metals. Various machining operations such as milling, turning, sawing, and punching also involve plastic deformation. Plastic deformation may take place by slip, twinning or combination of slip and twinning [1, 2].

Fatigue crack initiation usually occurs at locations where discontinuities are present or where plastic strain accumulates preferentially in the form of slip bands [3]. For components free of significant internal defects, the surface is frequently the site for fatigue crack initiation. When the strain range reaches to the level required for plastic deformation, long-range dislocation motion will take place. Since some fraction of dislocations continuously emerge at the surface while the others pile-up against internal obstacles, slip band on the surface evolve in the form of intrusions and extrusions, subsequently acting as stress concentrators and facilitating the nucleation of fatigue cracks. The growth of fatigue cracks, especially those are small in relation to the microstructural features, interact extensively with the microstructure which can alter their path away from the direction normal to the loading and can significantly influence their growth kinetics.

If a single crystal of a metal is stressed in tension beyond its elastic limit, it is slightly elongated and a step appears on the surface indicating relative displacement of one part of the crystal with respect to the rest. Increasing the load will cause another step. Each successive elongation requires a higher stress and

results in the appearance of another step, which is actually the intersection of a slip plane with the surface of the crystal. Progressive increase of the load eventually causes the material to fracture.

Slip occurs in directions in which the atoms are most closely packed, since this requires the least amount of energy. Figure 3.1 shows that when the plastic deformation is due to slip, the atoms move a whole interatomic space (moving from one corner to another corner of the unit cell). This means that overall lattice structure remains the same. Slip is observed as thin lines under the microscopes and these lines can be removed by polishing, as shown in Fig.3.2.

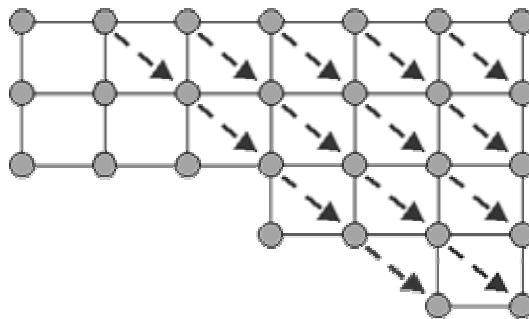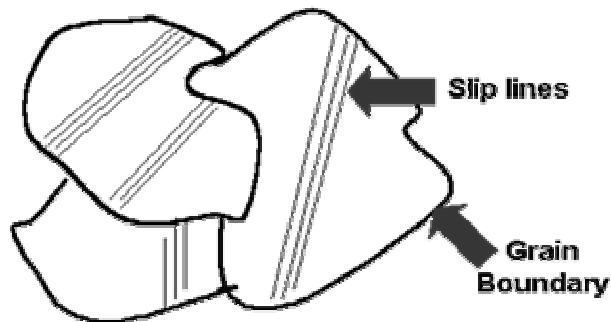Fig.3.1 The effect of slip on the lattice structure

Fig.3.2 Slip appears as thin lines under the microscope

Tensile test determines the strength of the material when subjected to a simple stretching operation. Typically, standard dimension test samples are pulled slowly at a uniform rate in a testing machine while the stress and strain are defined as [1, 2]:

$$\sigma = P / A \qquad (3.1)$$

$$\varepsilon_p = \left(l_p - l_0\right)/l_0 \tag{3.2}$$

where P is the applied force, A is the area of the cross section, σ is the engineering stress, ε_p is the engineering strain, l_p is the length after tensile test and l_0 is the original length of the tested specimen. For structural materials this behavior is of two types, linear elastic and plastic part. These behaviors are characterized by the properties that relate the applied stress to the response variable. The most common of these relations is between stress and strain, and the relevant properties are measured on the stress-strain curve. Figure 3.3 shows the stress-strain diagram of a ductile material where the linear portion of the graph indicates elastic deformation. The initial slope of the curve is called Modulus of Elasticity, also known as Young's Modulus, which indicates the stiffness of the material. It is related directly to the strength of the atomic bonds.

$$\text{Modulus of Elasticity (E)} = \sigma/\varepsilon \tag{3.3}$$

The maximum stress applied to the specimen (The highest point on the stress-strain diagram) is the tensile strength of the test material. This point in the engineering stress-strain curve indicates the beginning of necking. It is an important point, for it is part of the definition of the ultimate tensile strength, that is, the maximum load obtained by the engineering stress-strain curve divided by the original area. Ductility refers to the total elongation of the specimen due to
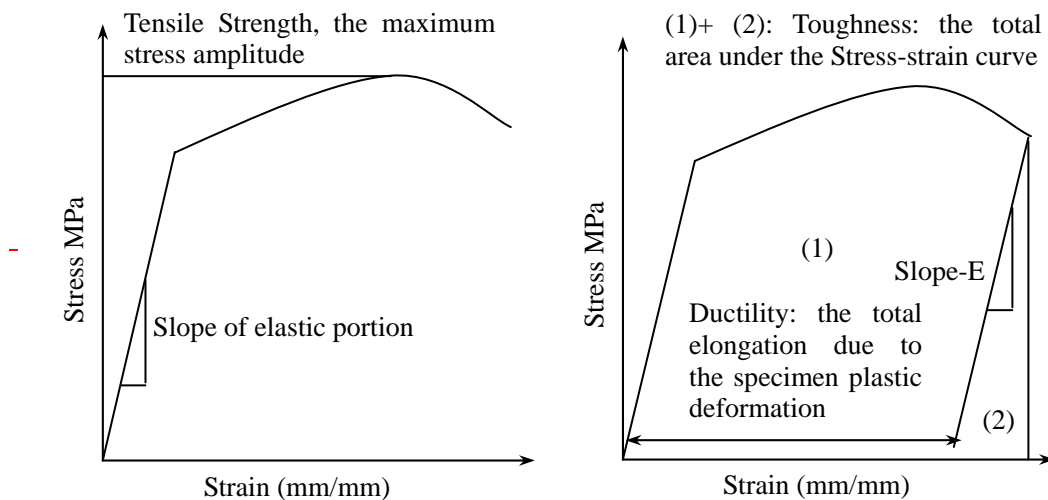

Fig.3.3 Parameters of mechanical properties in Stress-strain curves

plastic deformation, neglecting the elastic stretching, and toughness is the total area under the curve, which indicates the energy absorbed by the specimen in the process of breaking.

In this chapter, the relationship between tensile and compressive strain ratios and the surface deformation were investigated. It was concentrated on the initiation of slip lines in the surface and the translation phenomenon of slip lines to crack during the increasing of load in tension or compression test.

3.2 Experimental Results and Discussions

3.2.1 Mechanical Properties

The materials used in this test are four kinds of low and medium structural carbon steels, JIS S15C, S25C, S35C and S45C. The detail chemical compositions and heat treatment situations are the same as those listed in Chapter 2.

Specimens were annealed in vacuum at 600°C for 30 minutes and then electro-polished to the depth of more than 50μm in diameter to relieve the residual stress and remove the work hardened layer caused by mechanical machining. The tensile test was performed by a universal test machine (Shimadzu AG-IS 100) with a loading speed of 20mm/min. The microstructure of the specimen was observed by successively taken replica samples during the tensile test by pause some times.

Tensile test were applied on all of the test materials, the failure surface obtained through the test resembled a "cup and cone" fracture. Rupture occurs along a cone-shaped surface which forms an angle of approximately 45 ° with the original surface of the specimen. Table 3.1 lists the mechanical properties of the test materials.

Table 3.1 Mechanical properties of tensile test

	σ_Y, MPa	σ_B, MPa	EL.,%	ψ, %
S15C	288.4	445.9	27.9%	69.6
S25C	297.7	456.6	27.0%	58.5
S35C	299.3	550.3	21.6%	47.7
S45C	347.7	615.8	21.8%	45.7

σ_Y, Yield strength, σ_B, tensile strength, ψ, Reduction of area.

3.2.2 Stress-strain Curves

Figure 3.4 shows the stress-strain curves of the test materials. The necking strain ratios for S35C and S45C were almost the same and they were lower than that of S15C and S25C.

The yield strength and tensile strength increased with the increasing of carbon content, and the strength could be divided into two groups though the materials were heat treated to get same grain size. The fatigue strength of S35C and S45C were much higher than that of the other two kinds of materials. However the yield strength of S35C was near to that of S15C and S25C.
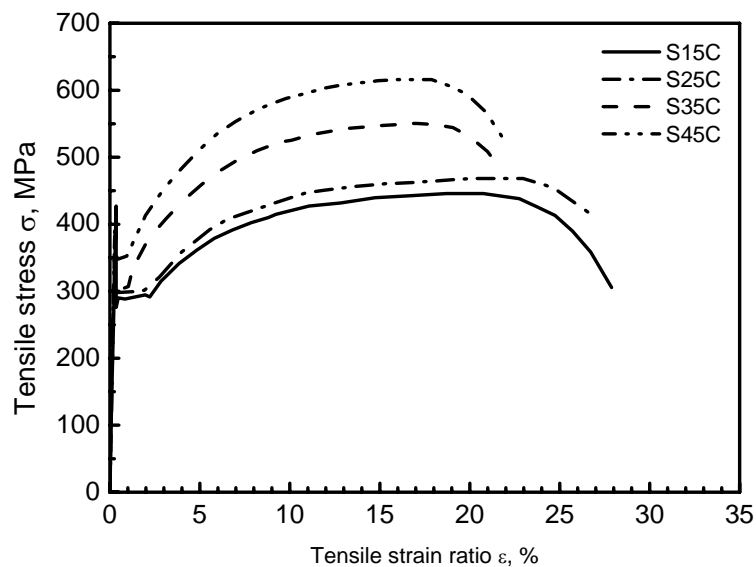

Fig. 3.4 Stress - strain curves of tensile specimens

3.2.3 Microstructure Behaviors Observation

The specimen surface was observed during the tensile by taken replica samples. Figure 3.5 to 3.12 show the microstructure behaviors of S15C, S25C, S35C and S45C by replicas taken from the same position on the surface of specimen.

There was no obvious change in microstructure in the elastic stage of the tensile test, and no remarkable slip line was observed during the elastic tensile stage and the yielding stage of the tensile test. With the increasing of tensile load, some slips initiated in ferrite grains or near the boundaries of the ferrite grains. The length of slip bands did not change at the beginning, only changed in the width, expressed as the color became deep at the slip band. When the slip bands concentrated for some while, they would be translated to short cracks in the
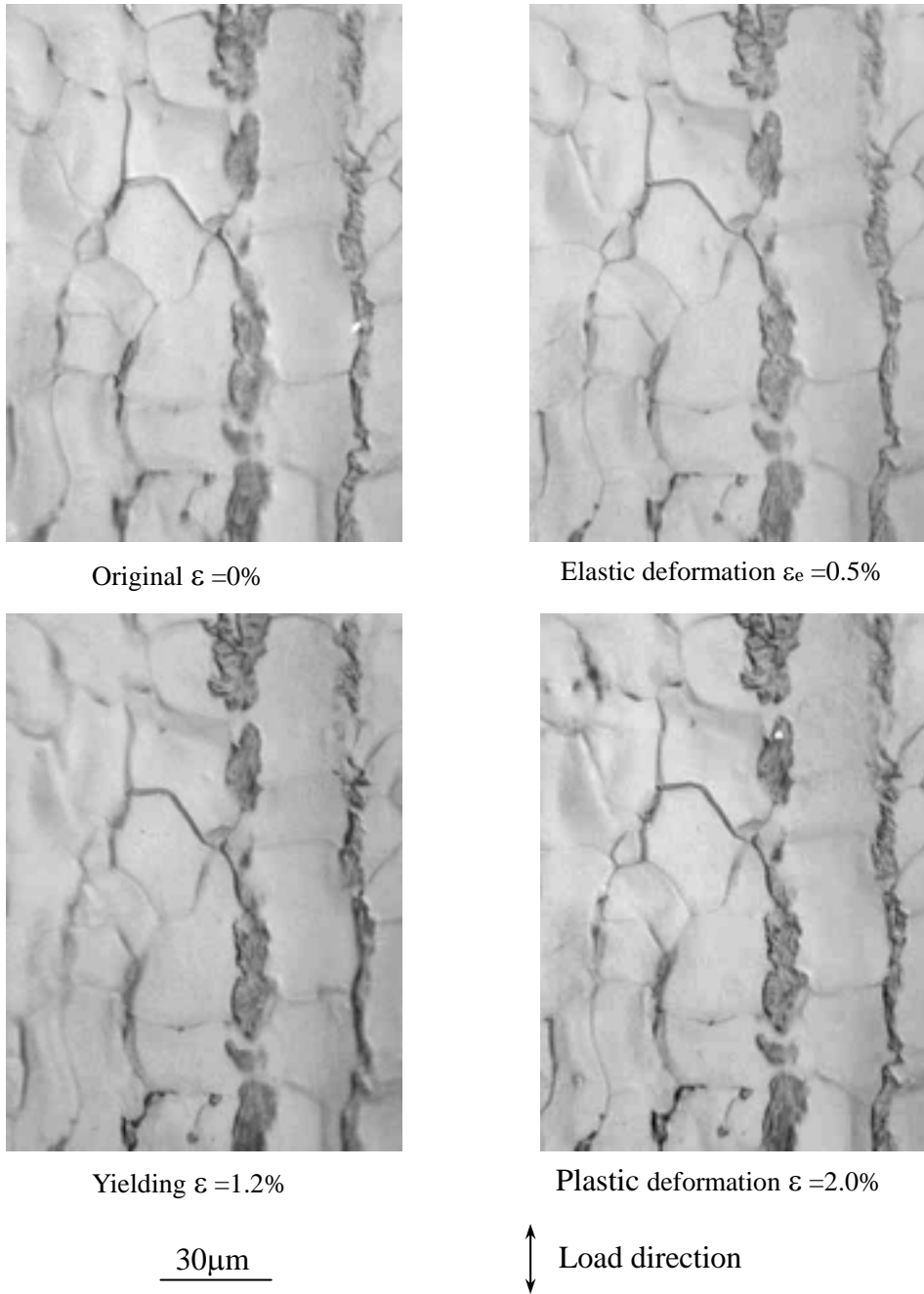
37

Original ε =0%

Elastic deformation ε_e =0.5%

Yielding ε =1.2%

Plastic deformation ε =2.0%

30μm   Load direction

Fig. 3.5 Microstructure behaviors in tensile test (S15C)

ε =5%

ε =8.1%

Necking ε =20.6%

ε =25.7%

30μm   Load direction
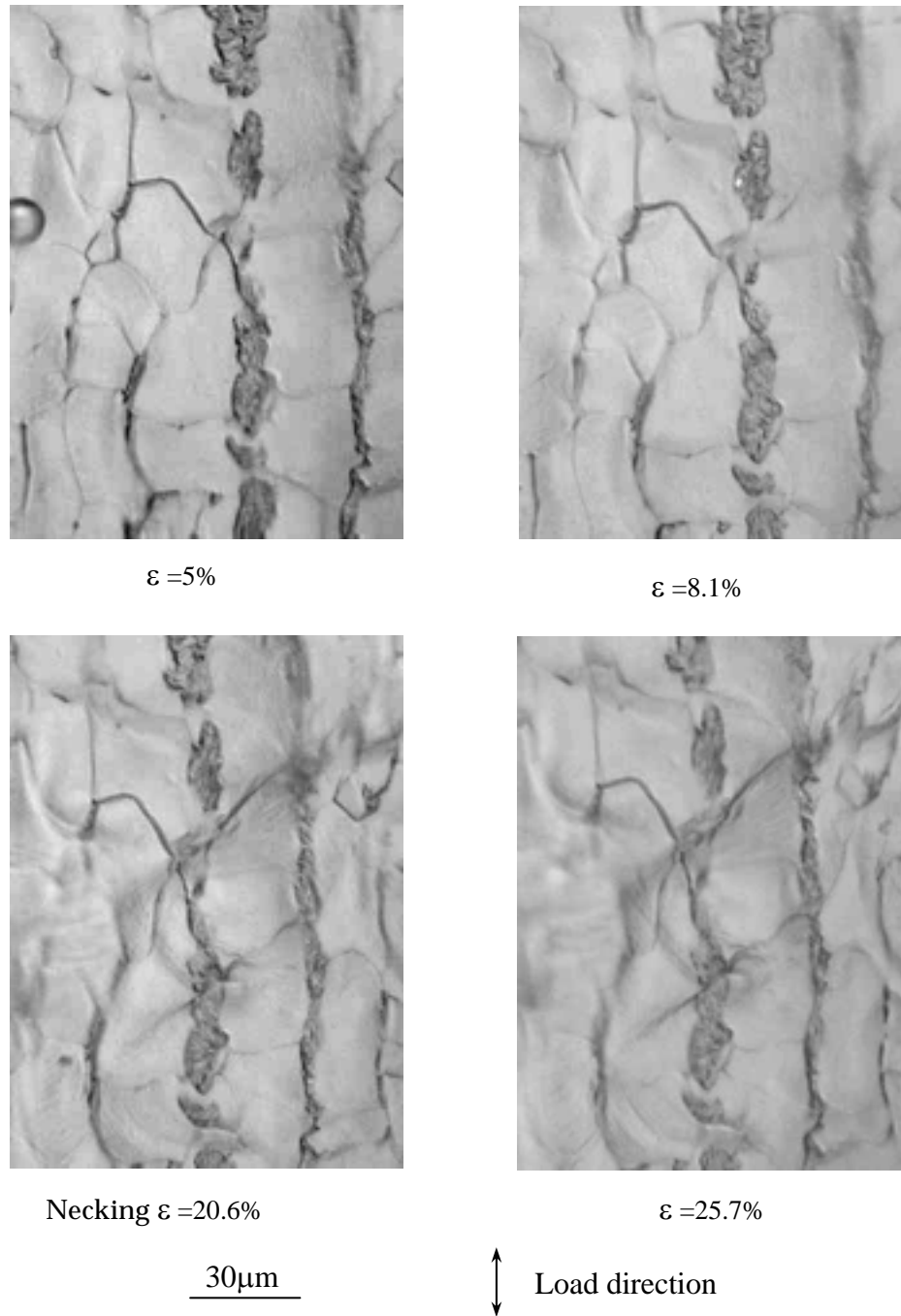
Fig. 3.6 Microstructure behaviors in tensile test
(S15C, plastic deformation stage)

Original ε =0%   Elastic deformation ε$_e$ =0.6%

Yielding ε =1.1%   Plastic deformation ε =1.5%

30μm   Load direction
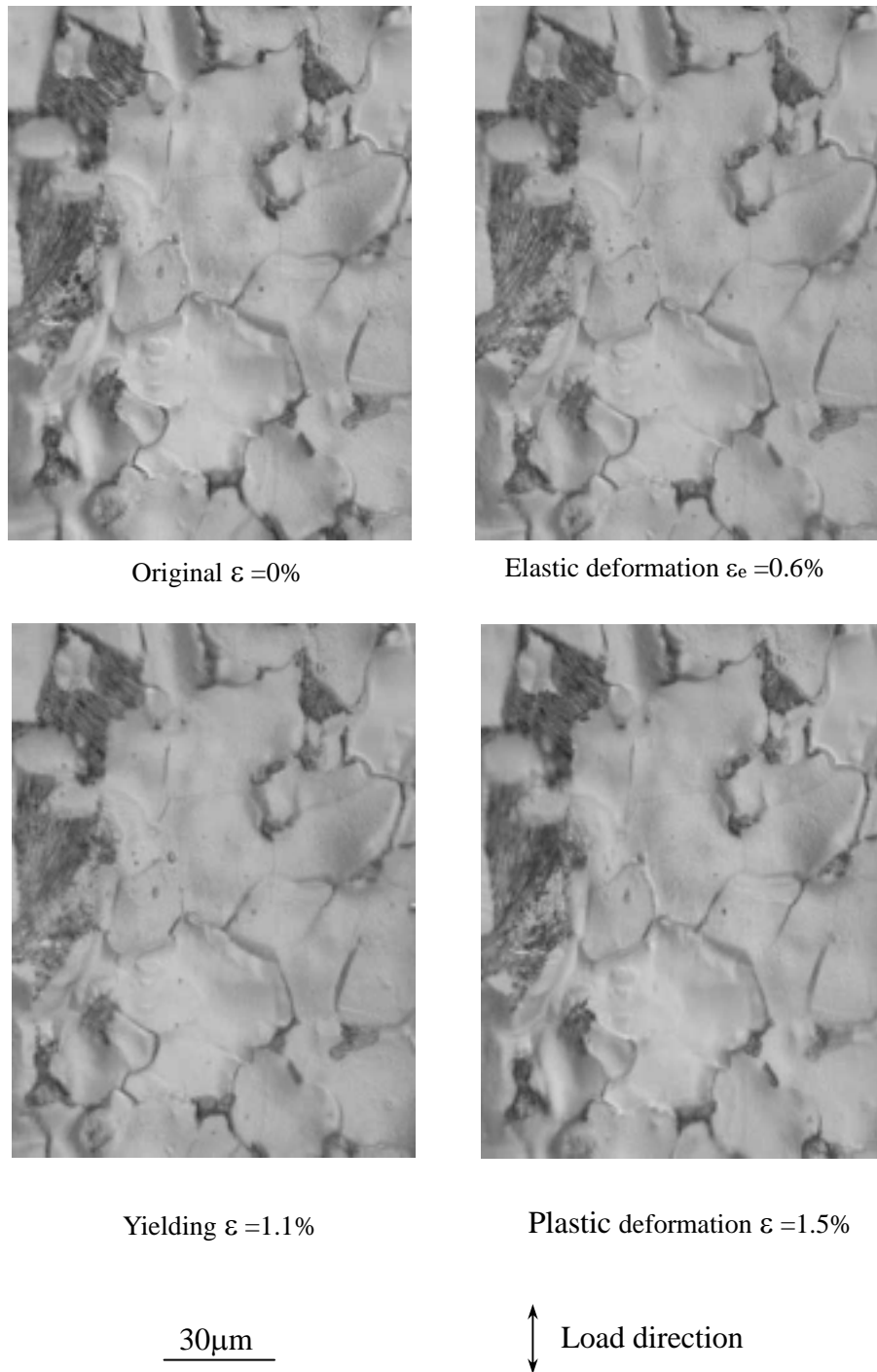
Fig. 3.7 Microstructure behaviors in tensile test (S25C)

ε =5%   ε =8%

ε =15%   ε =22%

30μm   ↕ Load direction
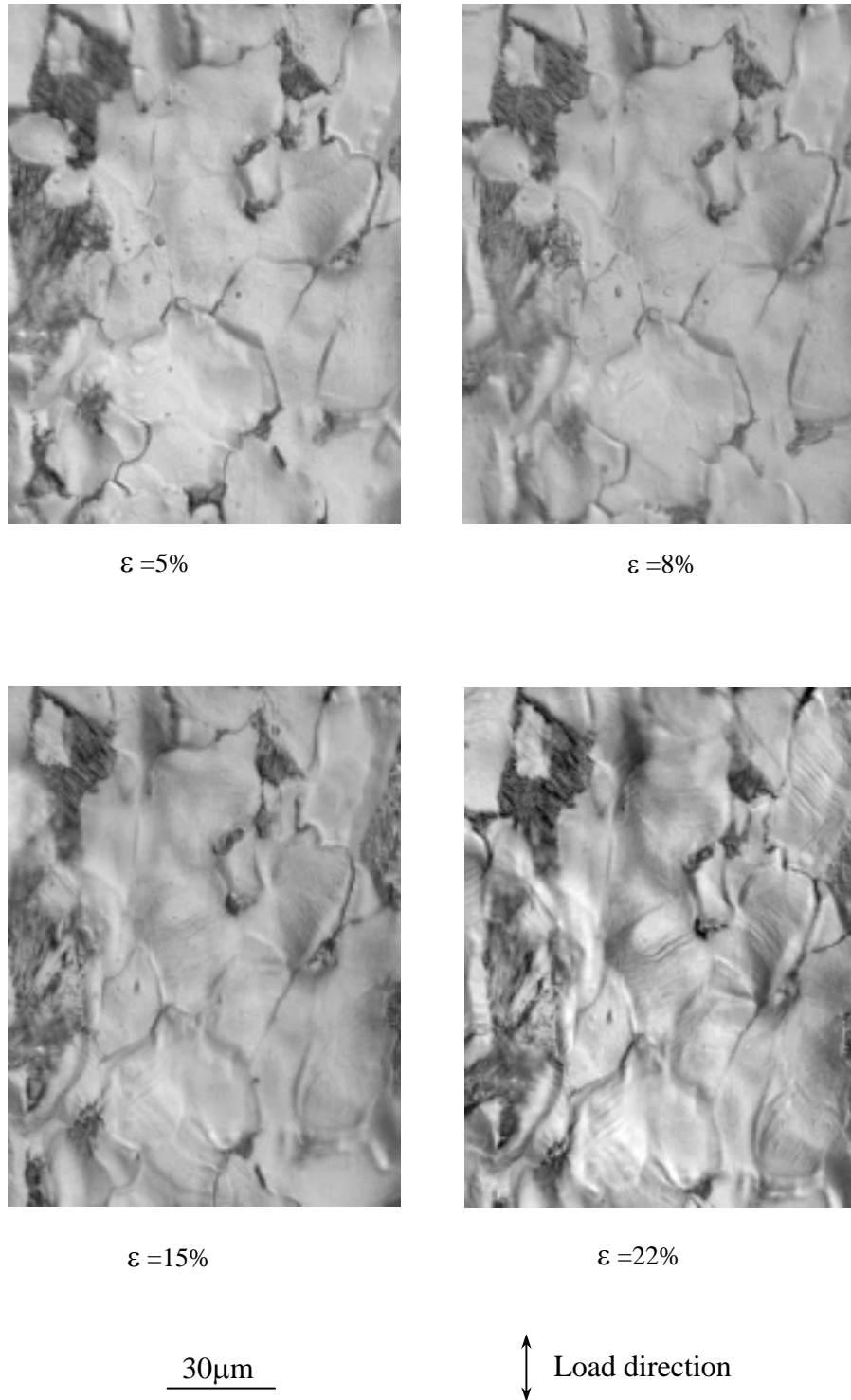
Fig. 3.8 Microstructure behaviors in tensile test
(S25C, plastic deformation stage)

Original ε =0%

Elastic deformation ε$_e$ =0.3%

Yielding ε =0.8%

Plastic deformation ε =2.0%

30μm

Load direction

Fig.3.9 Microstructure behaviors in tensile test (S35C)

ε =5.0%   ε =8.0%

ε =14.8%   ε =18.9%

30μm   Load direction
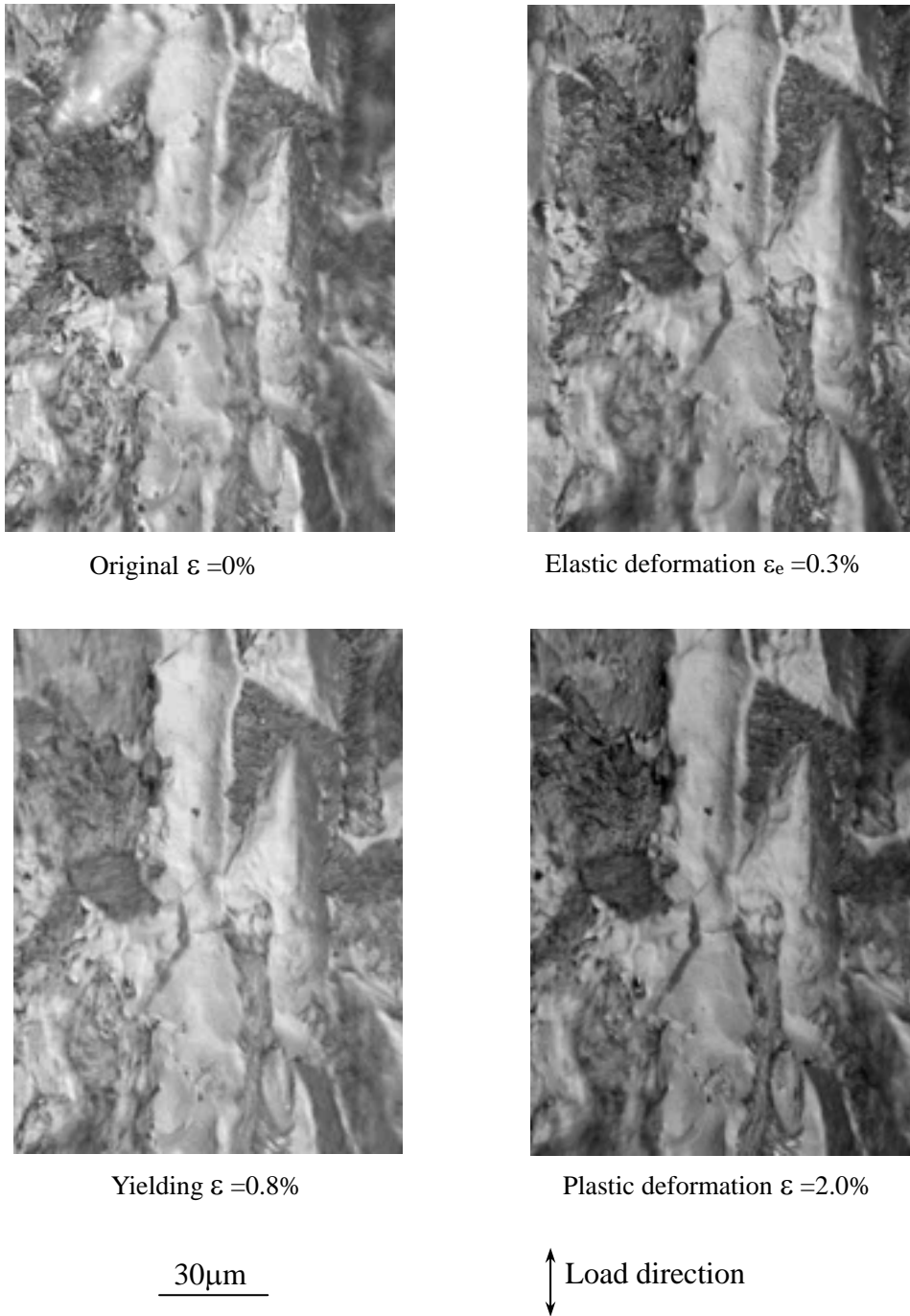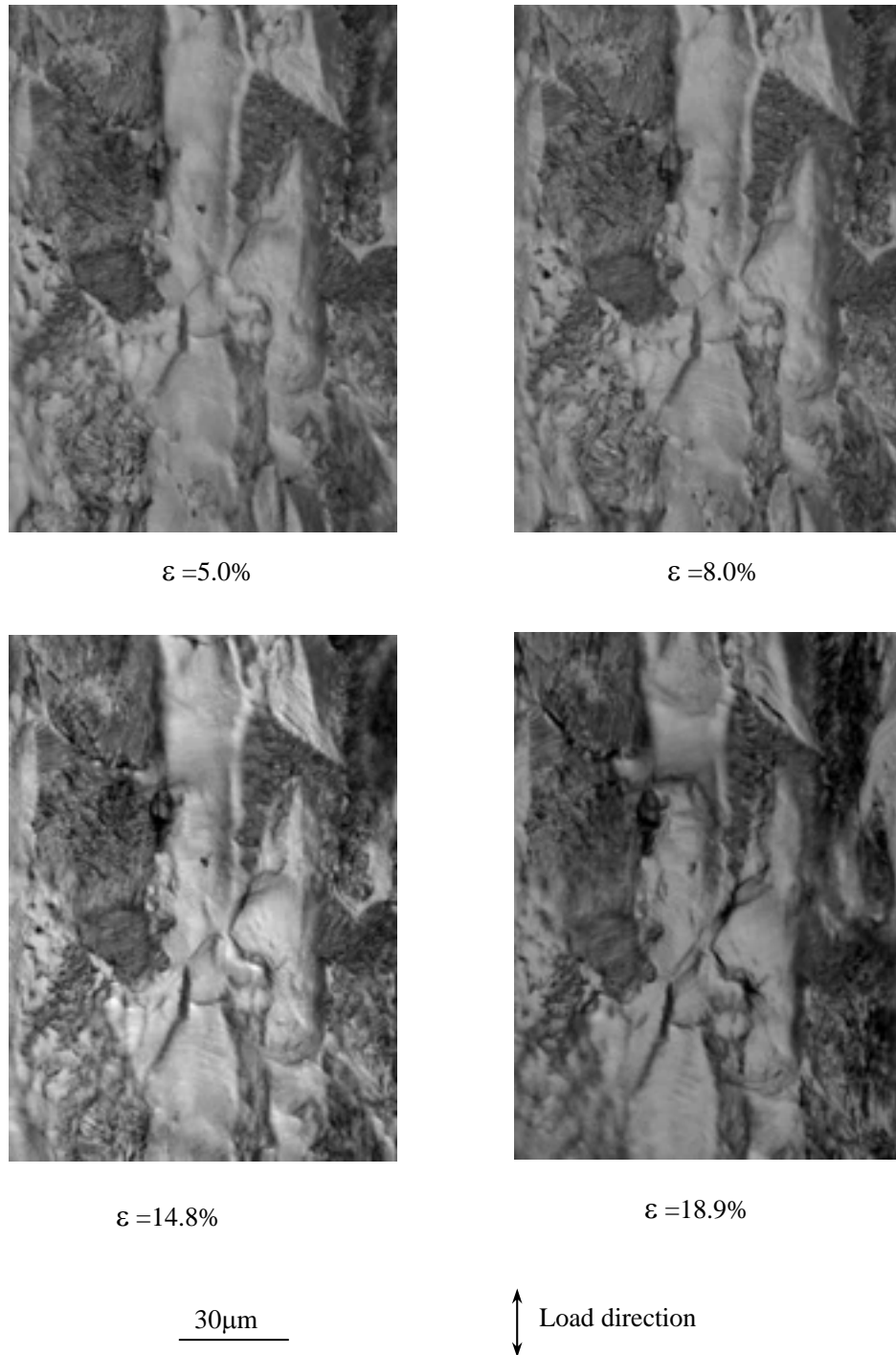
Fig.3.10 Microstructure behaviors in tensile test
(S35C, from slip lines to crack)

Original ε=0

Elastic deformation ε_e =0.1%

Yielding ε=0.5%

Plastic deformation ε=1.9%

30μm

Load direction

Fig.3.11 Microstructure behaviors in tensile test (S45C)

ε=5.0%   ε=8.0%

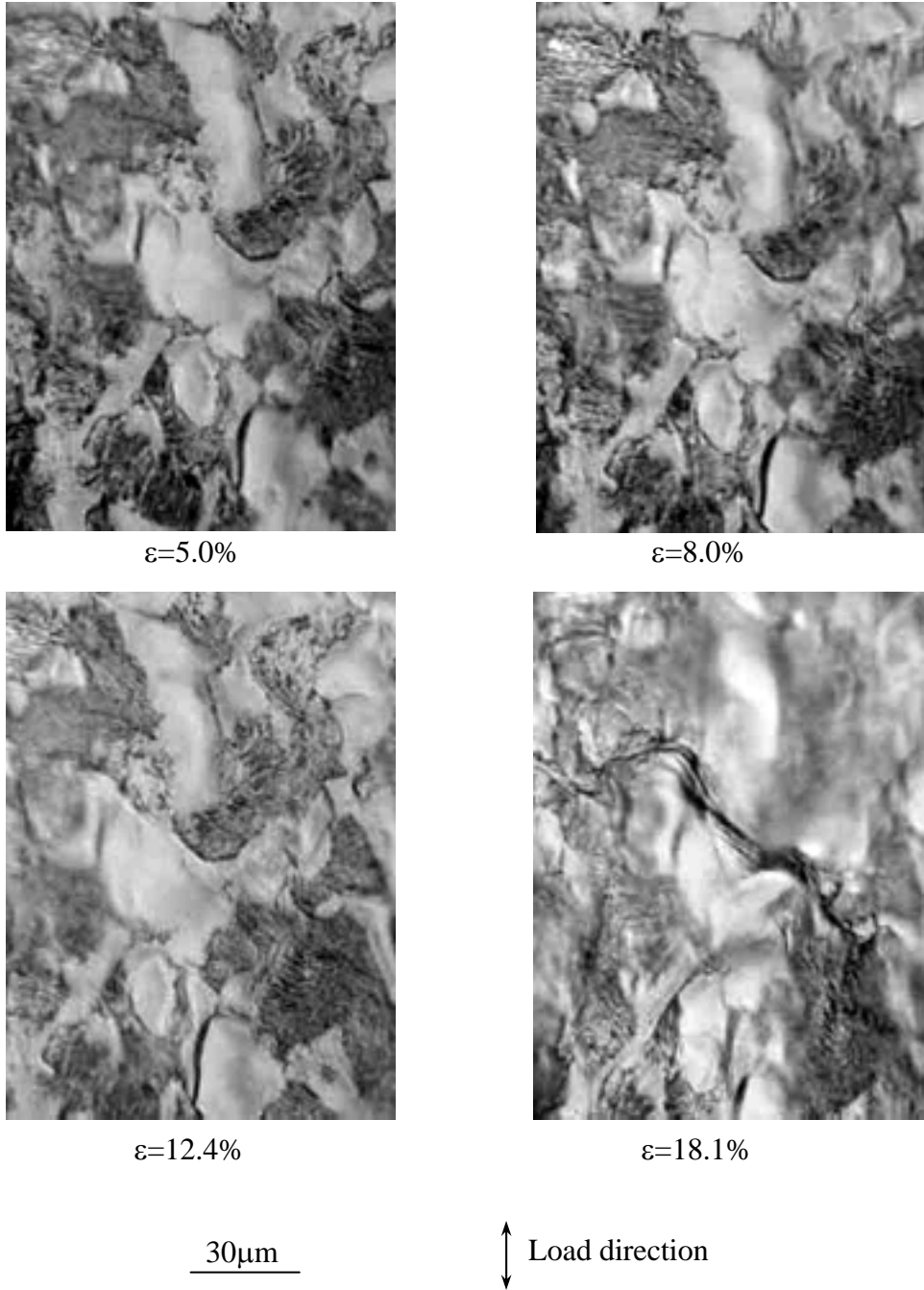ε=12.4%   ε=18.1%

30μm   ↕ Load direction
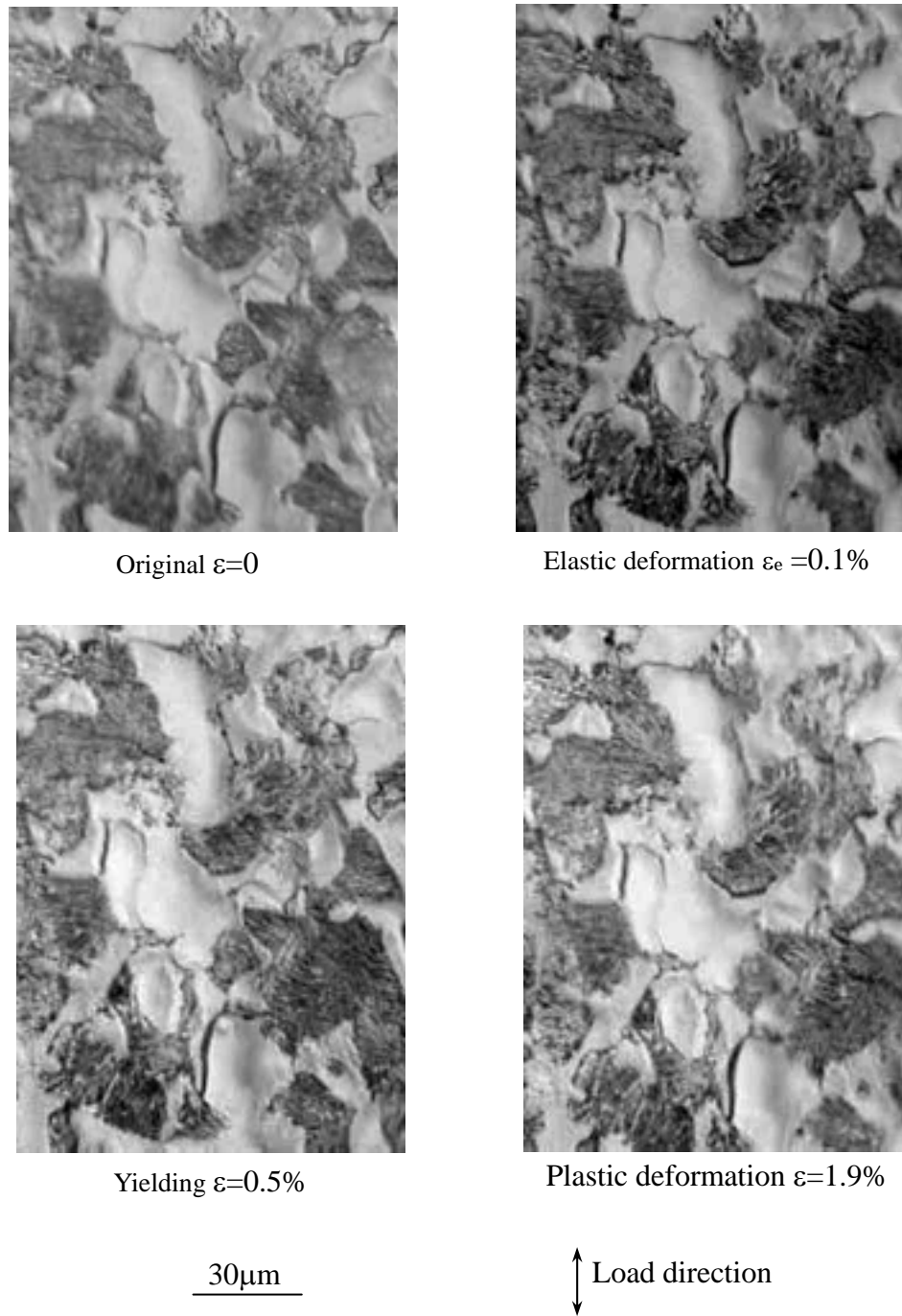
Fig.3.12 Microstructure behaviors in tensile test
(S45C, from slip lines to crack)

surface of specimens. The slip bands translated much faster for S45C than that of the other three kinds of materials. When tensile stress was applied to specimens and tensile strain ratio becomes to 5%, there were only slip lines in the surface of S15C, S25C and S35C, however some of the slip lines have translated to short cracks for S45C. Moreover, the short crack for S35C was about 45° to the axial direction, while the direction of the short crack in S45C had changed to the direction vertical to the axis before the fracture.

Deformation or strain is temporary when the material is stressed below its elastic limit. When the stress is beyond the elastic limit of the material, plastic or permanent deformation takes place, and it will not return to its original shape by the application of force alone. The yield strength of a crystalline material can be viewed as the stress required initiating dislocation motion. With the increasing of tensile stress load, the deformations changed from dislocations to slip lines, then finally translated to cracks and caused the failure of specimen. With the change of carbon content, the translate strain ratio because lower, because pearlite content increased with the increasing of carbon content, and the ferrite content decreased at the same time. When tensile stress was applied on the specimen, tensile lines were firstly happen in the ferrite grains or near the boundaries. For high ferrite content material, the slips would disperse widely, while ferrite content is much lower, and the slips would concentrate more easily than in the low carbon content materials. Consequently, the slip lines would be more easily translated to short cracks in high carbon content materials that in the lower ones.

3.3 Conclusions

This chapter was focused on investigating the relationship between tensile strain and the surface deformation of three kinds of structural carbon steels with same grain size.

Tensile strength and yield strength increase with the increasing of carbon content. Necking strain ratio for S15C and S25C are higher than that of S35C and S45C. There is no remarkable slip line in elastic deformations stage and the yielding stage, and all of the slips are observed by the optical microscope in the plastic deformation stage. The translation strain ratio gets lower for S15C, S25C, S35C and S45C. For S35C, the slip lines may translate to short cracks, but for S45C, the slip lines have translated to short cracks, and even the short crack has changed to the direction vertical to the axial direction before the fracture.

Reference

[1]. S. Timoshenko and D. H. Young, Strength of Materials, Fifth Edition, D. Van Nostrand Company, Inc., Princeton, New Jersey,1968.

[2]. William F. Smith, Foundations of Material Science and Engineering, Second Edition, McGraw-Hill Inc., Singapore, 1993.

[3]. K. Kubota, Master Degree Thesis, Saga University, Japan, 1994.

[4]. D. Miao, Doctor Degree Thesis, Saga University, Japan, 2001.

[5]. W. Sun, Doctor Degree Thesis, Saga University, Japan, 2004.

[6]. J. A. Collins, Failure of materials in mechanical design analysis prediction prevention, A wiley-interscience publication John Wiley & Sons Inc., 1981.

CHAPTER 4

Effect of Tensile Pre-strain on the Torsional Fatigue Properties

4.1 Introduction

It is reported that more than 80-90% of mechanical component failures are caused by fatigue failure [1]. Bending fatigue and torsional one are the most two normal fatigue styles in engineering. Though the fatigue properties have been studied for more than 150 years since the first fatigue study by Wöhler experimentally [2], most of the studies were focused on the rotating and bending fatigue or the tensile and compressive fatigue styles. Researches were not only focused on metal materials, including structural carbon steels [3-6], Aluminum alloy [7-9], Titanium alloy [10-12], etc., but also concentrated on the fatigue properties of the non-metallic materials and composite materials, such as Suresh (1990) and Robbern (1996) on ceramics, Hertzberg and Manson (1980), Hertzberg (1985) on polyatomic materials [13-16]. However, it is difficult to find out reports and detail researches on the torsional fatigue properties.

In the past 50 years, there have been extensive researches on the rotating and bending fatigue properties on the structural carbon steels, many of them were focused on the studies influence of pre-strain [17-20]. Based on these study results, the influence of pre-strain on the bending fatigue properties can be summarized as following:

At room temperature, the fatigue strength will be improved when carbon steels are subjected to tensile pre-strain because of the work hardening, and the improvement will increase with the increasing of tensile pre-strain ratio. However, when tensile pre-strain ratio is too large or very small, the fatigue strength will decrease. Pre-strain does not affect the growth rate of long fatigue cracks, while it influences much on the crack initiation and the micro crack propagation. Small pre-strain can cause the acceleration of slip initiation and crack initiation, and

increase the growth rate of a small surface crack, decrease the fatigue limit and fatigue life.

It is very difficult to find the systematic studies on the torsional fatigue properties until now, most the torsional properties were almost calculated from the bending fatigue properties by certain relationship. The objects of this chapter are to: (1) evaluate the effect of the tensile pre-strain on the torsional fatigue strength, (2) investigated the tensile pre-strain influence on the torsional fatigue crack initiation crack propagation behaviors; and (3) study the effect of tensile pre-strain on the non-propagating torsional fatigue crack behaviors.

4.2 Fatigue Strength

4.2.1 Experimental Results

The values listed in Table 4.1 are the fatigue limit values of test materials with different pre-strain ratios, and Figures 4.1, 4.2, 4.3 and 4.4 show the S-N

Table 4.1 Fatigue limits of specimens with different pre-strain ratio, MPa

	$\varepsilon_p=0\%$	$\varepsilon_p=2\%$	$\varepsilon_p=5\%$	$\varepsilon_p=8\%$
S15C	135	140	160	175
S25C	140	145	160	175
S35C	145	150	165	180
S45C	160	160	185	200
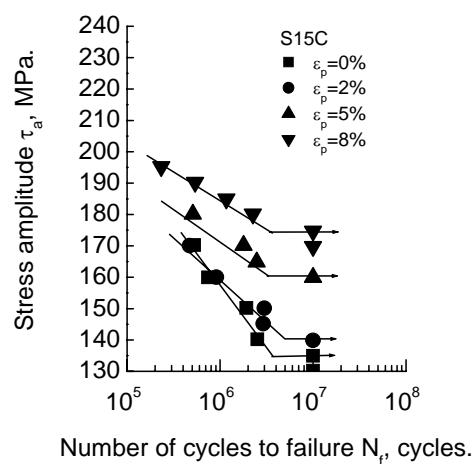
Fig.4.1 S-N curves of S15C with different pre-strain ratios
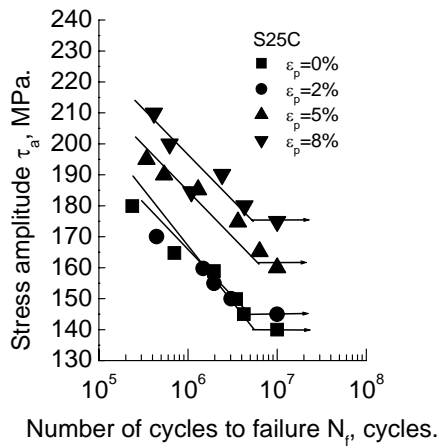
Fig.4.2 S-N curves of S25C with different pre-strain ratios
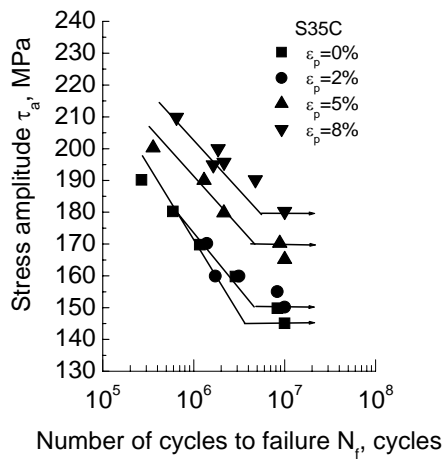

Fig.4.3 S-N curves of S35C with different pre-strain ratios
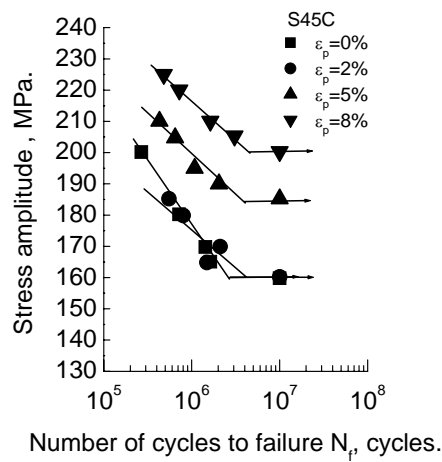

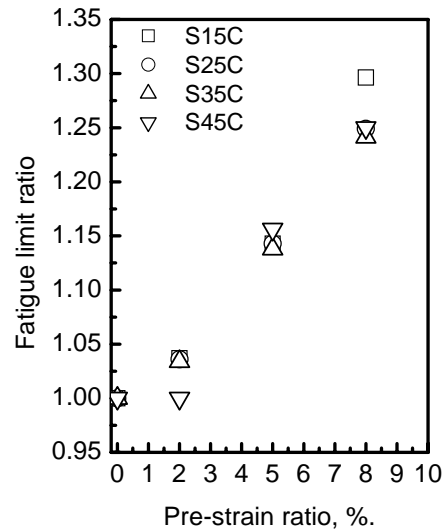Fig.4.4 S-N curves of S45C with different pre-strain ratios

Fig.4.5 Relationship between fatigue limit ratio and pre-strain ratio

curves of the different test materials with different pre-strain ratios (0%, 2%, 5% and 8%), respectively. The table and the figures show that torsional fatigue limits are improved after tensile pre-strain for all of the four kinds of test materials. For 2% tensile pre-strained specimens, the torsional fatigue limit is same as that of the original one for S45C, and a little higher than that of the non-pre-strained ones for the other three materials. For the same material, the S-N curve's slope of non-pre-strained specimens is larger than those of the pre-strained specimens, and it crosses with the lines of pre-strained specimens, i.e., the fatigue life is prolonged after tensile pre-strain.

Figure 4.5 is the relationship between pre-strain ratios and fatigue limit ratios based on the fatigue limit of non-pre-strained specimens. The fatigue limits increased a little for the lower tensile pre-strain ratio, and then increased much more with further pre-strains of 5% and 8% in this study.

4.2.2 Discussions

The above phenomena could be explained by the following aspects: the system of slips generated by tensile pre-strain and the torsional fatigue test; the work hardening effect and the change of tensile slip lines density.
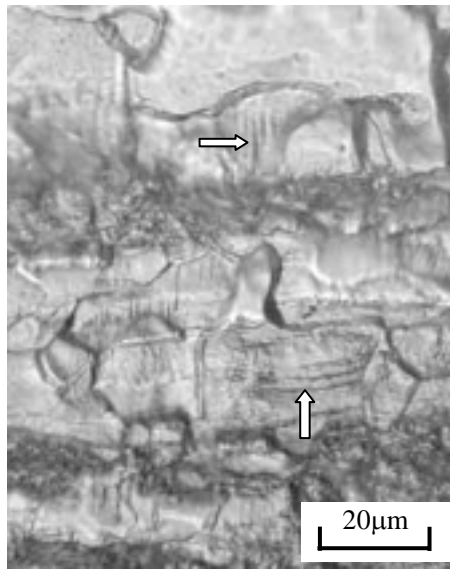
Systems of Tensile and Torsional Slips

As it is known that crack initiation is a local phenomenon and the plastic deformations are not uniform in one crystal grain. The slip system in polycrystal

51
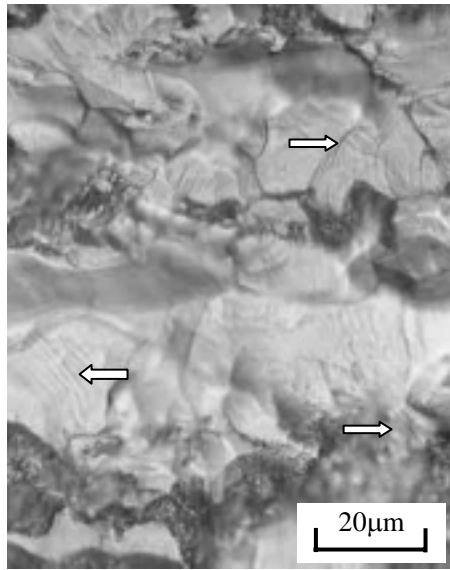
S35C, ε_p=8%, N=0

Tensile and axial direction $\Longleftrightarrow$ $\Longrightarrow$ Slip lines

Fig.4.6 Tensile slip lines

S35C, ε_p=8%, τ_a=190MPa, N=1.05×10^6cycles

N_f=1.64×10^6cycles

Tensile and axial direction $\Longleftrightarrow$ $\Longrightarrow$ Slip lines

Fig.4.7 Torsional fatigue slip lines

material differs at each grain, and there occurs a nonconformity compensation of deformation. Tensile slip lines caused by pre-strain at or near the grain boundaries, are about 45° to the axial direction, as shown in Fig.4.6, and the direction of torsional fatigue slip lines is along or vertical to the axial direction, as shown in Fig.4.7. The specimen in torsional fatigue test is suffered with shearing stress, and its direction is in agreement with that of torsional slip lines. Comparing Figs. 4.6and 4.7, it is clear that the two kinds of slip lines are different in direction. It is considered to be more difficult with comparing to the above case that the torsional fatigue crack would initiate in the grains with tensile slip lines. In fact, tensile slip lines are not observed in the area where the grains are torsional fatigue slipped, as shown in Fig 4.7. Therefore, tensile slip lines may be one of the main reasons why the torsional fatigue limits increase after tensile pre-strain.

Relation between the Parameters

Figures 4.8, 4.9 and 4.10 show the relationship between the torsional fatigue limit τ_w and the tensile pre-strain ratio ε_p, surface hardness HV, and the pre-strain tensile stress σ_a.

According to Fig. 4.8, the fatigue limit increases with the increasing of tensile pre-strain ratio. During the tensile pre-straining, the surface of specimens
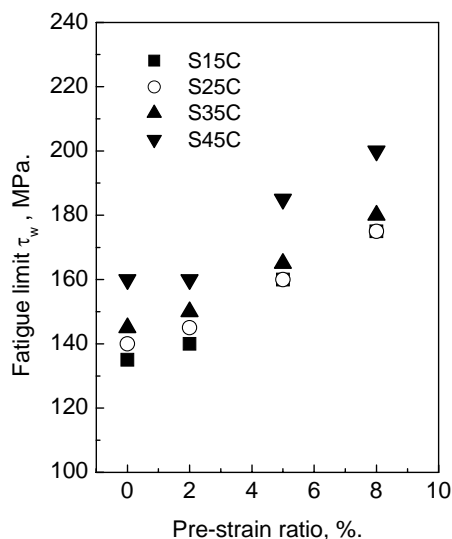

Fig.4.8 Relationship between fatigue limit τ_w and the pre-strain ratio ε_p

Table 4.2 Average surface hardness of ferrite grains, HV (0.49N)

	$\varepsilon_p = 0\%$	$\varepsilon_p = 2\%$	$\varepsilon_p = 5\%$	$\varepsilon_p = 8\%$
S15C	134	147	158	172
S25C	152	163	171	185
S35C	169	178	189	204
S45C	189	190	210	220

is work hardened and the hardness increases with the increasing of pre-strain ratio, as shown in Table 4.2.

Figure 4.9 shows the relationship between fatigue limits and the surface hardness of all the test materials. The solid lines are fitted by the actual fatigue limits from the fatigue test and the values of dot dashed lines are calculated by the following experiential equation [23, 24]:

$$\tau_w = C \cdot \sigma_w, \quad \sigma_w = 1.6Hv \tag{4.1}$$

Where, σ_w is the bending fatigue limit, τ_w is the torsional fatigue limit, Hv is the surface hardness of specimens. For the conventional structural carbon steels, C
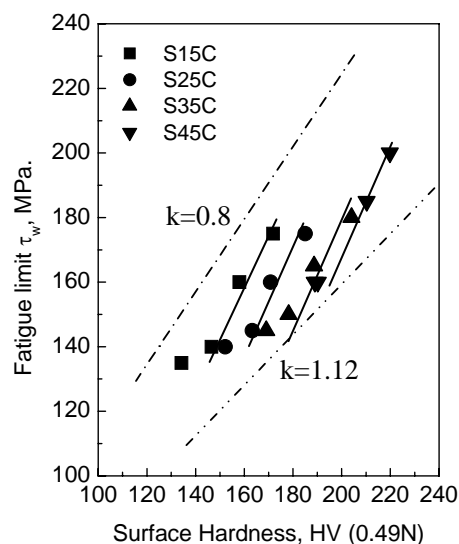
Fig.4.9 Relationship between torsional fatigue limit τ_w and the surface hardness HV
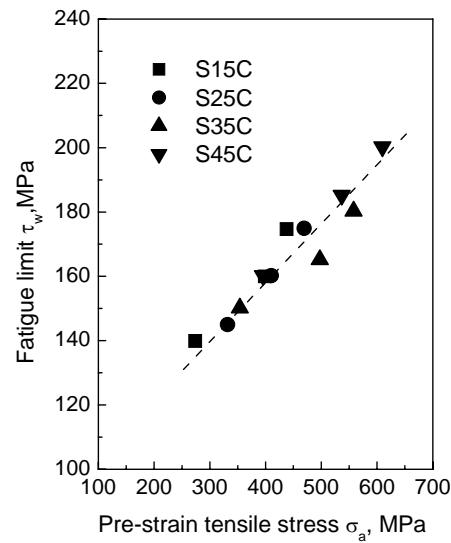
Fig.4.10 Relationship between fatigue limit τ_w and
pre-strain tensile stress σ_a

is in the range of 0.5-0.7 [24], therefore,

$$\tau_w = k \cdot Hv = (0.8 \sim 1.12)Hv \qquad (4.2)$$

According to Fig. 4.9, the torsional fatigue limits are all included in the range of values calculated by equation (4.2). The relation between the actual fatigue limits of pre-strained specimens and the surface hardness can be expressed as:

$$\tau_w = k \cdot Hv - b = 1.5Hv - b \qquad (4.3)$$

Here, b is a constant related to the tensile pre-strained material, which becomes larger with the increasing of carbon content of the common structural carbon steels. In other words, the fatigue limit τ_w of pre-strained specimens still increases linearly with the surface hardness Hv. However, the proportional parameter k after tensile pre-strain is larger than the experiential value. This might be one aspect that results in increasing of the fatigue limit after tensile pre-strain.

Figure 4.10 shows the relationship between torsional fatigue limits and the pre-strain tensile stress. Fatigue limits increase almost linearly with the increasing of pre-strain tensile stress. Since the grain size of test materials are almost the same, the density of slip lines should increase with the increasing of tensile stress, and the density of slip lines increases with the increasing of tensile pre-strain ratio, as shown in Fig.4.11.
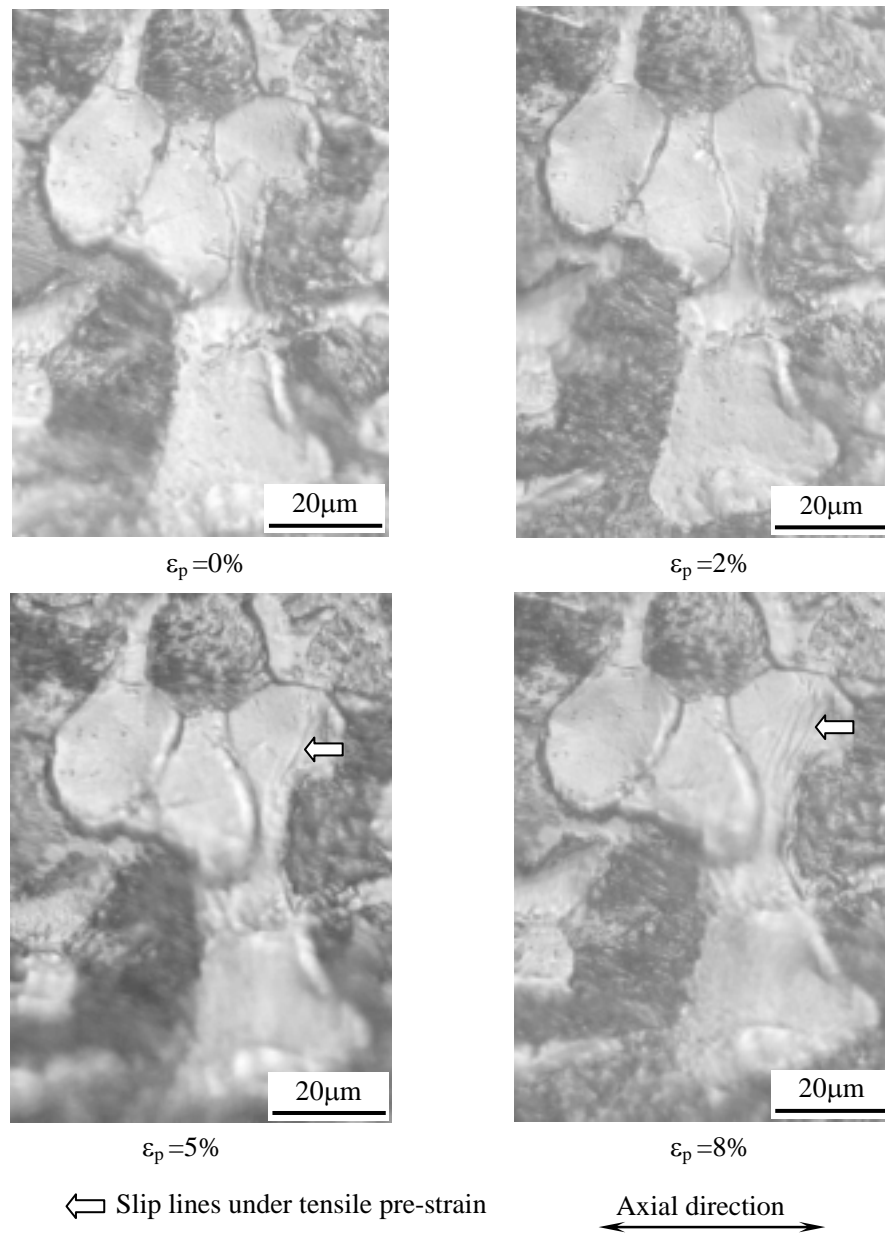
$\varepsilon_p = 0\%$ $\varepsilon_p = 2\%$

$\varepsilon_p = 5\%$ $\varepsilon_p = 8\%$

⇦ Slip lines under tensile pre-strain   Axial direction

Fig.4.11 Microstructure behaviors of tensile slip lines

4.3 Crack initiation and Propagation Behaviors

Fatigue crack initiation usually accounts for a significant fraction of the lives of engineering components such as helicopter rotors subjected to cyclic loading. A detailed understanding of both fatigue crack initiation and growth is essential for predicting remaining life, for improving the total fatigue life and for reliably

detecting cracks in order to take corrective actions to avoid catastrophic failures in critical components.

4.3.1 Crack Initiation

The torsional fatigue crack initiation and propagation behaviors were observed with replica samples through a microscope. Fig.4.12 shows some examples of crack initiation points. According to the microstructure observation, most of the

| N=0 | N=1.5×10^{5}cycles |

(a) S15C, ε_p=0%, τ_a=145MPa, N_f =1.29×10^{6}cycles

| N=0 | N=3.5×10^{5}cycles |

(b) S25C, ε_p=2%, τ_a=155MPa, N_f =1.96×10^{6}cycles

| N=0 | N=1.0×10^{5}cycles |

(c) S35C, ε_p=5%, τ_a=175MPa, N_f =2.98×10^6 cycles

| N=0 | N=1.0×10^{5}cycles |

(d) S45C, ε_p=8%, τ_a=210MPa, N_f =6.88×10^5 cycles

Axial direction ←——→   ——→ Arrow mark: crack initiation point
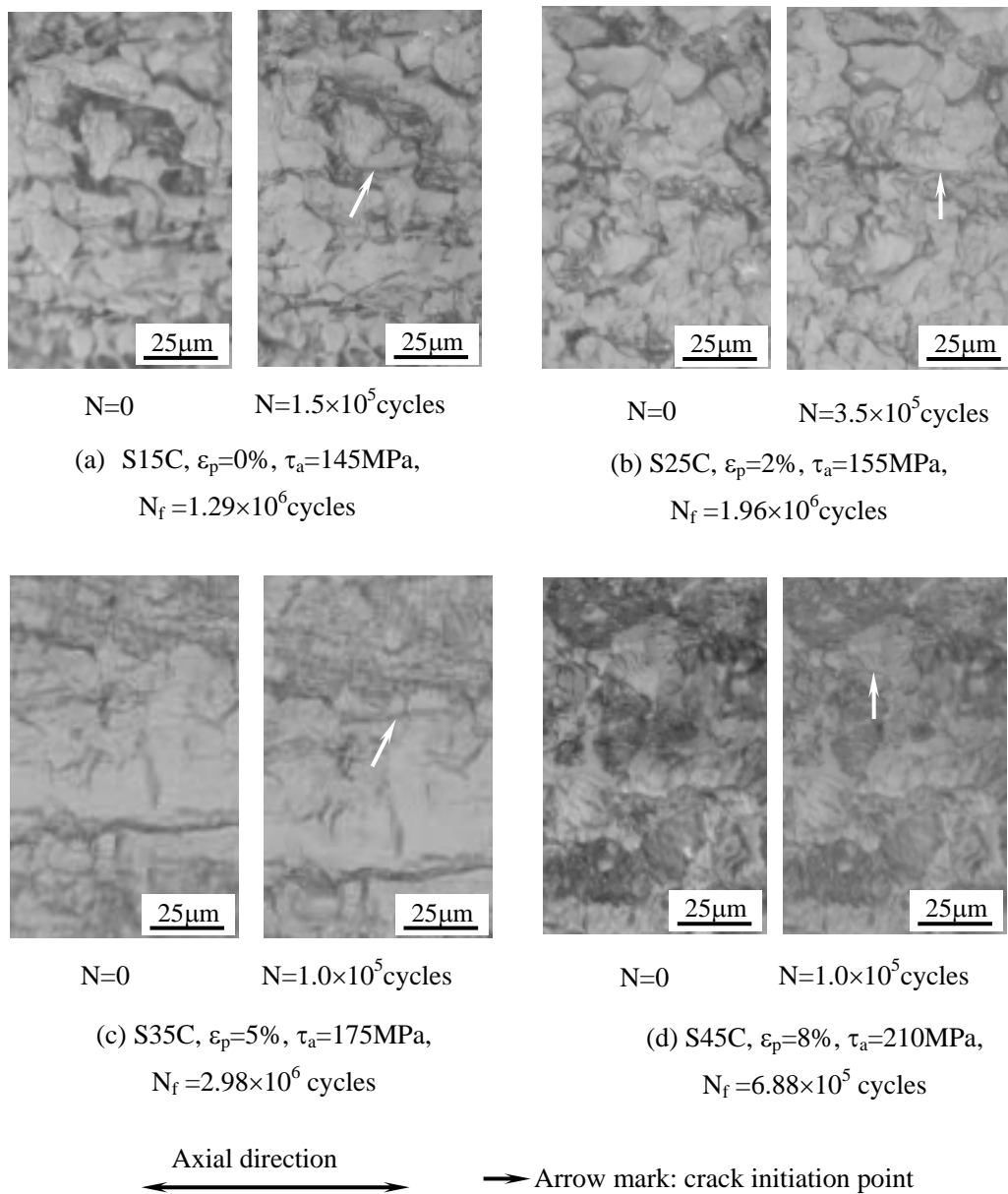
Fig.4.12 Microstructure of torsional fatigue crack initiation points

torsional fatigue cracks initiate at the weak part in the ferrite grains, where is slipped easily during the torsional fatigue test, and there is no obvious relation between the initiation point and the tensile pre-strain ratio.

This is due to the local phenomenon of tensile pre-strain. Some of the weak ferrite grains are slipped and some are not. When torsional fatigue test is applied on the specimens, the shearing stress makes the crack to initiate more easily in the weak ferrite grains in which there is no tensile slip line. The specimen is suffered with shearing stress in torsional fatigue test, the crack would initiate from the weak part, the ferrite grains where there is no tensile slip lines. Therefore, tensile pre-strain almost does not affect the initiation point of torsional fatigue crack.

4.3.2 Microstructure Behaviors of Crack Propagation

Figures 4.13, 4.14, 4.15 and 4.16 are the microstructure behaviors of the torsional fatigue crack propagation of the same materials with different pre-strain   ratios. It is shown in these figures that after the initiation, the crack maintains for some time and then propagates by Mode II style in the shearing stress direction. Based on the observation results, it was clear that most of the cracks stop in the axial direction and branch to the direction of Mode I style driven by the normal stress. This phenomenon could be attributed to the stress status of specimens in the torsional fatigue test, as shown in Fig.4.17. At the early stage, the torsioanl stress played the main part leading the grains to be torsional slipped, fatigue crack initiation and propagation. With the increasing of fatigue crack, when the length elongated to curtain value, it would be easier for cracks to propagate in the direction of the normal stress than in that of the torsional one. Consequently, the propagation in the axial direction would be stopped and branched to the direction about 45° to the axial direction.

When fatigue cracks initiated, there was not only one initiation point, but also many points and they propagated separately. With the growth of crack, some cracks would connect to each other and formed one much longer crack, which would grow to the fracture of the specimens and the final cracks were connected by plural short cracks. Table 4.3 lists the statistic results of the final cracks of the checked specimens.
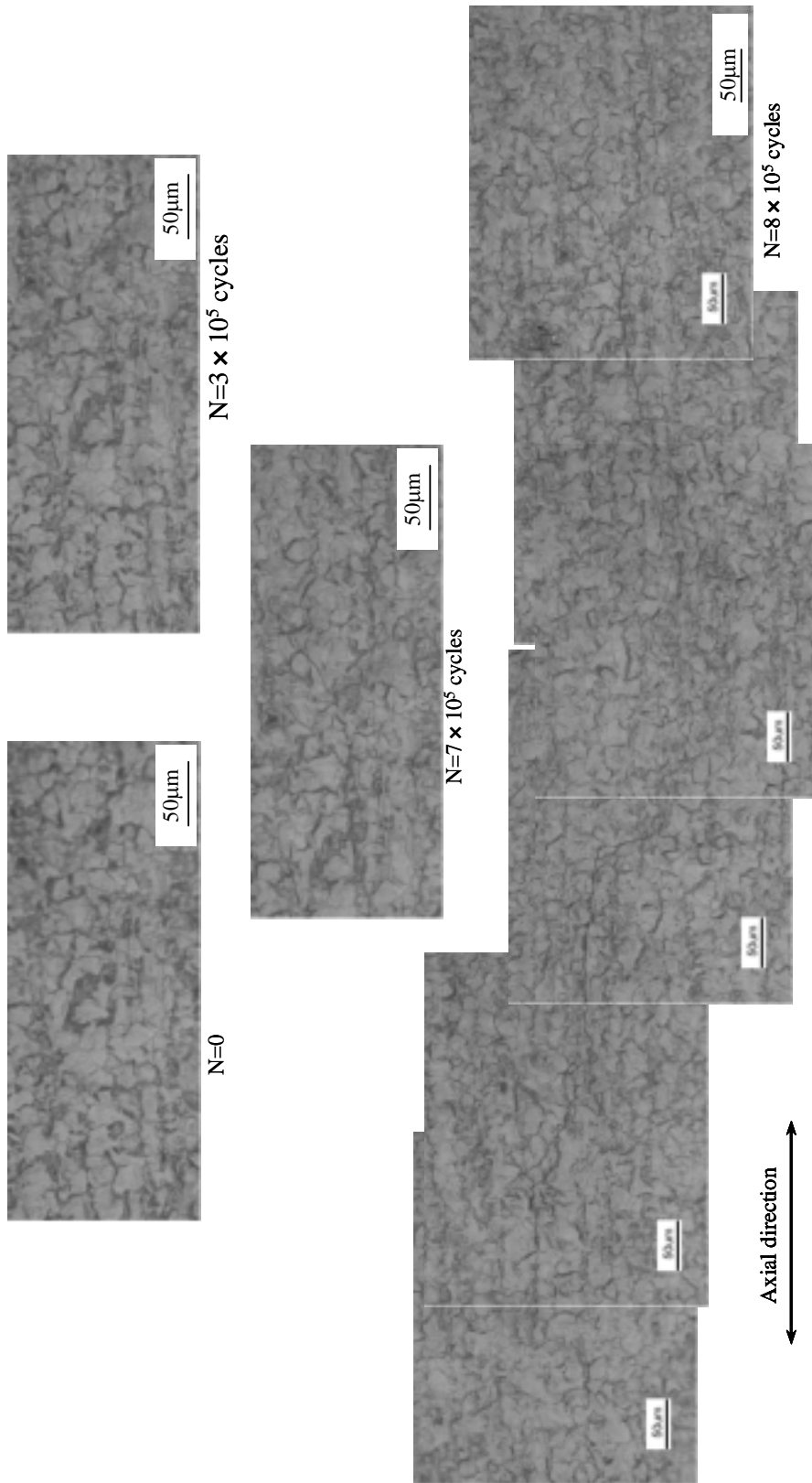
Fig.4.13 Microstructure behaviors of torsional fatigue crack propagation (S15C, 0%)
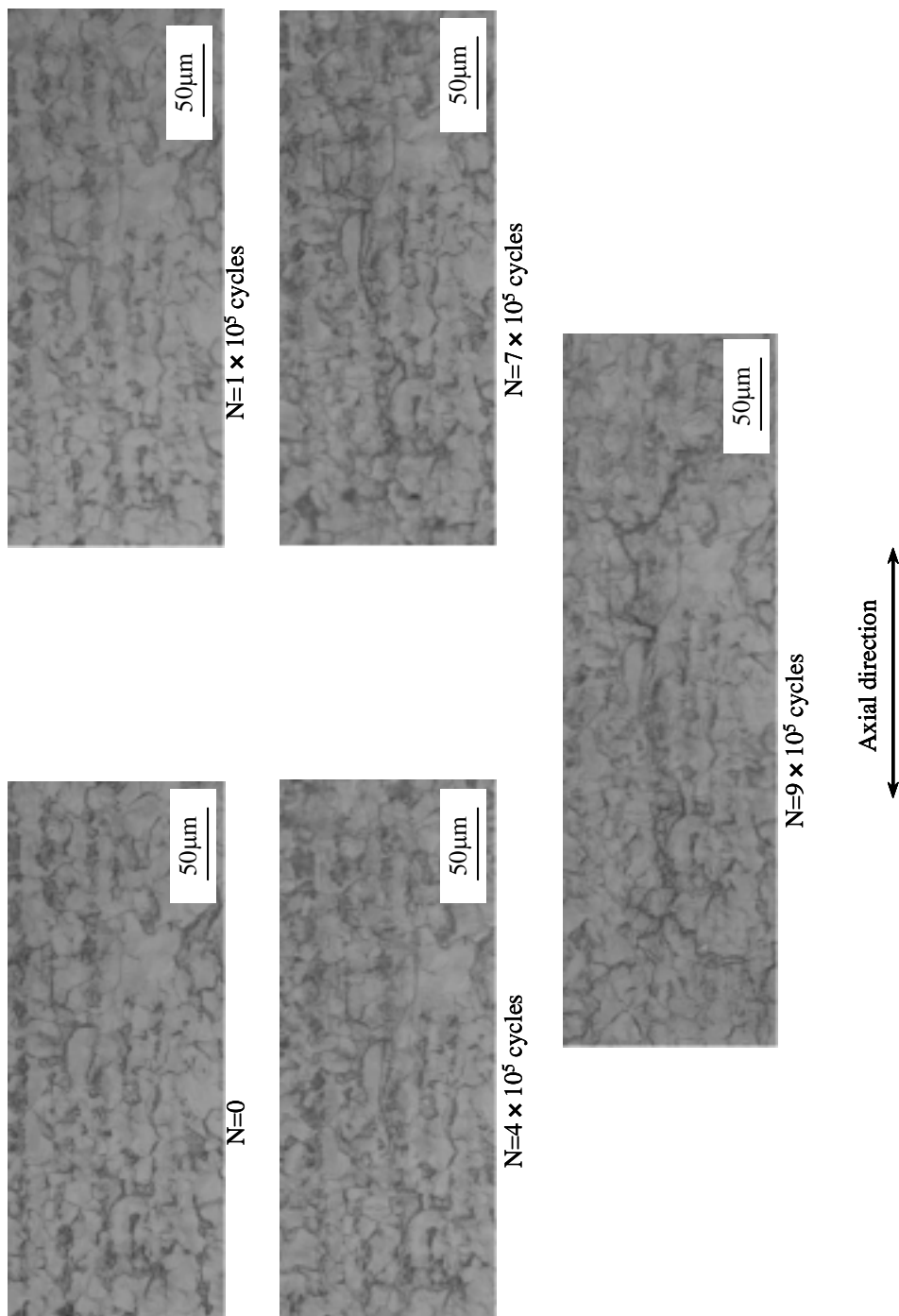
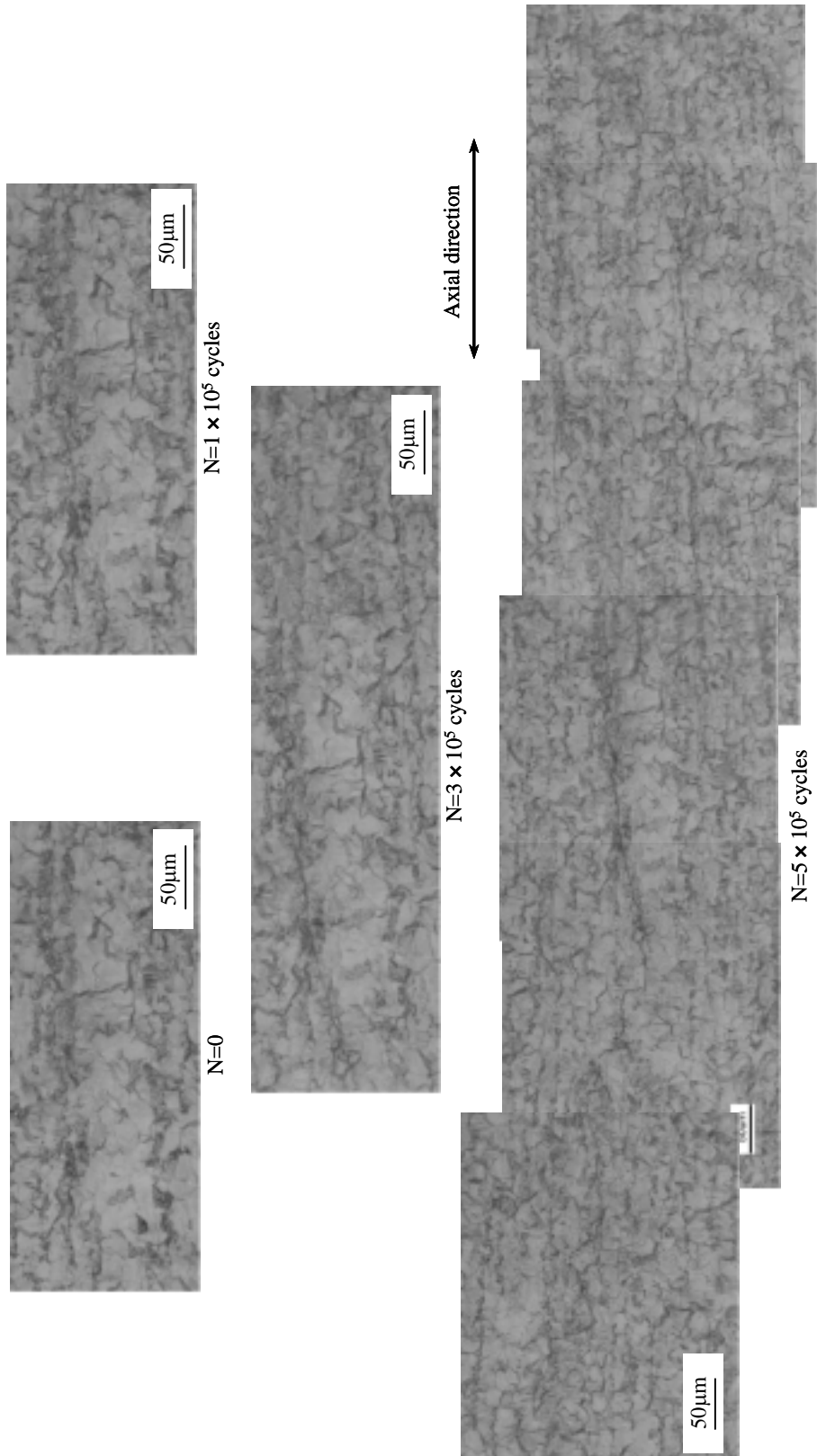Fig.4.13. Microstructure behaviors of torsional fatigue crack propagation (S15C, 2%)

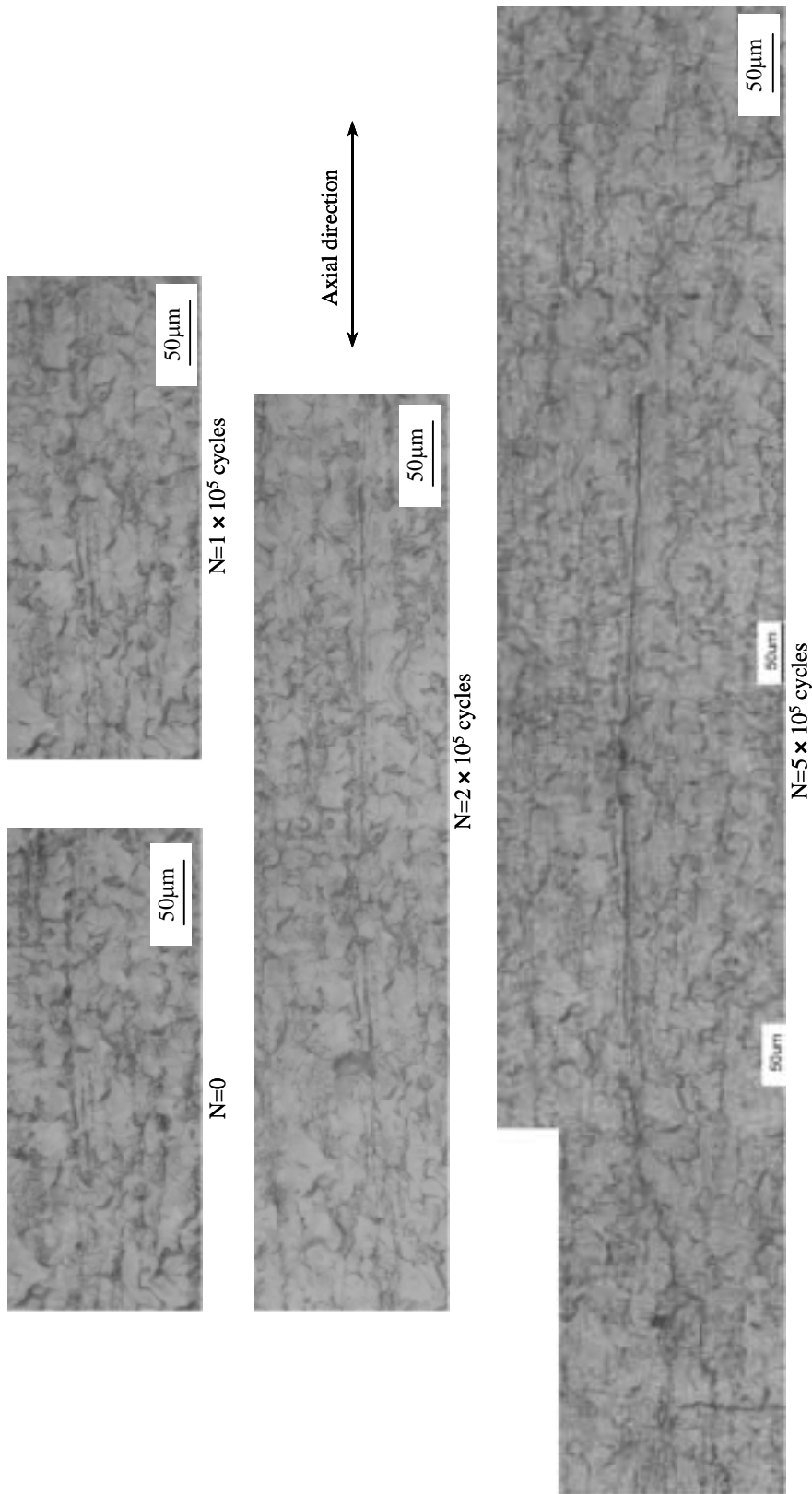Fig.4.13 Microstructure behaviors of torsional fatigue crack propagation (S15C, 5%)

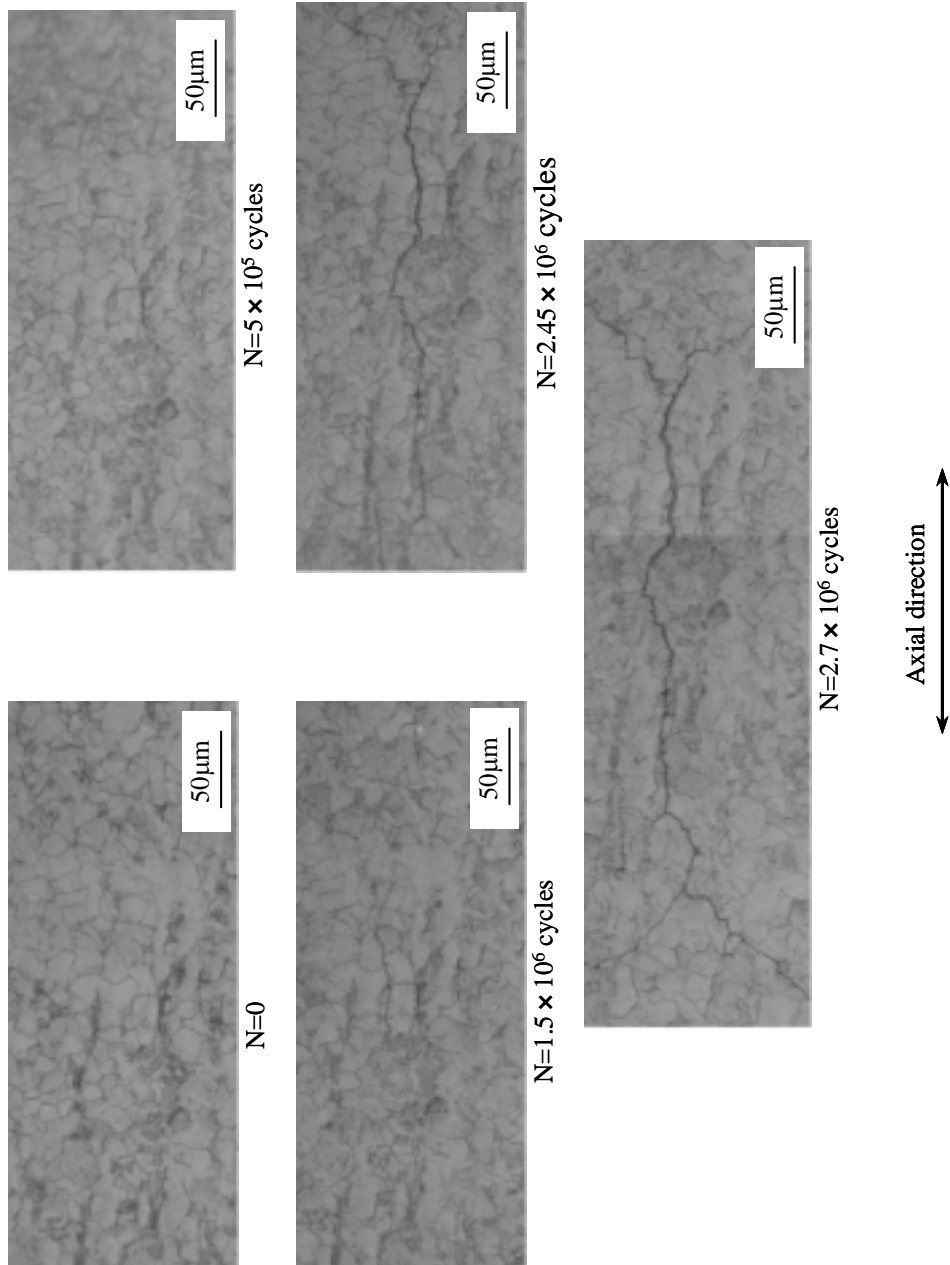Fig.4.13 Microstructure behaviors of torsional fatigue crack propagation (S15C, 8%)

Fig.4.14 Microstructure behaviors of torsional fatigue crack propagation (S25C, 0%)
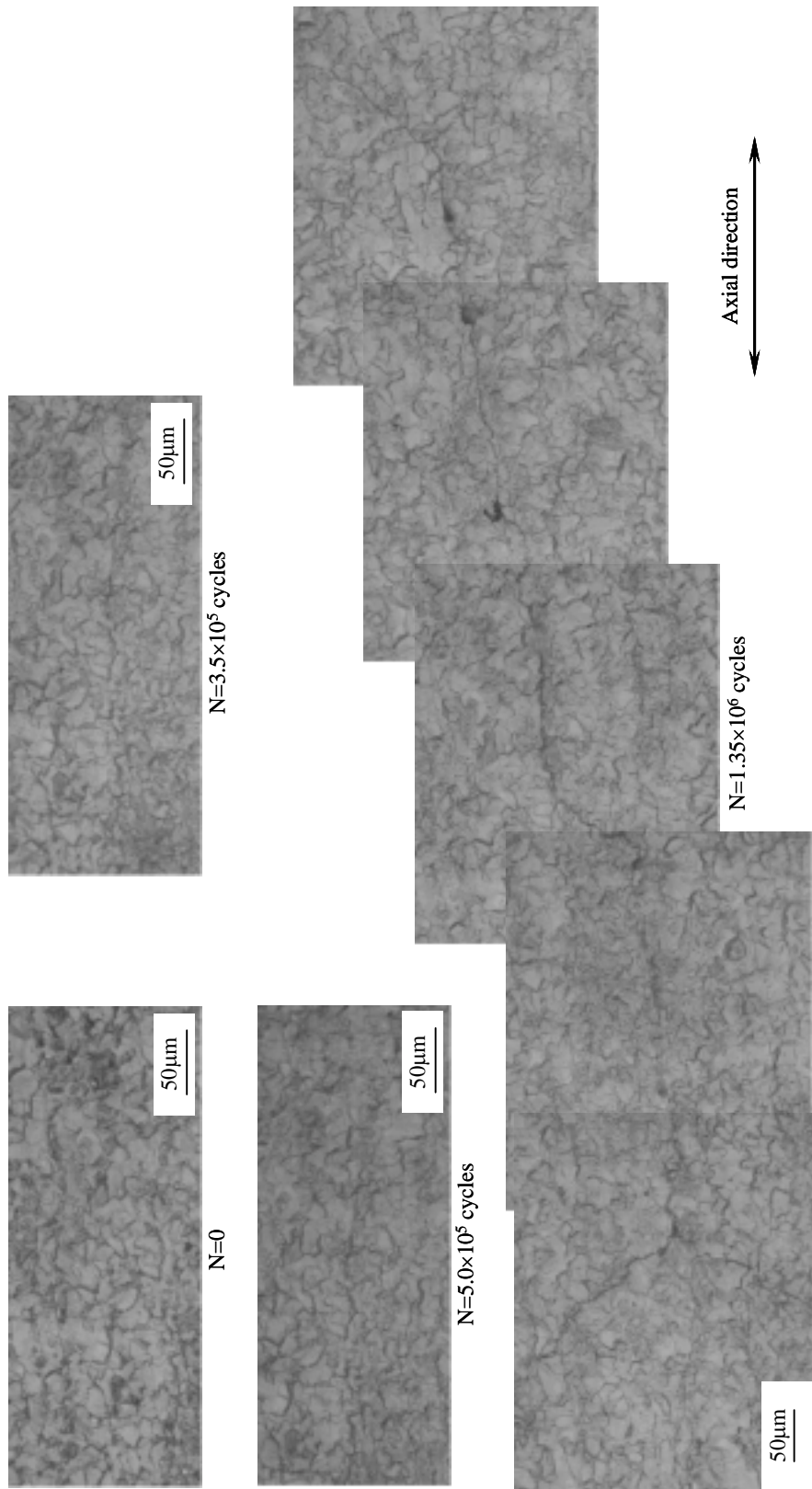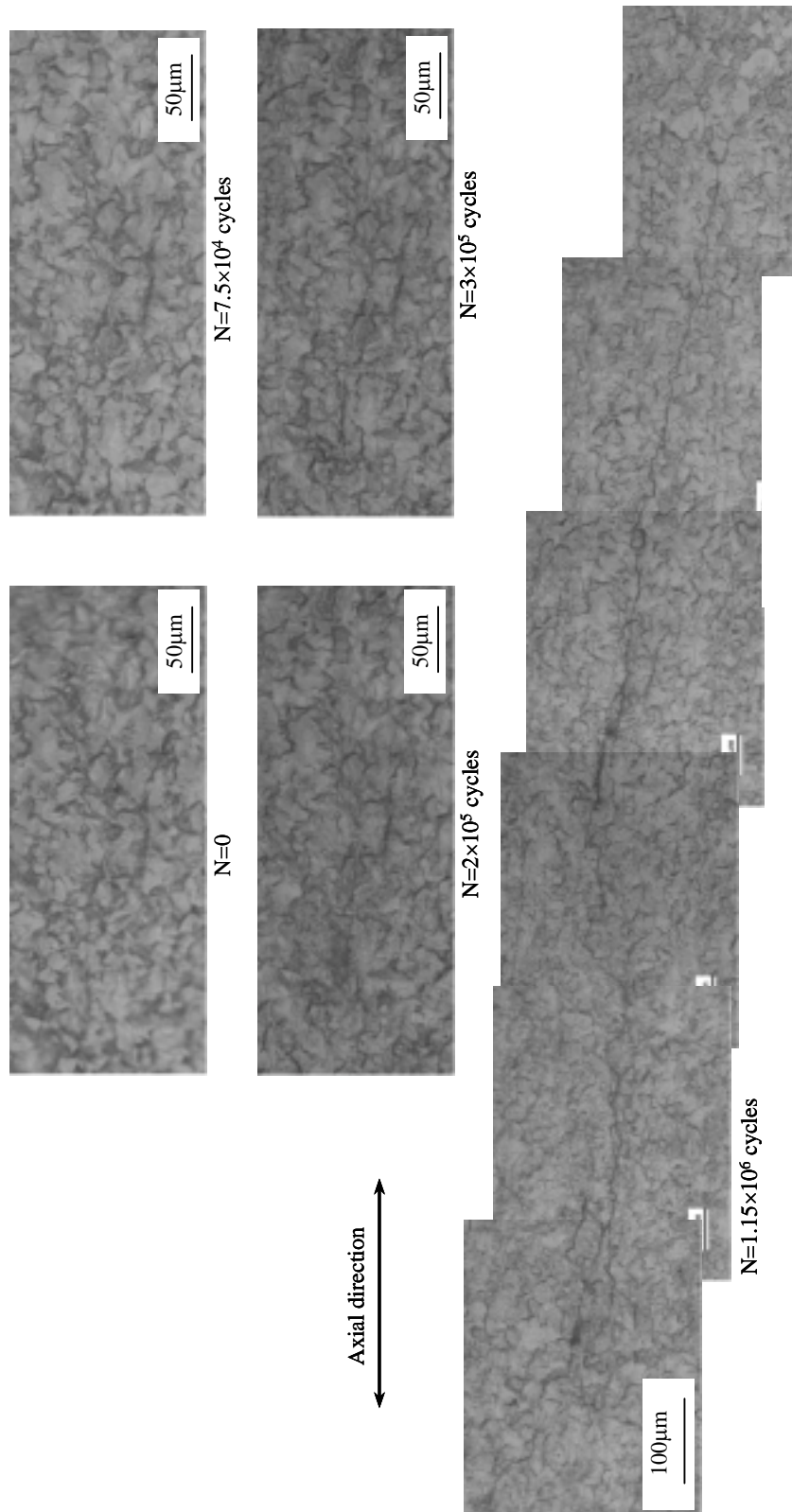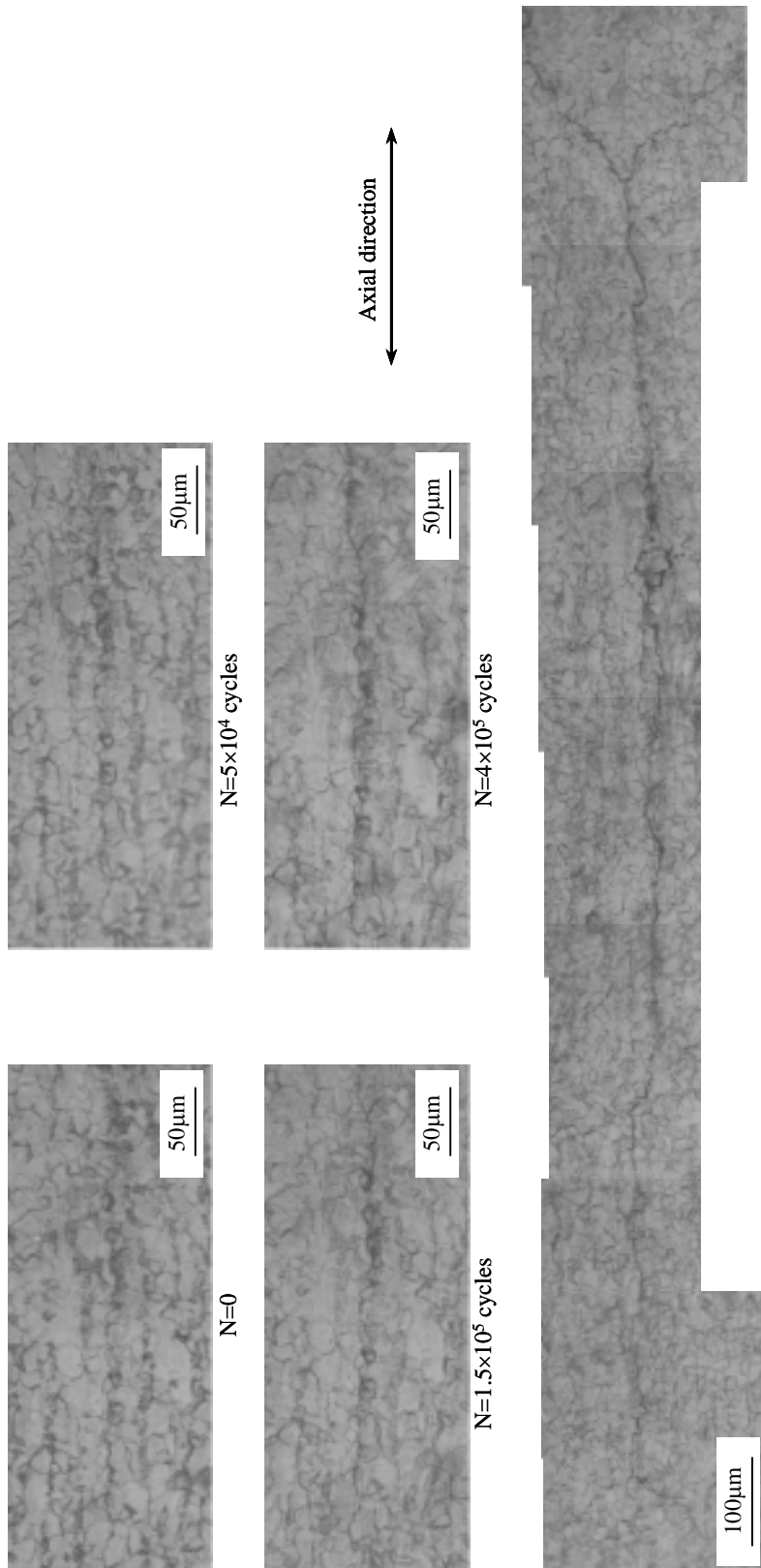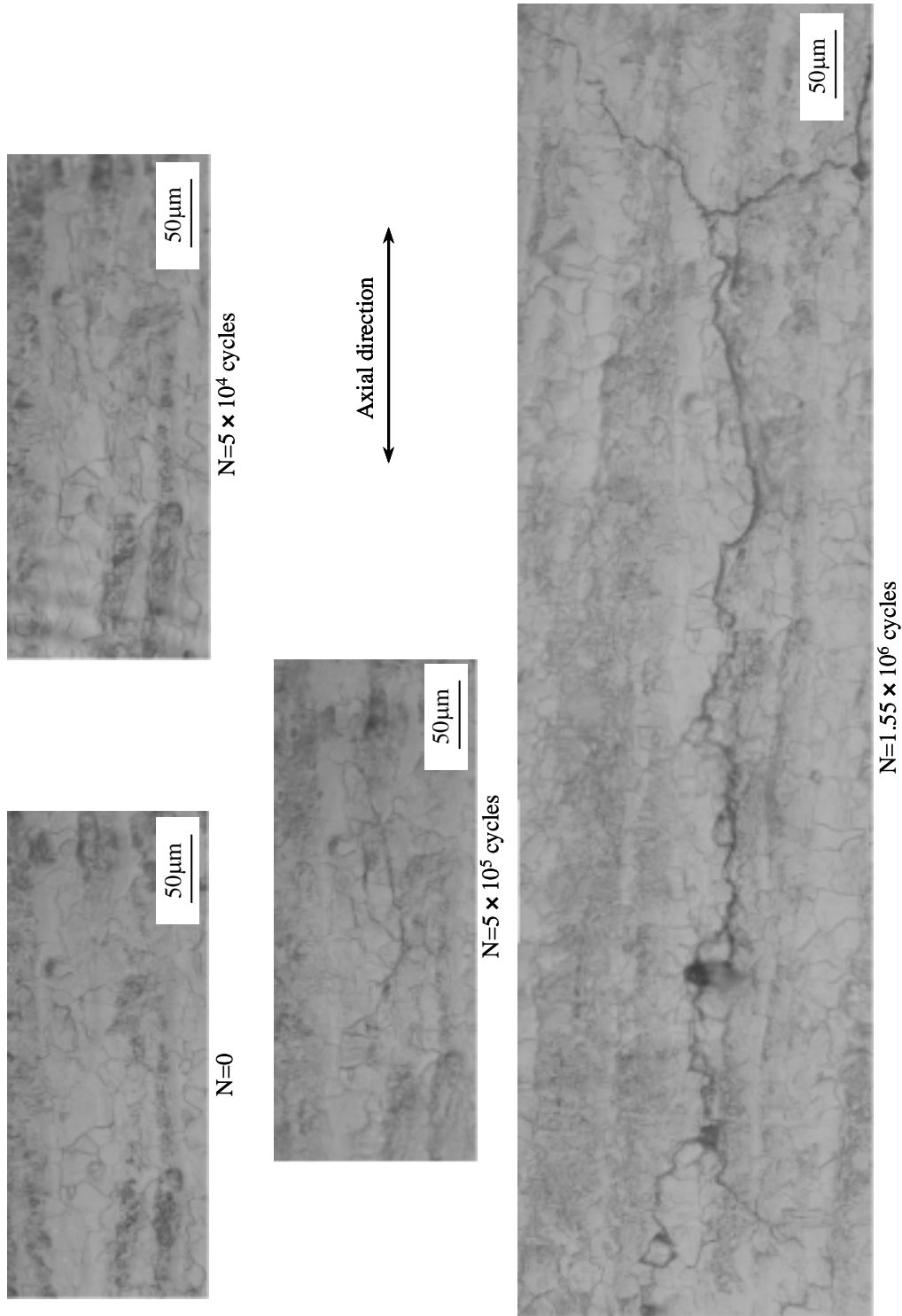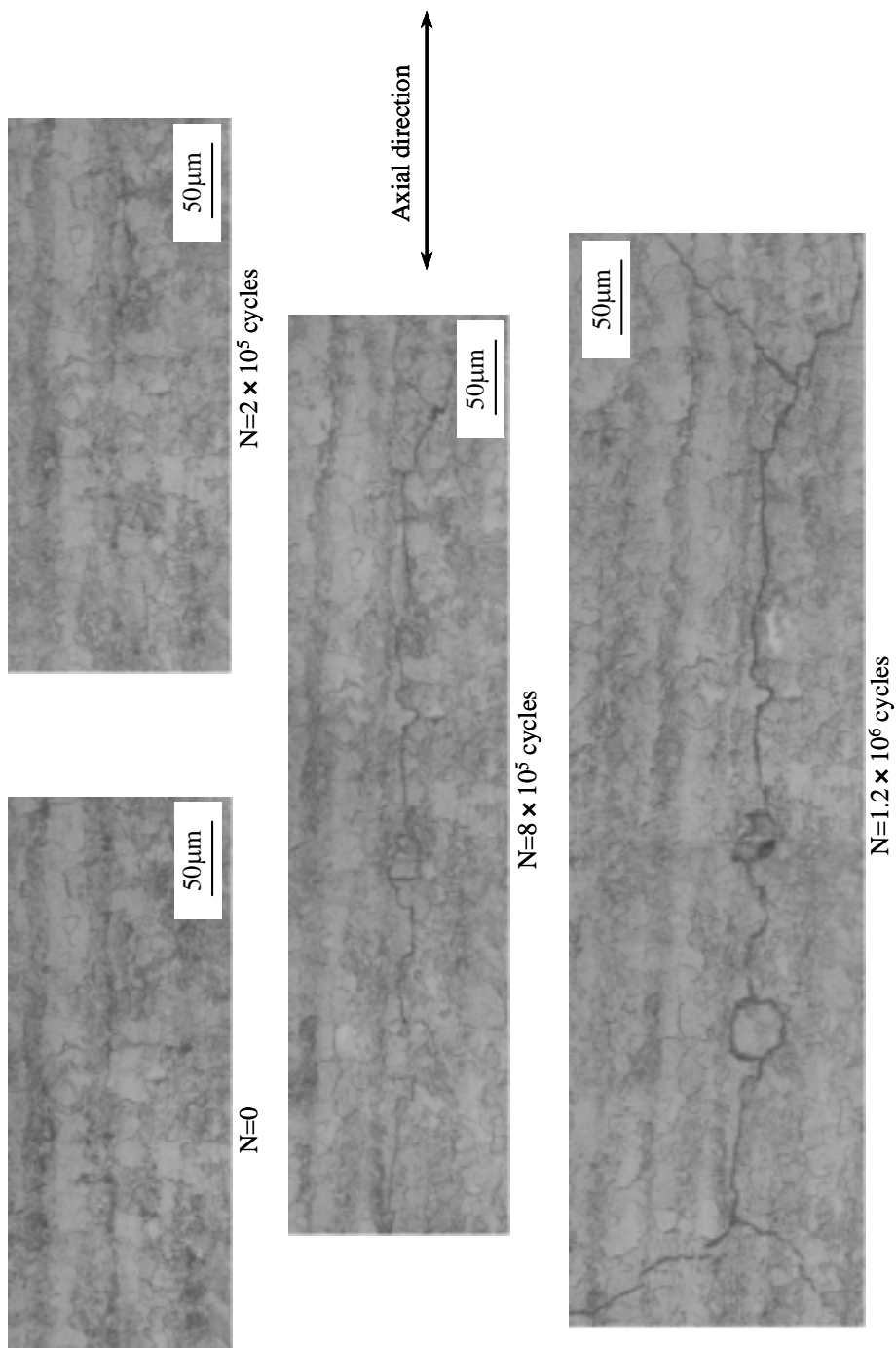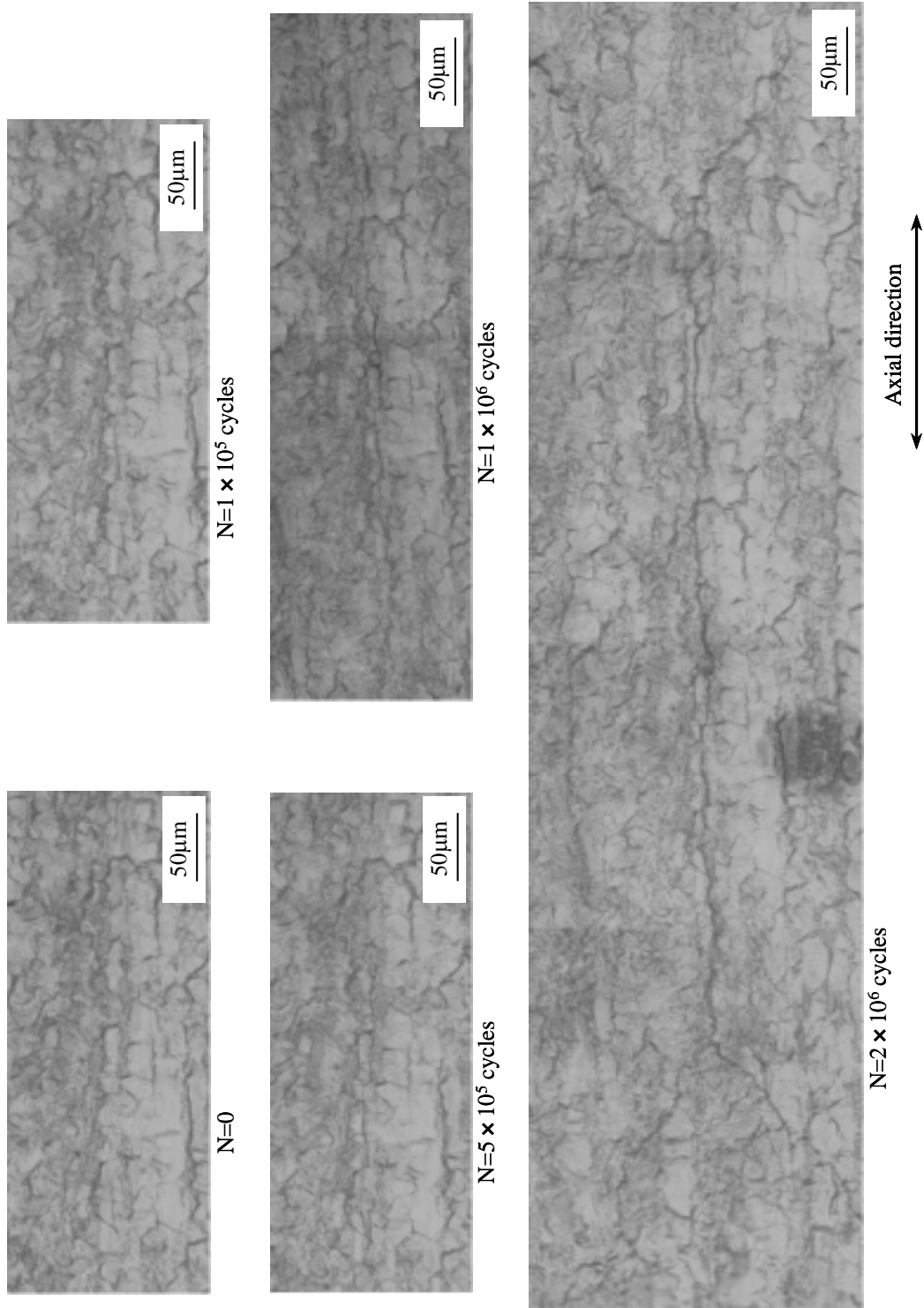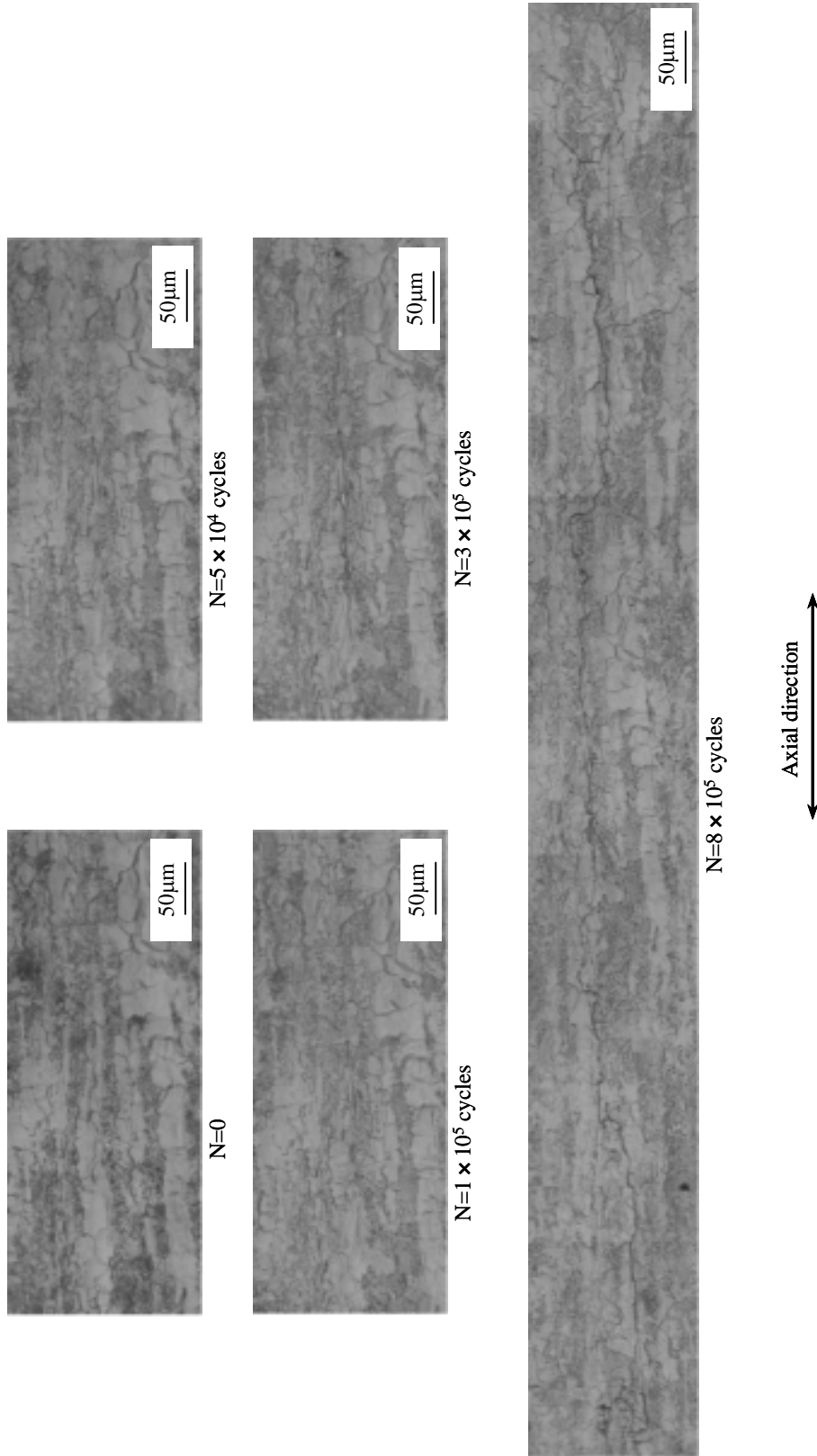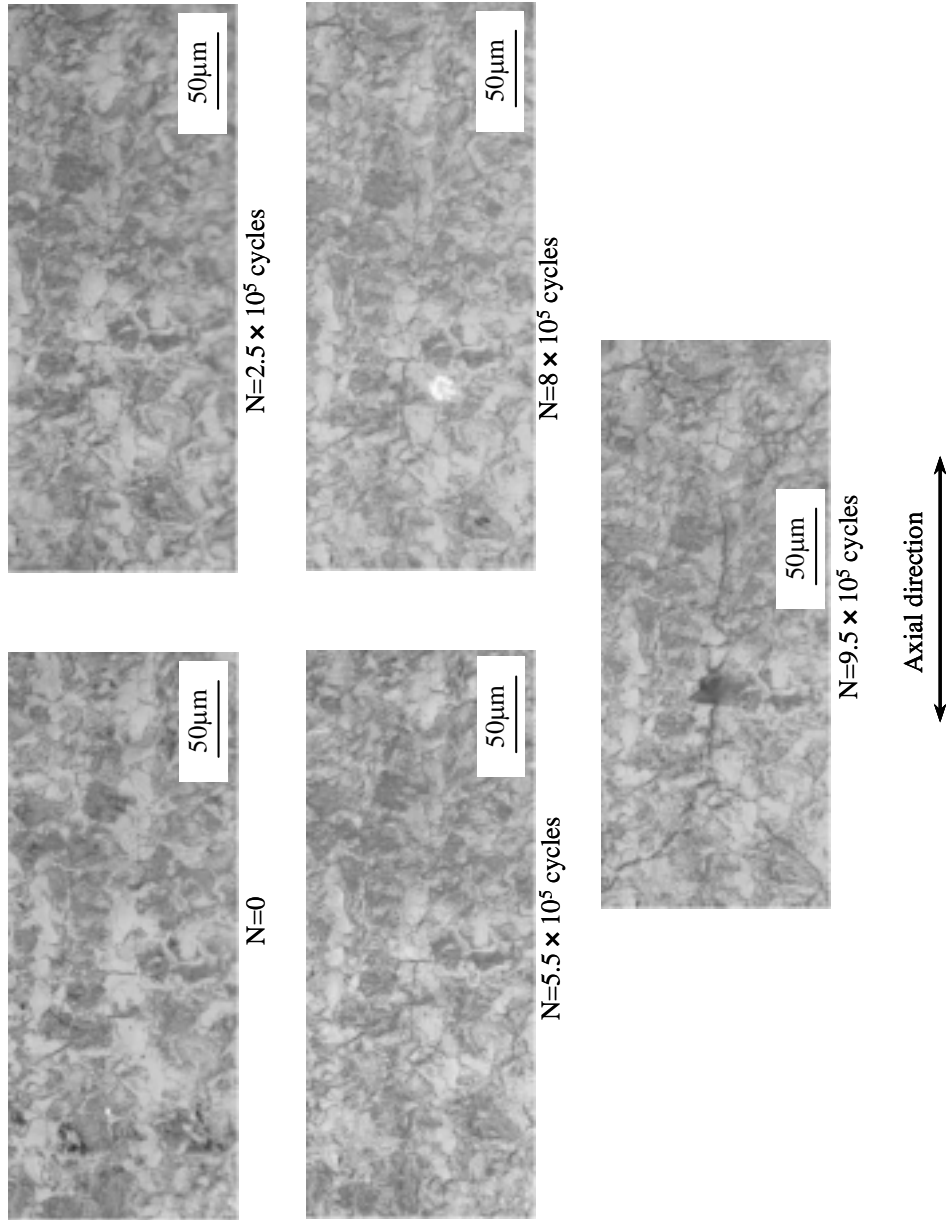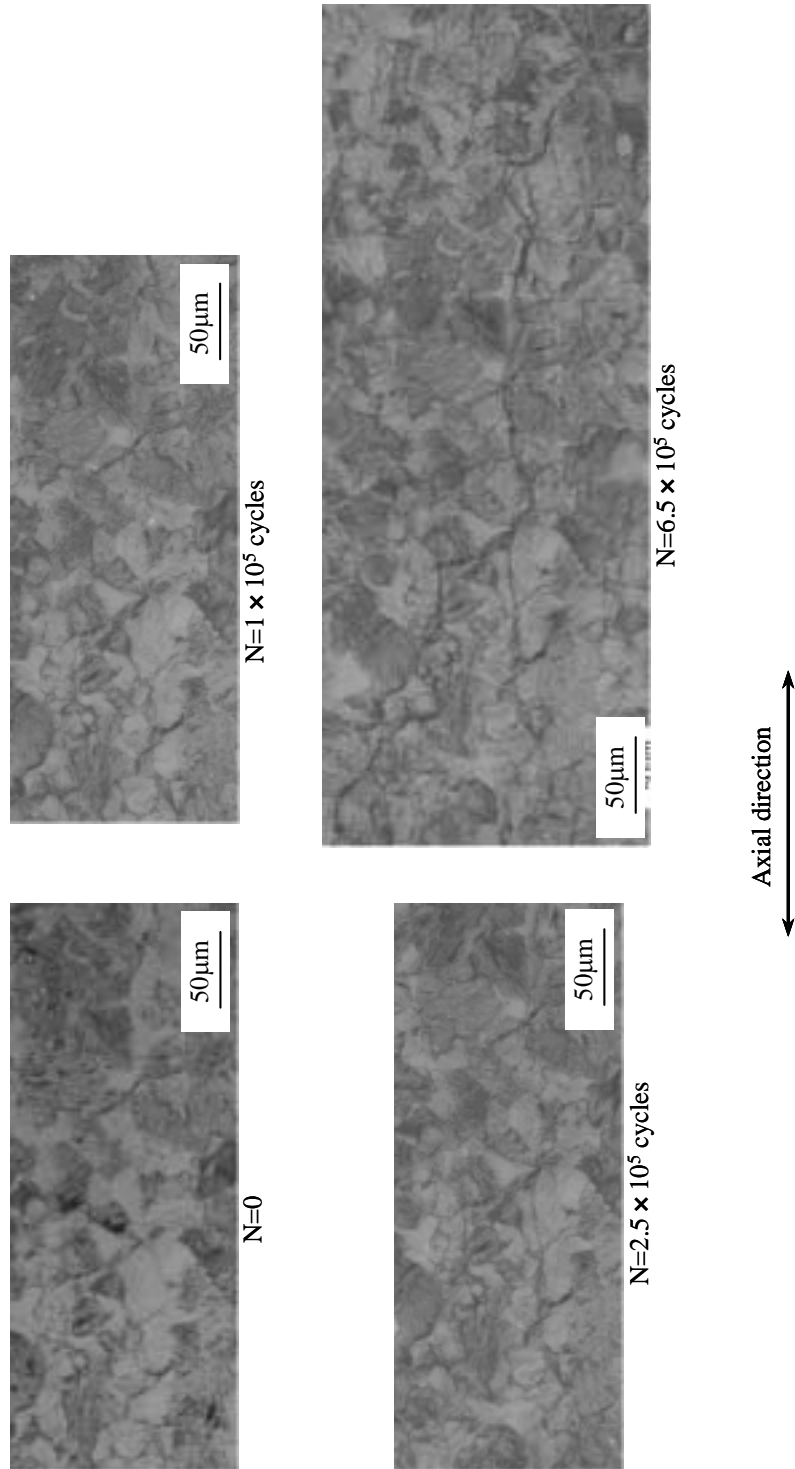
Fig.4.14 Microstructure behaviors of torsional fatigue crack propagation (S25C, 2%)

Fig.4.14 Microstructure behaviors of torsional fatigue crack propagation (S25C, 5%)

Fig.4.14 Microstructure behaviors of torsional fatigue crack propagation (S25C, 8%)

Fig.4.15 Microstructure behaviors of torsional fatigue crack propagation (S35C, 0%)

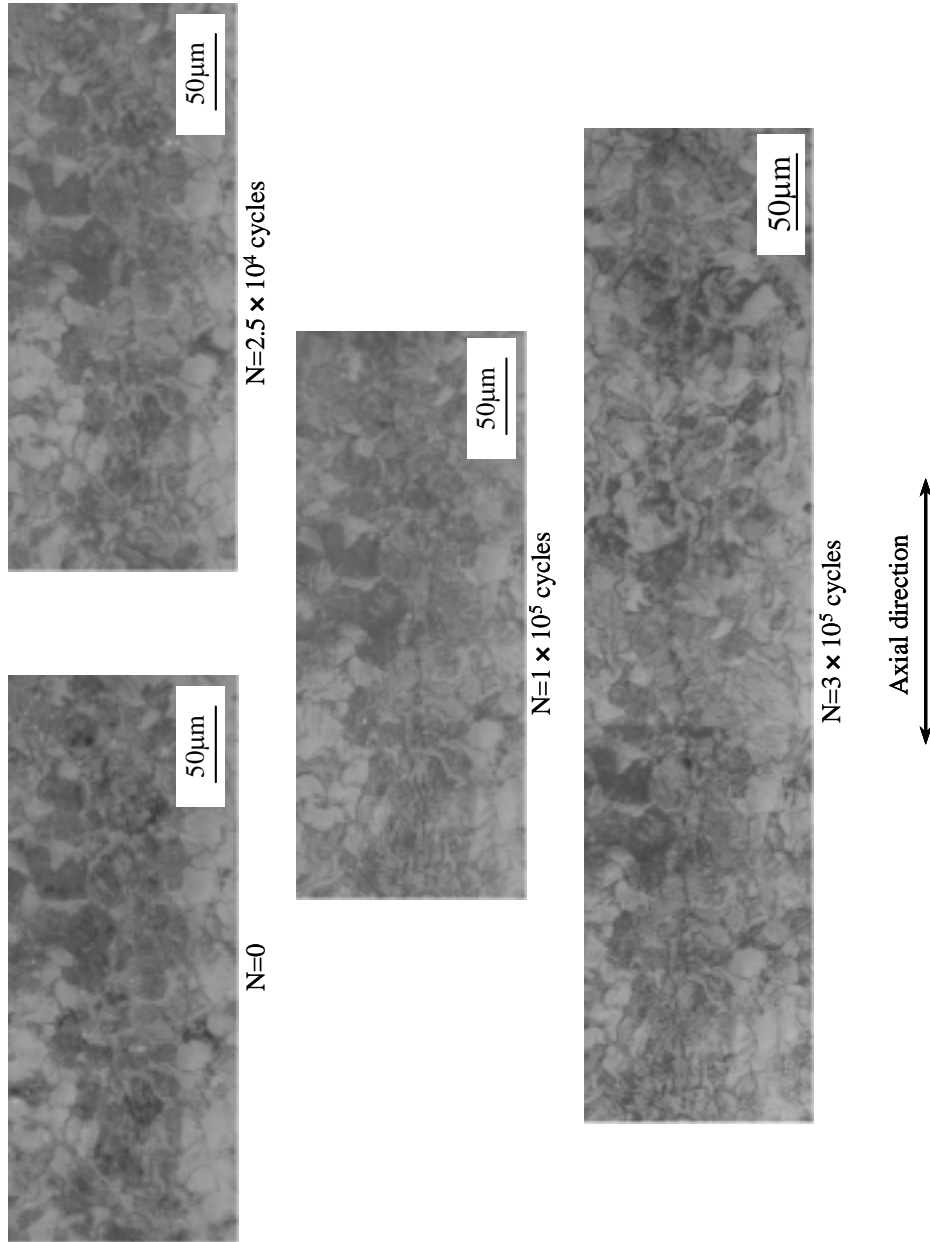Fig.4.15 Microstructure behaviors of torsional fatigue crack propagation (*S35C*, 2%)

Fig.4.15 Microstructure behaviors of torsional fatigue crack propagation (S35C, 5%)

Fig.4.15 Microstructure behaviors of torsional fatigue crack propagation (S35C, 8%)

Fig.4.16 Microstructure behaviors of torsional fatigue crack propagation (S45C, 0%)

Fig.4.16 Microstructure behaviors of torsional fatigue crack propagation (S45C, 2%)

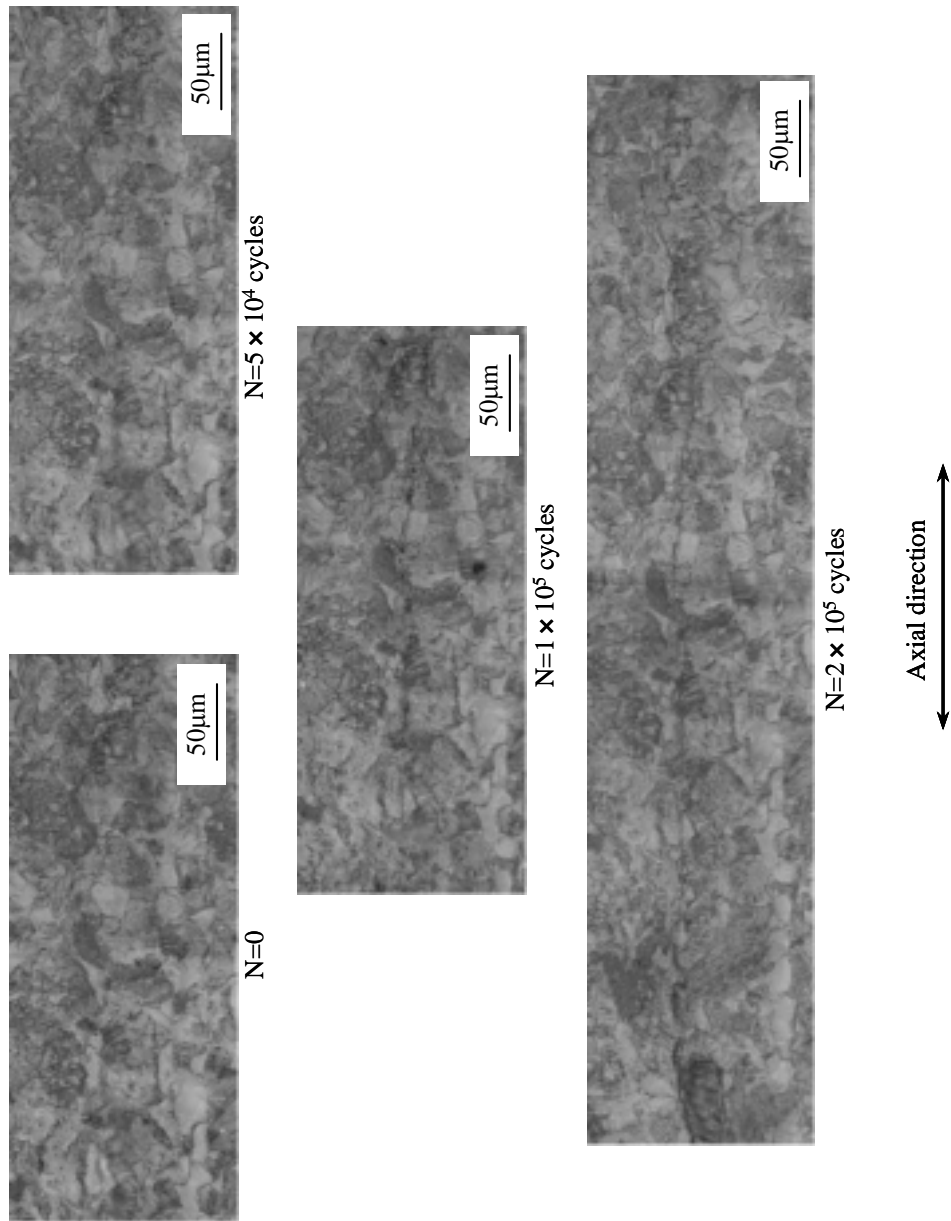Fig.4.16 Microstructure behaviors of torsional fatigue crack propagation (S45C, 5%)

Fig.4.16 Microstructure behaviors of torsional fatigue crack propagation (S45C, 8%)

Table 4.3 Statistic results of the final crack in checked specimens

|	$\varepsilon_p=0\%$	$\varepsilon_p=2\%$	$\varepsilon_p=5\%$	$\varepsilon_p=8\%$
S15C	Plural	Single	Plural	Plural
S25C	Single	Plural	Plural	Plural
S35C	Plural	Single	Plural	Plural
S45C	Plural	Plural	Plural	Single
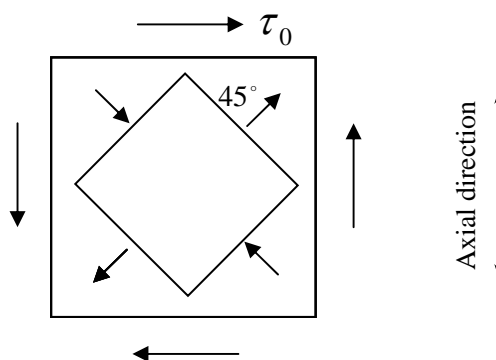
Fig.4.17 Stress status of torsional fatigue

4.3.3 Stress Amplitude Influences

Figure 4.18 is the crack initiation and propagation behaviors of S15C with different pre-strain ratios under the same stress amplitude, both the crack initiation lives (number of cycles to the fatigue crack initiation) and fatigue lives become longer with the increasing of tensile pre-strain ratio, and the crack growth rate becomes slower at the same time, as shown in Fig.4.18 (a). However, the crack initiation life of specimens with different pre-strain ratios is still in the range of 10-20% of the fatigue life, as shown in Fig.4.18 (b). The fatigue limit of S15C with 2%, 5% and 8% pre-strain ratio is 140, 160 and 175MPa, respectively. The stress amplitude difference, $\Delta\tau=\tau_a-\tau_w$, becomes smaller with the increasing of tensile pre-strain ratio, and it could be up to 45MPa for 2% pre-strained specimen, which is more than 30% of its own fatigue limit. When such high stress amplitude is applied on the 2% pre-strained specimen, the crack would initiate very quickly. Once the crack initiated, the crack would propagate very fast until the specimen is broken. For the cases of $\varepsilon_p=5\%$ and 8%, the cracks initiate slowly not only because of the decreasing of the net driving stress amplitude, but also the increasing of surface hardness, which retaining the crack initiation and

(a) l-N (τ_w =185MPa)
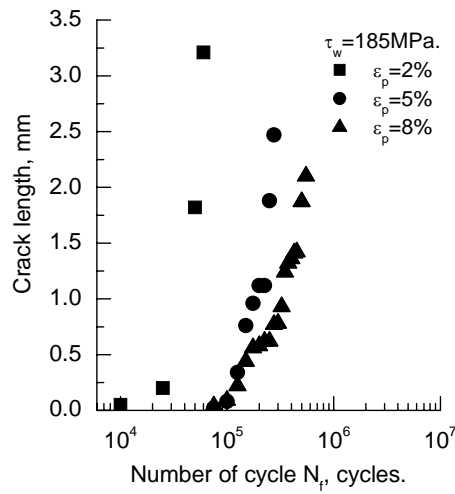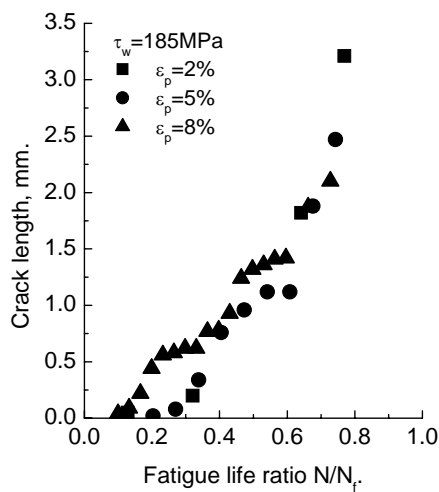
(b) l-N/N$_f$ (τ_w =185MPa)

Fig.4.18 Crack initiation and propagation behaviors
of S15C under the same stress amplitude

propagation. On the other hand, under the stress amplitude of $\tau_w = \tau_{wo} + 10$MPa, same stress amplitude of 10MPa is added to their own fatigue limits respectively. The stress amplitude for the higher pre-strained (ε_p =8%) specimen is much higher than that of the lower pre-strained (ε_p =2%) one. The stress amplitude difference between them is 35MPa. The increased stress may lead the crack to initiate earlier with the increasing of tensile pre-strain, as shown in Fig.4.19.
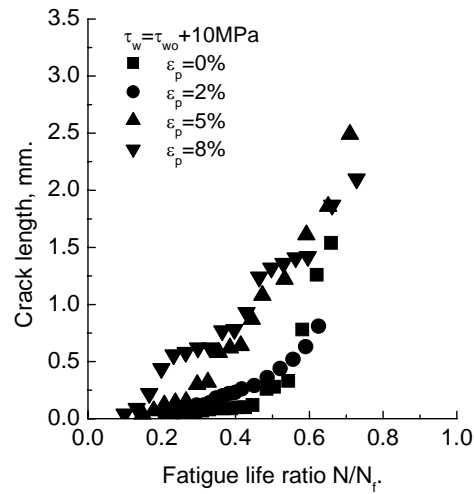
Fig.4.19 Crack initiation and propagation behaviors of
S15C under stress amplitude $\tau_w = \tau_{wo} + 10\text{MPa}$

Figures 4.20, 4.21 and 4.22 are the crack initiation and propagation behaviors of S45C under the same stress amplitudes, stress amplitude of $\tau_w = \tau_{wo} + 5\text{MPa}$ and $\tau_w = \tau_{wo} + 10\text{MPa}$, respectively. Under the same stress amplitude, fatigue life became longer and the crack growth rate got slower with the increasing of tensile pre-strain ratio. Under the stress amplitude $\tau_w = \tau_{wo} +$ constant MPa, the crack
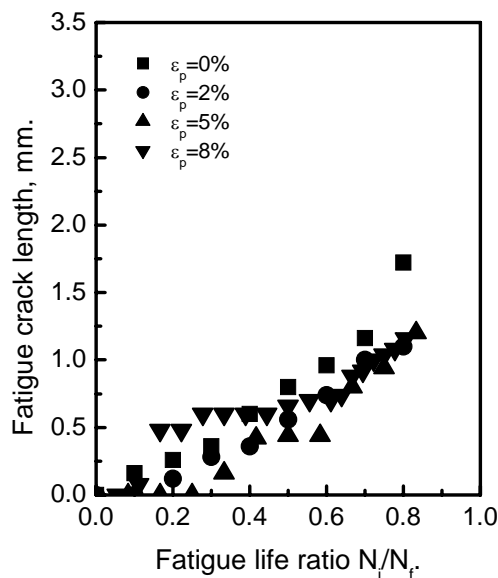

Fig.4.20 Crack initiation and propagation behaviors of
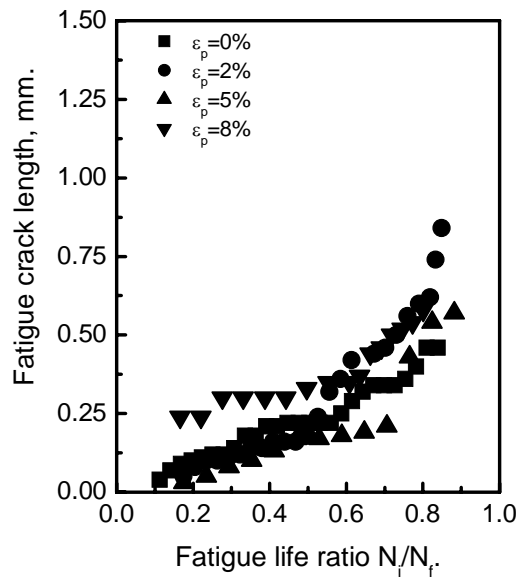S45C under same stress amplitude, 205MPa

Fig.4.21 Crack initiation and propagation behaviors of
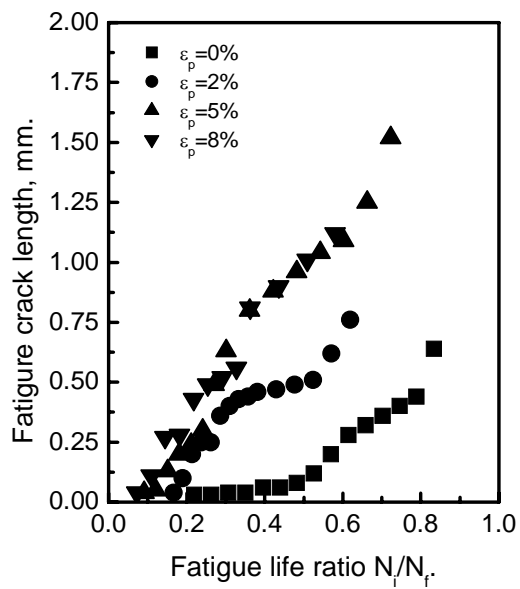S45C under stress amplitude $\tau_w = \tau_{wo} + 5$MPa

Fig.4.22 Crack initiation and propagation behaviors of
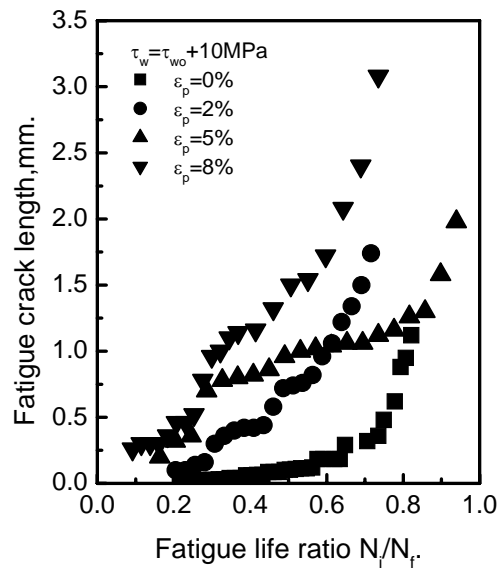S45C under stress amplitude $\tau_w = \tau_{wo} + 10$MPa

Fig.4.23 Crack initiation and propagation behaviors of
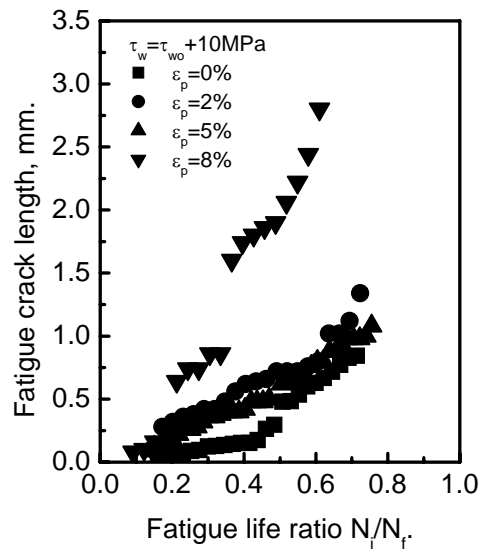S25C under stress amplitude $\tau_w = \tau_{wo} + 10$MPa

Fig.4.24 Crack initiation and propagation behaviors of
S35C under stress amplitude $\tau_w = \tau_{wo} + 10$MPa

initiated earlier with the increasing of tensile pre-strain, the crack growth faster with the increasing of tensile pre-strain ratio. And the difference in the crack growth rate gets larger when the constant stress value is larger. Figures 4.23 and 4.24 are the behaviors of S25C and S35C with different pre-strain ratios, respectively. The behaviors were almost the same with that of the S15C and S45C.

4.3.4 Crack Branch Behaviors

Based on the replica observation, the torsional fatigue cracks branched after propagating in Mode II style for some while. Figure 4.25 shows the branch points of the test materials. According to the figure, torsional fatigue cracks branch at the boundaries of grains, irrespective of ferrite or pearlite grains, and there is no relationship with the tensile pre-strain ratio. During the crack propagation, Mode I and Mode II styles exist at the same time. At the early stage of the torsional fatigue test, due to the specimen is suffered with shearing stress; the crack would initiate and propagate more easily by Mode II style. With the increasing of crack length, the Mode I style crack propagation becomes easier. When the crack propagates to the boundary of grains, it needs more energy to make the crack propagate through the grain by Mode II than along the boundary by Mode I, the crack would branch and propagate by Mode I style until failure. As the crack propagates by Mode I, the Mode II stress intensity factor would decrease and the crack propagation would stop in the axial direction.

Figure 4.26 is the shapes and directions of the branched cracks with different pre-strain ratios of same material. Though the directions of branched cracks are not same, due to the scatter of the crystallographic orientations of grains ahead of the crack tip, they eventually propagated to the direction perpendicular to the principal stresses, i.e. 45° to the axial direction.

4.4 Non-propagating Micro Crack Behaviors

Non-propagating micro crack behaviors were observed by successive taken replica examples after 10^7 cycles at the stress amplitude of the fatigue limit.

Figures 4.27, 4.28, 4.29 and 4.30 are the microstructure behaviors of the non-propagating cracks for S15C, S25C, S35C and S45C with different tensile pre-strain ratios from 0% to 8%, respectively. Non-propagating cracks initiate from the weak part of the ferrite grain in the surface and stop at the grain boundaries before branching, irrespective of ferrite grains or pearlite blocks.
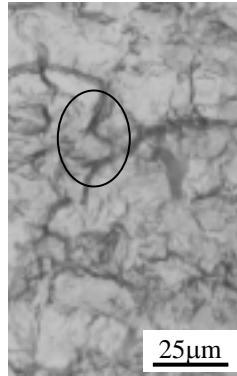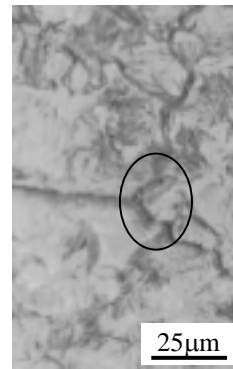
(a) ε_p =0%, τ_a=145MPa,
S15C, N=8.0×10^5cycles
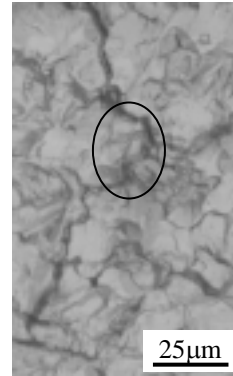
(b) ε_p =2%, τ_a=155MPa,
S25C, N=1.3×10^6 cycles
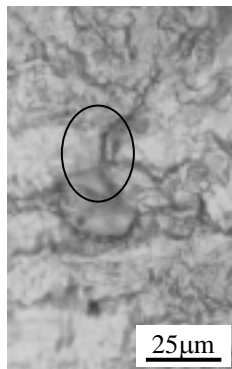
(c) ε_p =5%, τ_a=175MPa,
S35C, N=2.0×10^6 cycles

(d) ε_p =8%, τ_a=210MPa,
S45C, N=4.0×10^5 cycles

Circle mark: crack branch point

Fig.4.25 Microstructure of crack branch points
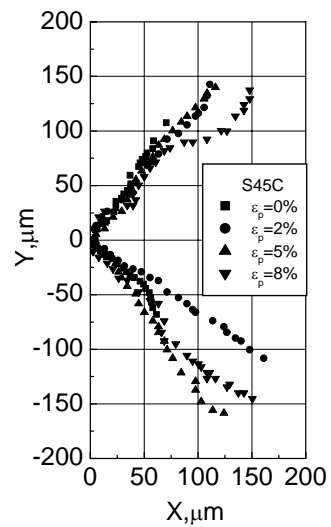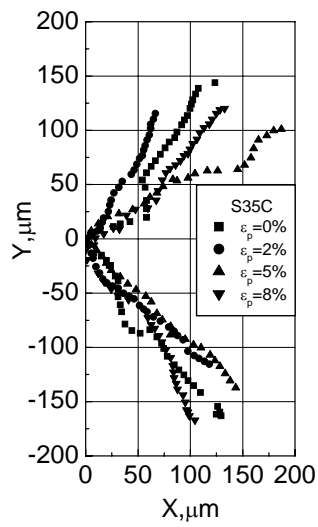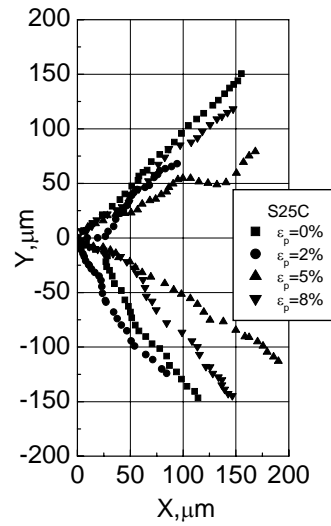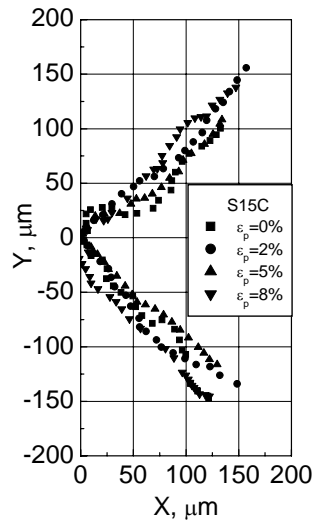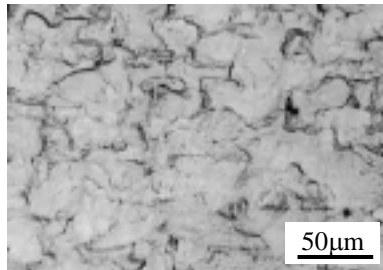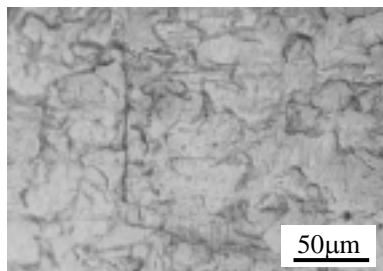
$\varepsilon_p = 8\%$, $\tau_a = 175$MPa, N=0

$\varepsilon_p = 8\%$, $\tau_a = 175$MPa, N=6×10^6 cycles
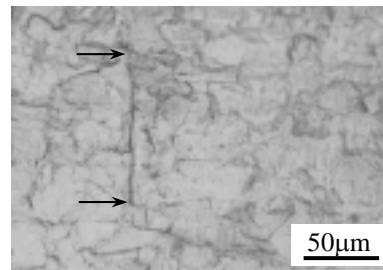
$\varepsilon_p = 8\%$, $\tau_a = 175$MPa, N=1×10^7 cycles

Arrow mark: tip of non-propagating micro crack

Axial direction

Fig.4.27 Microstructure of non-propagating micro crack of S15C with
8% pre-strain
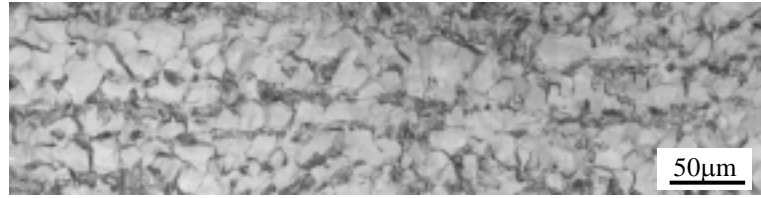
N=0

N=5×10^5 cycles
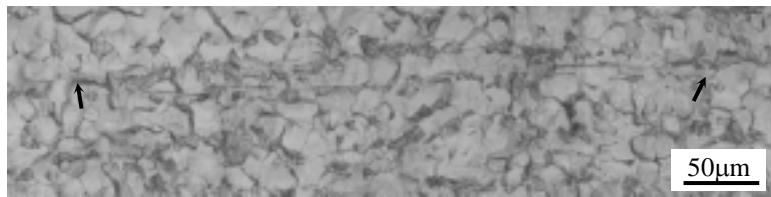
N=6×10^6 cycles

N=1×10^7 cycles

Arrow mark: tip of non-propagating micro crack

Axial direction

Fig.4.28 Microstructure of non-propagating micro crack of S25C with 2% pre-strain (τ_a=145MPa)

N=0

N=1×10⁵cycles

N=6×10⁶cycles

N=1×10⁷cycles

Arrow mark: tip of non-propagating micro crack

Axial direction

Fig.4.28 Microstructure of non-propagating micro crack of S25C with
5% pre-strain (τ_a=160MPa)

N=0

N=2×10^5cycles

N=6×10^6cycles

N=1×10^7cycles

Arrow mark: tip of non-propagating micro crack

Axial direction

Fig.4.28 Microstructure of non-propagating micro crack of S25C with 8% pre-strain (τ_a=175MPa)

N=0

N=1.0× 10^6 cycles

N=6.0× 10^6 cycles
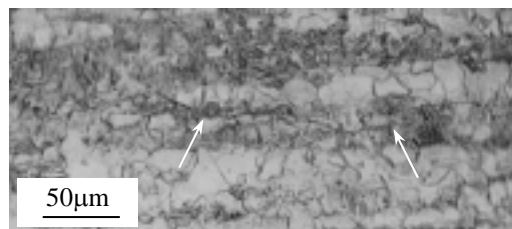
N=1.0× 10^7 cycles

Axial direction

Arrow mark: tip of non-propagating micro crack

Fig.4.29 Microstructure of non-propagating micro crack for S35C without pre-strain (τ_a=145MPa)
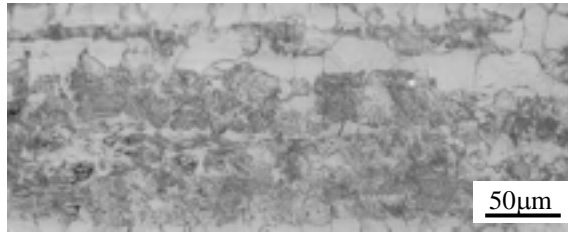
N=0
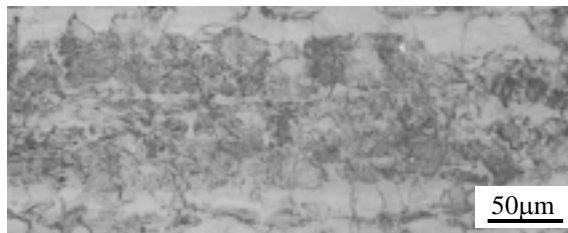
N=1×10^5 cycles
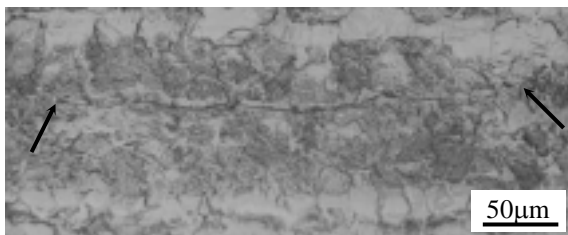
N=5×10^6 cycles

N=1×10^7 cycles

Arrow mark: tip of non-propagating micro crack

Axial direction
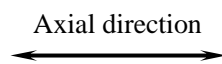
Fig.4.29 Microstructure of non-propagating micro crack of S35C with 2% pre-strain (τ_a=150MPa)

N=0

N=1×10^7 cycles

Arrow mark:
tip of non-propagating micro crack

Axial direction
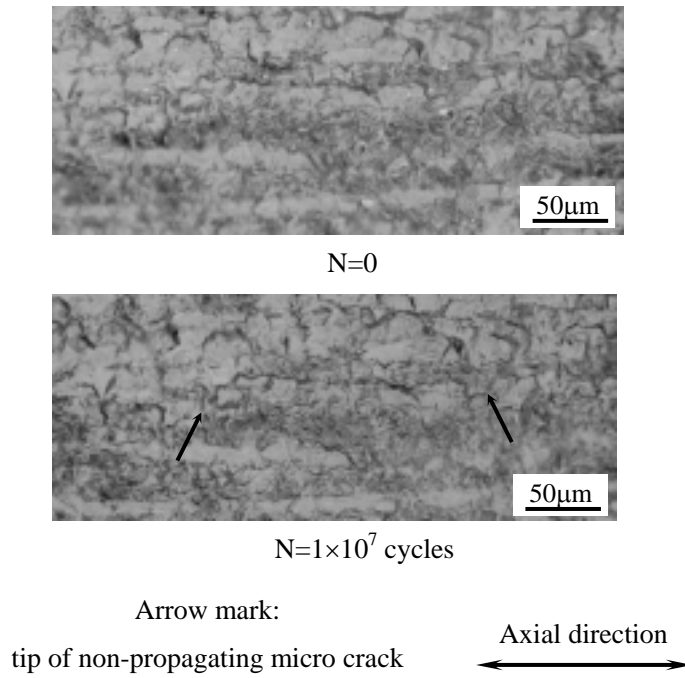
Fig.4.29 Microstructure of non-propagating micro crack of S35C with 5% pre-strain (τ_a=165MPa)
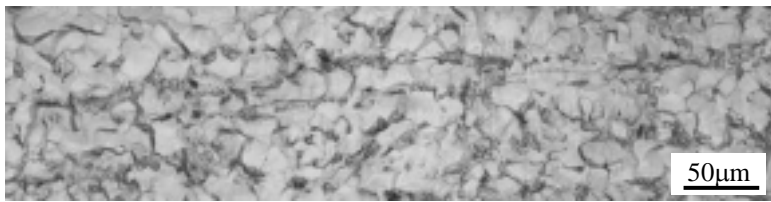

N=0

N=1×10^7 cycles

Arrow mark: tip of non-propagating micro crack

Axial direction
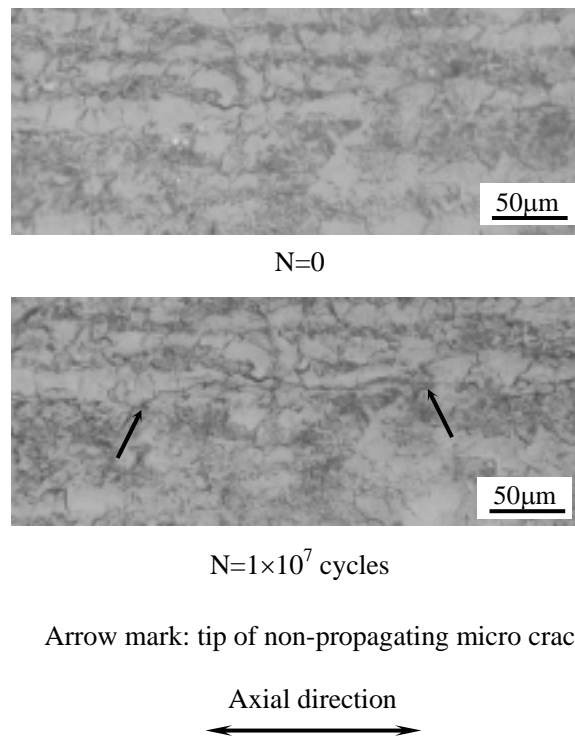
Fig.4.29 Microstructure of non-propagating micro crack of S35C with 8% pre-strain (τ_a=180MPa)

N=0
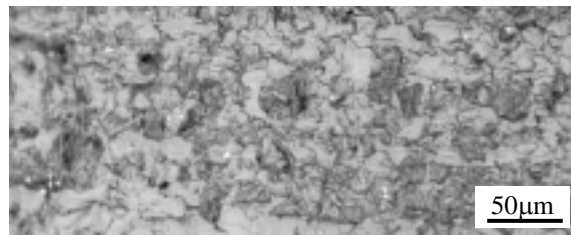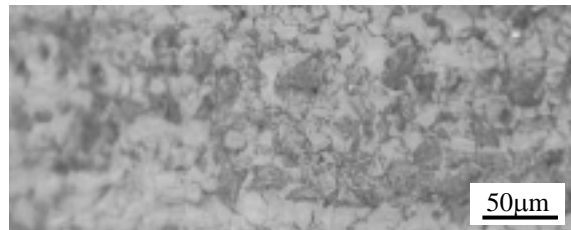
N=1×10^5 cycles
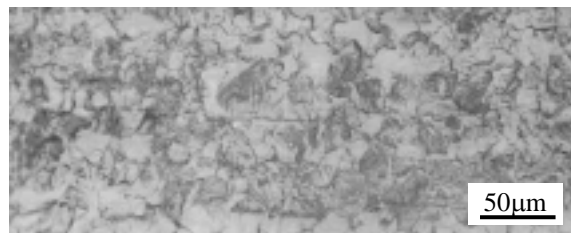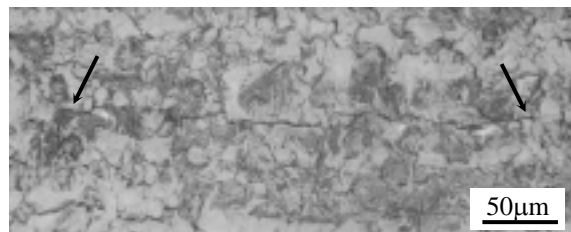
N=1×10^6 cycles

N=4×10^6 cycles
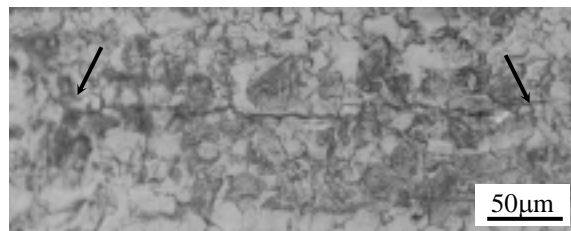
N=1×10^7 cycles

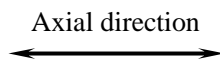Arrow mark: tip of non-propagating micro crack ⟷ Axial direction

Fig.4.30 Microstructure of non-propagating micro crack of S45C
without pre-strain (τ_a=160MPa)

90

N=0
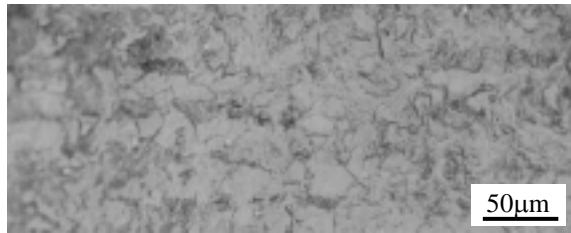
N=1×10^5 cycles

N=1×10^6 cycles
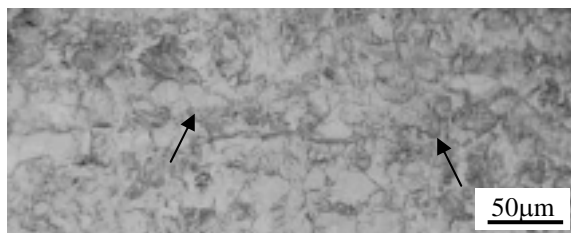
N=3×10^6 cycles

N=1×10^7 cycles

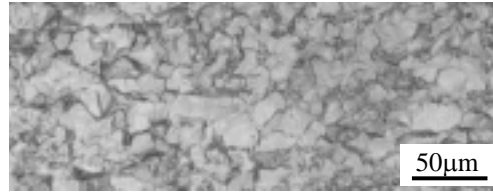Arrow mark: tip of non-propagating micro crack   Axial direction

Fig.4.30 Microstructure of non-propagating micro crack of S45C with
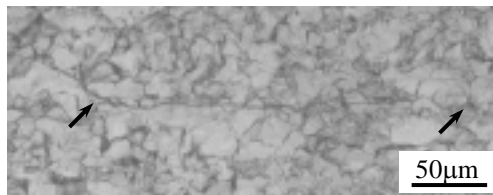2% pre-strain (τ_a=160MPa)
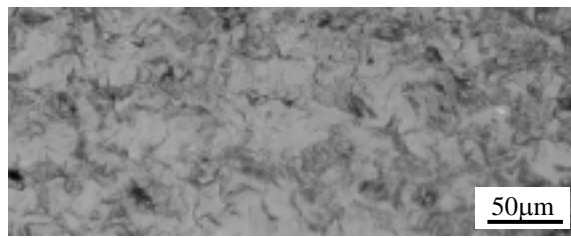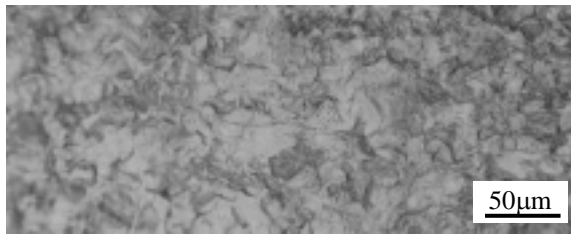
N=0

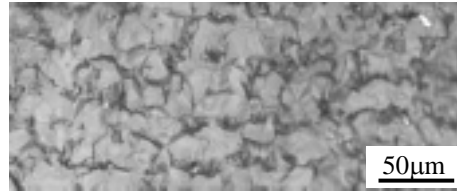N=1×10^6 cycles
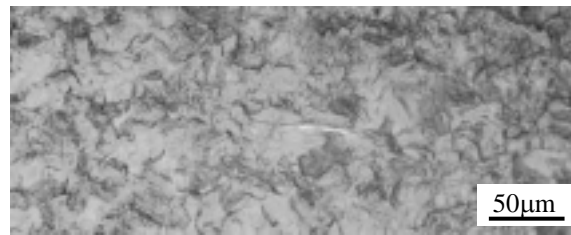
N=3×10^6 cycles
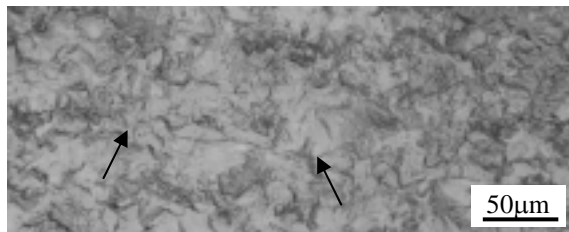
N=1×10^7 cycles

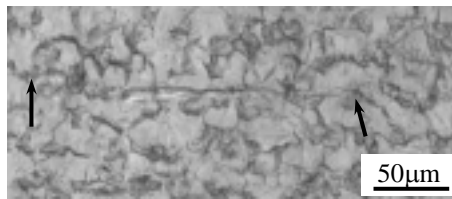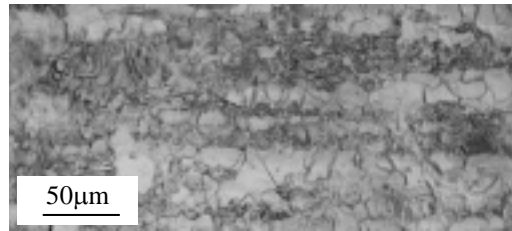Arrow mark: tip of non-propagating micro crack

Axial direction

Fig.4.30 Microstructure of non-propagating micro crack of S45C with
8% pre-strain (τ_a=200MPa)

The length of the non-propagating cracks of the same material became shorter with the increasing of tensile pre-strain ratio. This phenomenon might be explained by the following equation:

$$K_{II} = \tau_w \Phi \sqrt{\pi l} \tag{4.4}$$

τ_w is the fatigue limit, Φ is a modified factor that is decided by the shape, dimension of the specimen and the way the stress is applied, l is the length of the non-propagating crack, and K_{II} is the torsional stress intensity factor. Under the given test condition, K_{II} and Φ are constant, consequently the crack length l is only related to the stress amplitude τ_w. The non-propagating crack length l decreases since the fatigue limit τ_w increases with the increasing of tensile pre-strain.

4.5 Comparison to the Rotating and Bending Fatigue

Effects of tensile pre-strain on the rotating and bending fatigue properties have been studied by many researchers during the long years of fatigue studies. Some researches have studied on the effects of tensile pre-strain on the rotating and bending fatigue properties of the conventional structural carbon steels [26, 27]. Compared the torsional fatigue test results with the previous reports, it is founded that the influences were much different for the tensile pre-strain on the bending or torsional fatigue properties.

4.5.1 Fatigue Limits

Rotating and bending fatigue limits decreased a little at the small pre-strain ratio, and then increased with larger tensile pre-strain. When the pre-strain is too large, fatigue limit will decrease contrarily. The relationship between fatigue limit ratios and the pre-strain ratios of the four kinds of test materials is shown in Fig.4.31.

For rotating and bending test, the fatigue limits of tensile pre-strained specimens were lower than that of the virgin ones which were not tensile pre-strained before the fatigue test. While for the torsional fatigue test, the fatigue limits of tensile pre-strained specimens were equal or higher than that of the non-pre-strained specimens, the improvements were much higher than that in the rotating and bending fatigue test. For 8% pre-strained S15C specimens, the fatigue limit was improved to about 130% of that of the non-pre-strained one. Even for the lowest improvement of the 8% pre-strained S45C, it was improved to
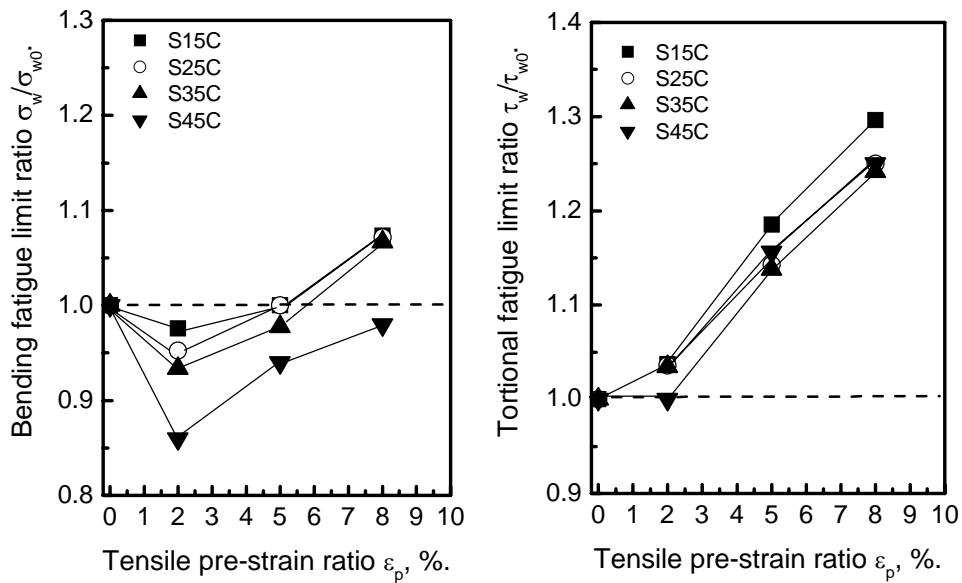
Fig.4.31 Relationship between fatigue limit ratios and tensile
pre-strain ratios
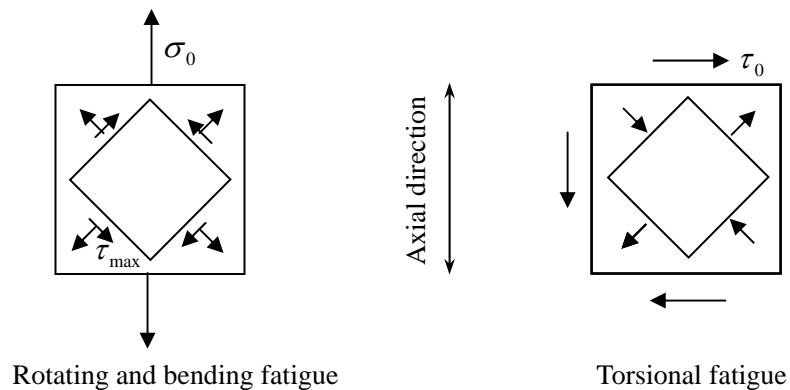
Fig.4.32 Stress states for rotating and bending fatigue
and torsional fatigue

25% of that of the virgin ones. Such a difference could be due to the different slip system in bending and torsional fatigue test. Figure 4.32 shows the stress states for the rotating and bending fatigue test and torsional fatigue test, respectively. For the tensile and bending fatigue, the direction of tensile slip lines is consistent with that of the maximum shearing stress, these tensile slip lines might become the initiation of tensile and bending fatigue cracks. However, in torsional fatigue test, the direction of tensile slips is about 45° to the maximum torsional stress

94

direction. It is much harder for the torsional slip lines to initiate in the areas with tensile slip lines than in those without tensile slip lines. Therefore, tensile slip lines decreased the fatigue limits of rotating and bending fatigue, but increased the torsional fatigue limits.

Table 4.4 Relationship between bending fatigue limits
and torsional fatigue limits.

		σ_w, MPa	τ_w, MPa	$\psi = \tau_w / \sigma_w$
S15C	ε_p=0%	205	135	0.659
	ε_p=2%	200	140	0.700
	ε_p=5%	205	160	0.780
	ε_p=8%	220	175	0.795
S25C	ε_p=0%	210	140	0.667
	ε_p=2%	200	145	0.725
	ε_p=5%	210	160	0.762
	ε_p=8%	225	175	0.778
S35C	ε_p=0%	225	145	0.644
	ε_p=2%	210	150	0.714
	ε_p=5%	220	165	0.750
	ε_p=8%	240	180	0.750
S45C	ε_p=0%	250	160	0.640
	ε_p=2%	215	160	0.744
	ε_p=5%	235	185	0.787
	ε_p=8%	245	200	0.816

On the other side, it is generally considered that based on the maximum pre-strain energy mechanism, the relationship between the fatigue limits of bending fatigue test and that of the torsional fatigue test could be expressed as the following equation, and for the isotropic carbon steels, it could be about 0.68 [28]. For the ductile materials, it can be 0.5-1.0.

$$\psi = \tau_w / \sigma_w \cong 0.58 \qquad (4.5)$$

Table 4.4 shows the fatigue limit values of bending and torsional fatigue tests for different carbon steels with different tensile pre-strain ratios. To the non-pre-strained specimens, it is 0.659, 0.667, 0.644 and 0.640 respectively for all of the four kinds of structural carbon steels. The values for the tensile pre-strained specimens are higher than that of the non-pre-strained specimens.

4.5.2 Crack Initiation Point

Most of the bending fatigue cracks initiated from the slip lines in the ferrite grains or between the ferrite grains and the pearlite blocks. While the torsional fatigue crack were mostly initiated from the torsional slip lines in the ferrite grains or near the grain boundaries between ferrite grains and the pearlite blocks. For the tensile pre-strained rotating and bending fatigue test, the fatigue cracks could initiate from the tensile slip lines of transcrystalline and intercrystalline or grain boundary between ferrite grain and pearlite block, and even from the pearlite blocks [25], just because the exist of tensile slip lines in those areas. For torsional fatigue test, when tensile pre-strain was applied on the specimens and some grains were tensile slipped, it would be much harder for the torsional slip lines initiation, and the slip lines would initiated in the weakest part in the surface of specimen. In other words, the torsional fatigue crack initiated in the weak ferrite grains where was not tensile slipped and not work hardened.

4.5.3 Crack Propagation

Comparing to the torsional fatigue test, tensile pre-strain also influenced much on the crack initiation and propagation behaviors for rotating and bending fatigue test [26, 27]. Under same stress amplitude, fatigue crack initiation life and fatigue life became longer, and the growth rate to the fatigue life became lower with the increasing of tensile pre-strain ratio. Under the stress amplitude of $\tau_w = \tau_{wo} + 10$ MPa, there was no obvious difference in crack initiation and propagation behaviors with the changing of tensile pre-strain.

4.5.4 Non-propagating Micro Cracks

Non-propagating micro cracks were observed in both non-pre-strained specimens and pre-strained ones, and there were no obvious influence of tensile pre-strain ratio on the non-propagating crack length, the length was about one grain size. However, for the torsional fatigue test, non-propagating micro cracks were observed in the pre-strained ones and the length were much longer than that in the bending fatigue test specimens, which got shorter with the increasing of tensile pre-strain ratio.

4.6 Conclusions

In this chapter, the effects of tensile pre-strain on the torsional fatigue properties were studied in detail. Based on the test results, it can be concluded as:

(1). Tensile pre-strain improves the torsional fatigue strength. Fatigue limits increase or equal to the non-pre-strained specimens at the low pre-strain ratio, then increase with the increasing of tensile pre-strain from 2% to 8%, and the highest improvement can be 130% to that of the non-pre-strained ones.

(2). Comparing to the cracks initiated from the tensile slip lines in the rotating and bending fatigue tests, the torsional fatigue cracks initiate from the torsional slip lines in the weak ferrite grains or near the grain boundaries between ferrite grains and the pearlite blocks. Tensile pre-strain does no obvious influence on the crack initiation points of torsional fatigue cracks.

(3). Under the same stress amplitude, torsional fatigue crack initiation life fatigue life become longer, and the growth rate becomes lower with the increasing of tensile pre-strain ratio. However there is no obvious difference in growth rate to the fatigue life ratios. Under the stress amplitude of $\tau_w = \tau_{wo} +$ constant MPa, the crack initiated earlier with the increasing of tensile pre-strain, and the crack grows faster with the increasing of tensile pre-strain ratios. Moreover, the difference in growth rate gets larger when the constant stress value is larger.

(4). Tensile pre-strain does not affect the fatigue crack branch point and branch directions.

(5). In specimens where non-propagating micro cracks are observed, the length of non-propagating cracks gets shorter with the increasing of pre-strain ratios for the same material.

(6). Fatigue limit ratios between bending fatigue test and the torsional fatigue test increase after tensile pre-strain. Tensile pre-strain affected the crack initiation point of the bending fatigue crack, while does no influence on the torsioanl fatigue crack initiation points. Length of non-propagating cracks for bending fatigue test is much shorter than the torsional ones, and there is no obvious relation between non-propagating crack length and the pre-strain ratio for bending fatigue test.

References

[1]. S. Nishida, Failure Analysis in Engineering Application, Butterworth Heinemann Ltd., 1992, p. 1-5.

[2]. A. Wöhler, Abstract in English, in Engineering, 1871, Vol. 11, p. 199.

[3]. J. Komotori, M. Shimizu, Y. Misaka and K. Kawasaki, Fatigue strength and fracture mechanism of steel modified by super-rapid induction heating and quenching, International Journal of Fatigue, Vol. 23, 2001, p. 225-230.

[4]. Scatter Characteristic of Fatigue life in Normalized 0.21% C Steel Plain Specimen, Journal of Society of Material Science, Vol. 42, 1993, p. 163-168.

[5]. D. H. Kim, J. H. Kim, J. H. Lee, B. H. Jeon and S. S. Cho, Low cycle fatigue life prediction of structural steels, APCFS and ATEM'01, JSME-MMD, 2001, p. 378-383.

[6]. H. Nisitani and R. Imai, Comparison of fatigue processes in 0.45% C steel specimens polished under different conditions, JSME, Vol.28, 1985, p. 2503-2510.

[7]. X. L. Yue, S. Nishida and N. Hattori, Fatigue Properties of Notched Aluminum Specimens after Hard Rolling, Materials Science Research International, Vol. 8, 2001, p. 53-59.

[8]. L. P. Borrego, J. M. Costa, S. Silva and J. M. Ferreira, Microstructure dependent fatigue crack growth in aged hardened aluminium alloys, International Journal of Fatigue, Vol. 26, 2004, p. 1321-1331.

[9]. T. S. Srivatsan, Meslet Al-Hajri and V. K. Vasudevan, Cyclic plastic strain response and fracture behavior of 2009 aluminum alloy metal-matrix composite, International Journal of Fatigue, Vol. 27, 2005, p. 357-371.

[10]. S. Nishida, K. Hayashi, N. Hattori, K. Nakano, Y. Yanagida and H. Tamasaki, Mechanical Properties of Tungsten Fiber Reinforced Ti-6Al-4V Alloy. Key Engineering Materials, Vol.183-187, 2000, p. 1243-1248.

[11]. S. Y. Son, S. Nishida, N. Hattori and K, Nakano, Fatigue Properties of Tungsten Fiber Reinforced Ti-6Al-4V Alloy. Key Engineering Materials, Vol.183-187, 2000, p. 963-968.

[12]. Mirco D. Chapetti, Application of a threshold curve model to high-cycle fatigue behavior of small cracks induced by foreign-object damage in Ti–6Al–4V, International Journal of Fatigue, Vol.27, 2005, p. 493-501.

[13]. S. Suresh, C. F. Shih, A. Morrone and N. P. O'Dowd, Mixed-mode fracture

toughness of ceramic material, Journal of American ceramic society 73, p. 1257- 1267.

[14]. G. Roebben, M. Steen, J. Bressers, O. Van Der Biest, Mechanical fatigue in monolithic non-transforming ceramic, Progress in Material Science 40, p. 265- 331.

[15]. R. W. Hertzerg and J. A. Manson, Micro mechanisms of fatigue crack advance in PVC, Journal of Material Science 8, p. 1554-1558.

[16]. R. W. Hertzerg, Deformation and fracture mechanism of engineering materials, 4th edition, New York: Wiley.

[17]. M. Goto, H. Nisitani, H. Miyagawa and A. Miura, Effect of pre-strain on the fatigue properties of a hear treated 0.45% C steel, JSME, Vol. 57, 1991. p. 1475-1480.

[18]. H. Nisitani, T. Teranishi, T. Takeno, S. Yamada and S. Tanaka, Effect of pre-strain on notched fatigue strength of 0.45% C steel, JSME, Vol. 64, 1998. p. 2502-2507.

[19]. H. Nisitani, M. Goto and H. Miyagawa, Effect of pre-strain on the fatigue life of 0.34% C steel plain specimens, JSME, Vol.53, 1987, p. 378-386.

[20]. H. Nisitani, S. Tanaka, S. Yamada and T. Teranish, Relation between micro-cracks and the coaxing effect of pre-strained low carbon steel, JSME, Vol.54, 1988, p. 190-195.

[21]. M. Goto, Y. Yanagawa and H. Nisitani, Statistical properties in the initiation and propergation of microcracks of a heat-treated 0.45% C steel, JSME International Journal, Vol.33, 1990, p. 235-242.

[22]. H. Nisitani, H. Noguchi, H. Uchihori and H. Nakase, An examination of the notch effect in fatigue of carbon steels based on linear notch mechanics, JSME International Journal, Vol.32, 1989, p. 439-443.

[23]. Y. Murakami, M. Endo. Effects of defects, inclusions and inhomogeneities on fatigue strength, International Journal of Fatigue, Vol.16, 1994, p. 163-182.

[24]. Y. Murakami, K. Takahashi, M. Takada and Y. Toriyama. Quantitative evaluation of effect of artificial small defects on torsional fatigue strength, JSME, Vol. 64, 1998, p. 271-276.

[25]. S. Nishida, Zhang W. and H. Kubota. Relationship between pre-strain and fatigue properties of plain carbon steels, Proceeding of ICM&M'97, Japan, 1997, p. 261-266.

[26]. Dehua Miao. Doctor degree thesis, Saga University, 2001.

[27]. Wenxian Sun. Doctor degree thesis, Saga University, 2004.

[28]. H. Nisitani and T. Fukuda. Fatigue limit and small-crack growth law in rotating bending and torsional fatigue of isotropic carbon steel plain specimen, JSME A, Vol.59, 1993, p.311-318.

CHAPTER 5

Influence of Carbon Content on Torsional Fatigue Properties

5.1 Introduction

Metals and alloys have many useful engineering properties and so have wide spread application in engineering designs. Iron and its alloys (principal steels) account for about 90 percent of the world's production of metals mainly because of their combination of good strength, toughness and ductility at relatively low cost [1].

Carbon steels constitute by far the largest tonnages of all steels sold. A full listing of their applications is obviously impossible. They are used as castings and forgings, pipes and tubes, sheets and plates, wires, rods, rails and structural shapes. Most of steels are made by oxidizing the carbon and other impurities in the pig iron until the carbon content of the iron is reduced to the required level. Carbon steels account for nearly 90% of the world's steel production. All carbon steels are defined as having less than 1.65% manganese, 0.6% silicon, and 0.6% copper. Carbon is the most important alloying constituent in steels, and it is chiefly responsible for the broad range of mechanical properties attainable in both wrought and cast products.

Plain-carbon steels are essentially alloys of iron and carbon with up to about 1.2% carbon. However, the majority of steels contain less than 0.5% carbon [1]. Based on the carbon content, carbon steels are usually grouped into 5 classes: ultra low carbon steels, extra low carbon steels, low carbon steels, medium carbon steels and high carbon steels. When carbon content is more than 2.0%, it is classified as cast iron. Plain carbon steels are metallurgically subdivided into hypo- and hypereutectoid grades, depending on whether their carbon content is less or more than 0.80%. Additional alloying elements (manganese, silicon, nickel, etc.) change the carbon content of this, the eutectoid point, and may even

eliminate it entirely. Limitations of carbon led to the development of micro-alloyed steels with low carbon content.

There have been extensive researches on the carbon steels in the past years. Many of them were focused on one single material, discussed on the overloads [3], cross sections [4], micro crack (short crack) propagation [5-7], pre-strain [8-11] and so on. But few of the studies have ever discussed on the effect of carbon content on the fatigue properties of structural carbon steels, especially on the torsional fatigue properties.

In this study, four kinds of structural carbon steels with different carbon content, JIS S15C, S25C, S35C and S45C were used to investigate the torsioanl fatigue properties, all of the materials were heat treated before machining to make them with same grain size. Some of the specimens were tensile pre-strained before the torsional fatigue test with three different pre-strain ratios of 2%, 5% and 8%. The specific treatment and procedure were introduced in Chapter 2 in detail. The objects of this chapter is to discuss how the carbon content influences the torsional fatigue properties of the fatigue strength, fatigue crack initiation and propagation behaviors, and also the microstructural behaviors of the non-propagating cracks of specimens with or without tensile pre-strain.

5.2 Influences of Carbon Content on Torsional Fatigue Properties

5.2.1. Fatigue Strength

Figures 5.1, 5.2, 5.3 and 5.4 show the S-N curves of the four kinds of test materials with different pre-strain ratios, including non-pre-strained specimens, pre-strained ones with the pre-strain ratios from 2% to 8%. For materials with same pre-strain ratios, both fatigue life and fatigue limit increased with the increasing of carbon content, and the slope of the curves were the same. Compared with other figures with different tensile pre-strain ratios, the slope of curves of tensile pre-strained specimens were a little smaller than that of the non-pre-strained ones, and the fatigue life differences became wider with the increasing of pre-strain ratio.

5.2.2. Crack Initiation and Propagation Behaviors

Figure 5.5 shows an example of the micro structural behaviors of torsional fatigue crack initiation and propagation.
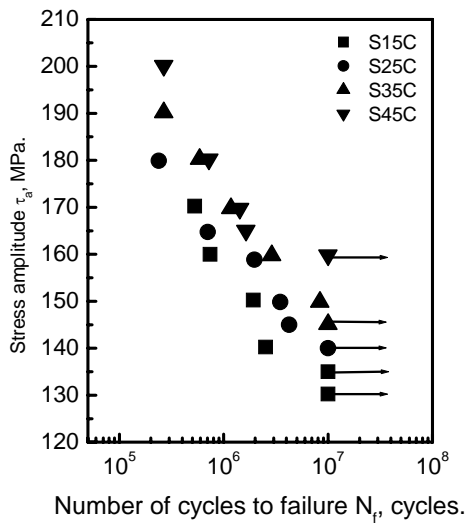
Fig.5.1 S-N curves of
non-pre-strained specimens
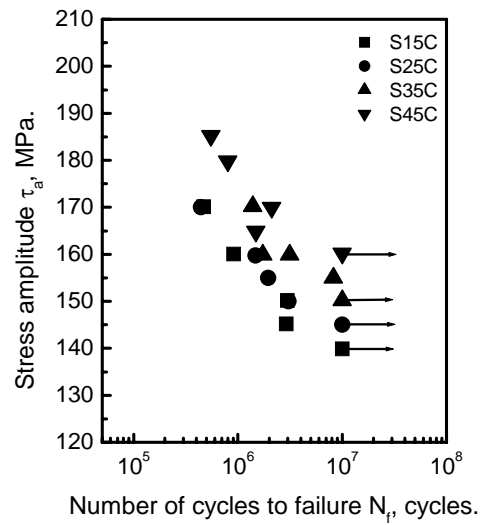
Fig.5.2 S-N curves of 2%
pre-strained specimens
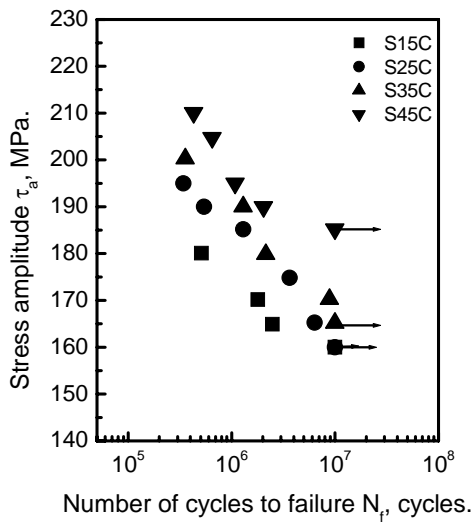
Fig.5.3 S-N curves of 5%
pre-strained specimens
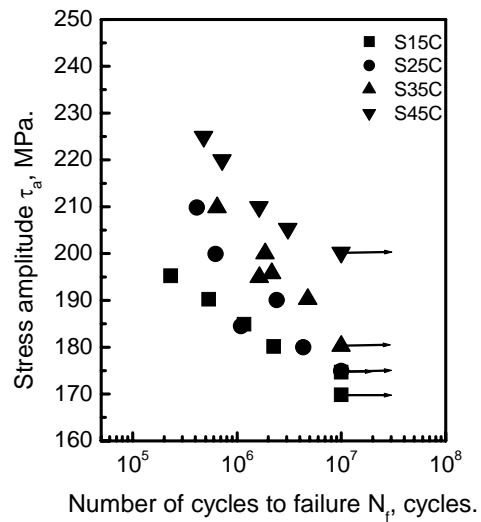
Fig.5.4 S-N curves of 8%
pre-strained specimens

Crack Initiation

According to the observation by successive taken replica samples, fatigue cracks initiated in the surface of specimens, as the shown example in Fig.4.5. For all of the four kinds of test materials, most of the fatigue cracks initiated from the

103

torsional slip lines in the soft ferrite grains, where is slipped easily. There was almost no obvious relation with the tensile pre-strain ratio and carbon content, not like the cracks in bending fatigue test, the intiation position would change with the change of tensile pre-strain or carbon content [12, 13]. In other words, tensile pre-strain and carbon content do not affect the torsional fatigue crack initiation position in the tortional fatigue test.

50μm

N=0

50μm

N=5× 10^5 cycles

50μm

N=1.5× 10^6 cycles

50μm

N=2.7× 10^6 cycles

Axial direction

S25C, $\varepsilon_p = 0\%$, τ_a=150MPa, $N_f = 3.47\times10^6$ cycles
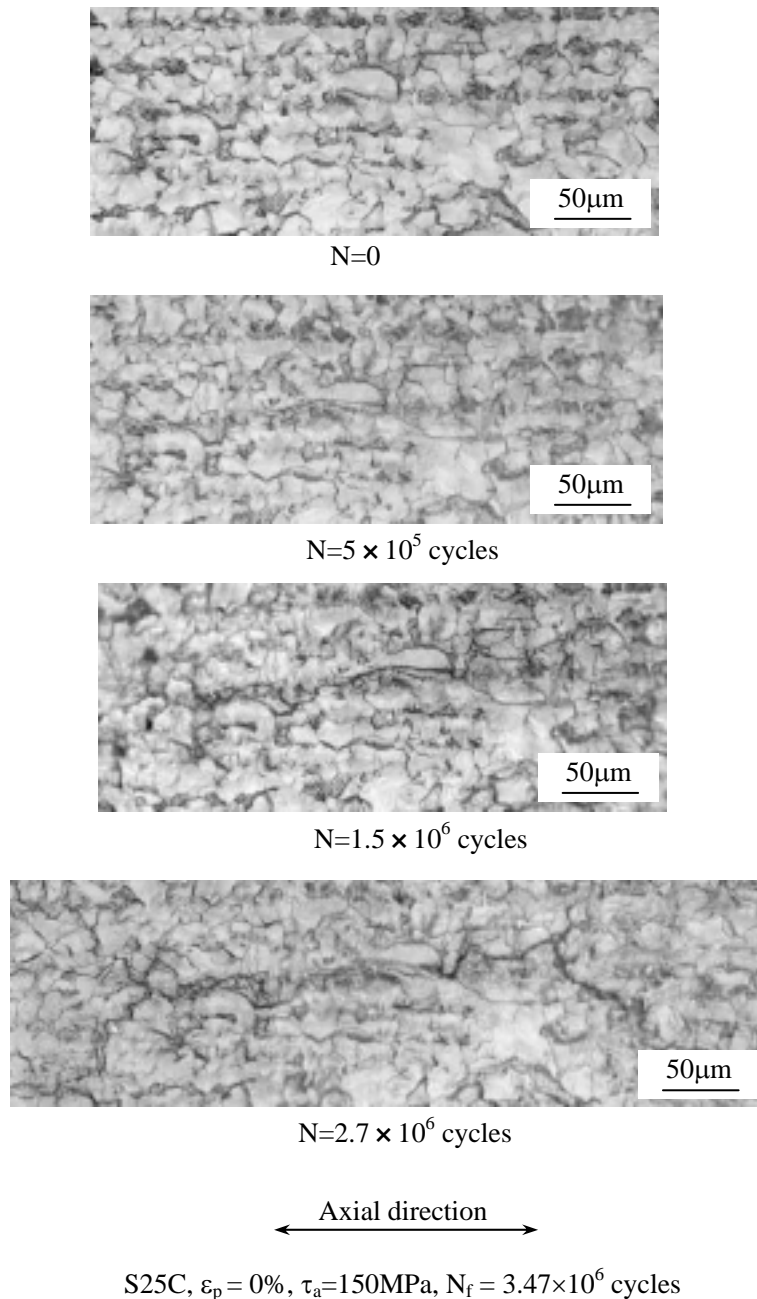
Fig.5.5 Micro structural behaviors of torsional fatigue crack propagation

Crack Propagation in Mode II and the Branch Behavior

After the fatigue crack initiated in torsional slips in the ferrite grains, it would propagate through the grains or along the grain boundaries in the axial direction. Comparing the crack length along the axial direction, it could be founded that for specimens with the same pre-strain ratio, it got shorter with the increasing of
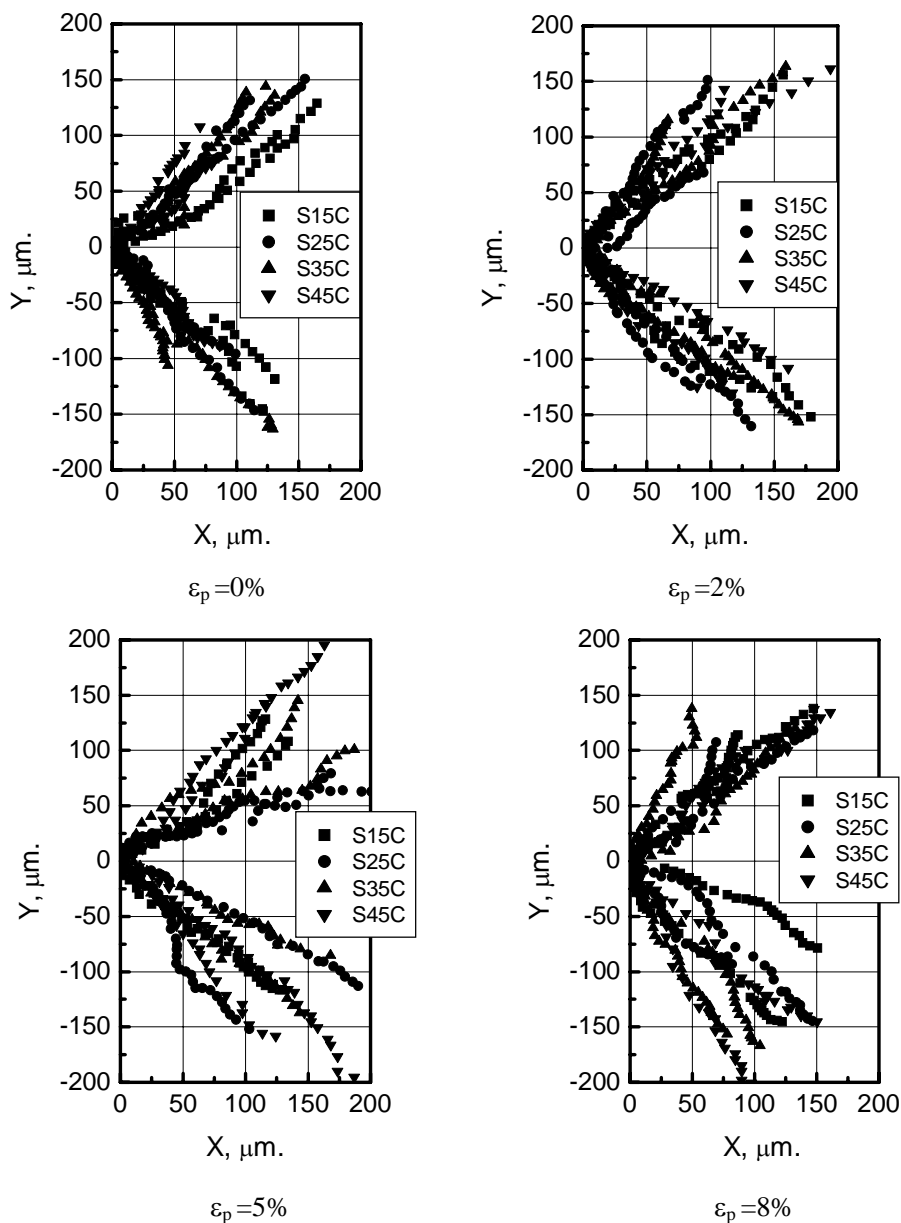
Fig.5.6 Crack branch of specimens with the same pre-strain ratios

carbon content, though the final crack might be long because of the connecting of plural short cracks. After the cracks propagated for some while by Mode II style in the axial direction, it would branched to Mode I style, and the propagation directions also changed to almost near vertical to the normal stress direction, that is, about 45° to the axial direction. Figure 4.6 shows the crack branch directions of materials with same tensile pre-strain ratio. During the Mode I style, the cracks might propagate along the grain boundaries or through the soft ferrite grains, therefore the direction of branched crack was not in the same direction all the time, it would change a little with the direction changing of the grain boundaries. Moreover, the cracks in Mode II styles were stopped at the grain boundaries between ferrite grains and ferrite grains, or between ferrite grain and pearlite blocks, no matter for the non-pre-strained specimens or the pre-strained ones of all of the four kinds of test materials. In other words, branch point and the branch directions are also independent with the carbon content and tensile pre-strain.

Crack Propagation Behaviors

The following figures, Figs. 5.7, 5.8, 5.9 and 5.10 show the relationship between fatigue life ratios and the crack length. It is shown that there is no obvious difference in crack growth rate for the different materials with the same pre-strain ratio. Comparing the different pre-strain ratios, it is evident that the fatigue cracks

Fig.5.7 Crack propagation of non-pre-strained specimen
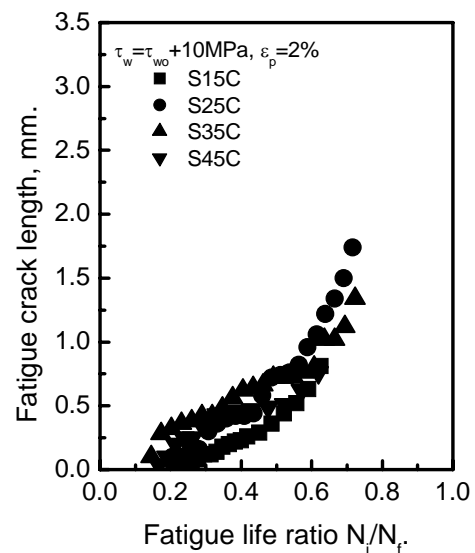
Fig.5.8 Crack propagation of 2% pre-strained specimens
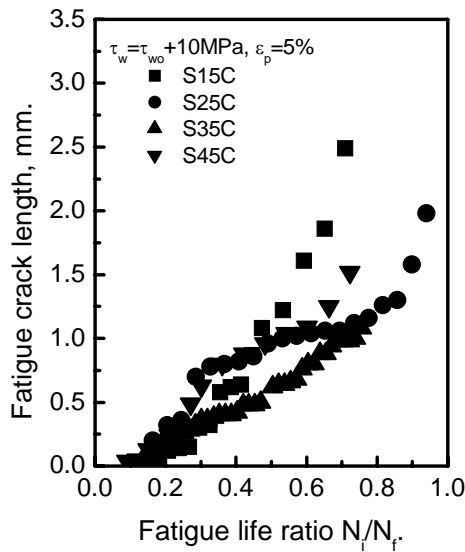
Fig.5.9 Crack propagation of 5%
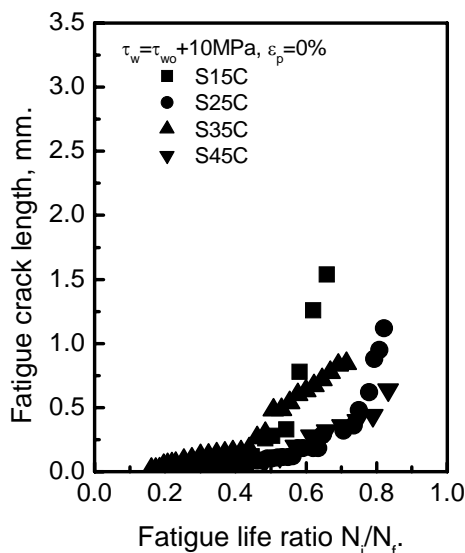pre-strained specimens
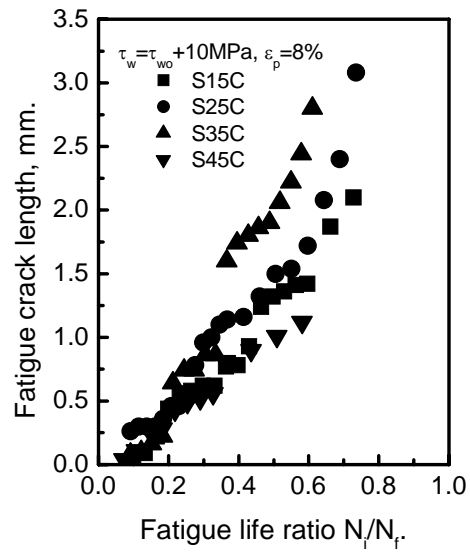
Fig.5.10 Crack propagation of
8% pre-strained specimens

initiated a little earlier with the increasing of tensile pre-strain ratios and the growth rate increased for all of the four kinds of material. The trends of the effect of pre-strain on the crack initiation behaviors are almost the same for the test materials with different carbon content. In other words, the effect of tensile pre-strain on the crack initiation behaviors is independent of the carbon content for the materials with same grain size. On the other hand, the difference of crack growth rate for materials with the same pre-strain ratio became larger with the increasing of pre-strain ratios.

5.2.3. Non-propagating Micro Crack Behaviors

Figures 5.11 and 5.12 are the comparison of the length of the observed non-propagating cracks with same tensile pre-strain ratios after they were applied with their own fatigue limit stress and the number of cycles was over 10^7 cycles. For 2% pre-strained specimens, the crack length was 0.45mm, 0.35mm and 0.18mm for S25C, S35C and S45C, respectively. And to the 8% pre-strained ones, the length of the cracks were 0.25mm, 0.24mm, 0.2mm and 0.1mm, respectively. All of the crack lengths decreased with the increasing of carbon content for the specimens with the same pre-strain ratio.

The following equation might be used to explain why the length of non-propagating crack decreased with the increasing of carbon content:

$$K_{II} = \tau_w \Phi \sqrt{\pi l} \qquad (5.1)$$

τ_w is the fatigue limit, Φ is a modified factor that is decided by the shape, dimension of the specimen and the way the stress is applied, l is the length of the non-propagating crack, and K_{II} is the torsional stress intensity factor. Under the given test condition, K_{II} and Φ are constant, consequently the crack length l is only related to the stress amplitude τ_w. For specimens of different material with same tensile pre-strain, the fatigue limit τ_w increases with the increasing of carbon content, as shown in Figs. 5.1 to 5.4. Therefore, the non-propagating crack length l decreased with the increasing of carbon content.

S25C, τ_a=145MPa

S35C, τ_a=150MPa
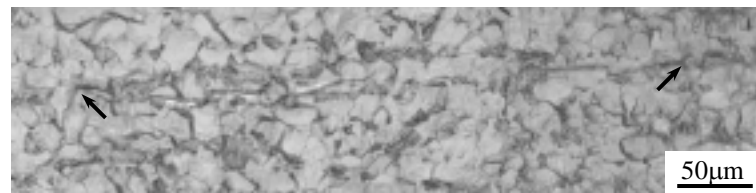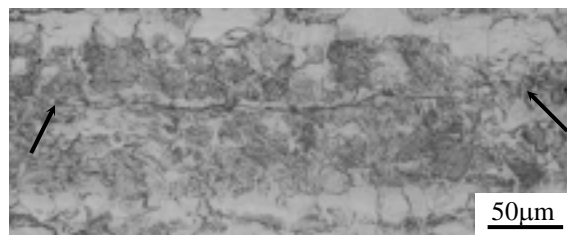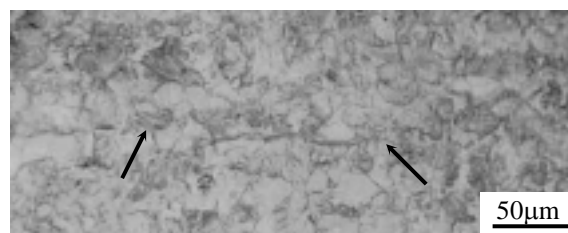
S45C, τ_a=160MPa

Arrow mark: tip of non-propagating micro crack

Axial direction

Fig.5.11 Length of non-propagating micro crack of
specimens with 2% pre-strain

S25C, τ_a=175MPa

S35C, τ_a=180MPa
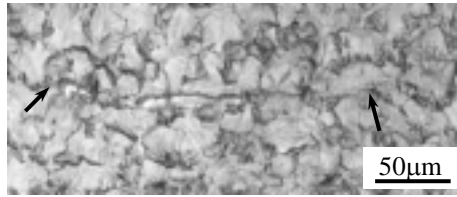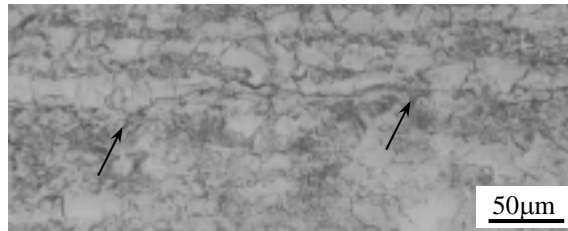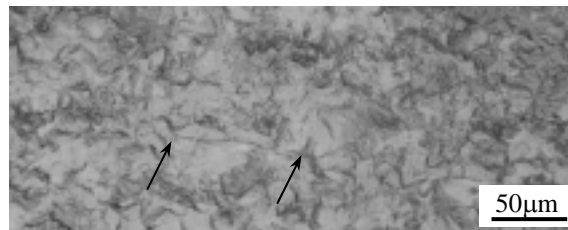
S45C, τ_a=200MPa

Arrow mark: tip of non-propagating micro crack

Axial direction

Fig.5.12 Length of non-propagating micro
cracks of 8% pre-strained specimens

5.3 Discussions

Table 5.1 lists the fatigue limits of all kinds of specimens of different materials
with different tensile pre-strain ratios and Fig. 5.13 is the relationships between
carbon content and the torsional fatigue limit ratios, taking the fatigue limits of
S15C as the original ones. The relationship was divided into two groups. The one
includes non-pre-strained specimens and 2% pre-strained ones, which could be
called low pre-strained group, and the other one including 5% and 8% pre-strain

was be called high tensile pre-strained group. For both of the two groups, fatigue limit ratios increased with the increasing of carbon content in totally, and the increase trends were almost the same for the materials for materials with different tensile pre-strain ratios, though the improvement of the higher tensile pre-strained group was almost lower than the other group by a constant value. This phenomenon is in contrast to the bending fatigue test, as shown in Fig. 5.15, taking the bending fatigue limits of S15C as the original ones. In this case, the fatigue limit ratios also increased with the increasing of carbon content, the improvements were much different, the highest one of non-pre-strained S45C was up to 122% to that of the S15C specimen, and the lowest one, that of the 2% pre-strained S45C specimen was only 7% improved than that of the original one.

Table 5.1. Fatigue limits of specimens, MPa

	S15C	S25C	S35C	S45C
$\varepsilon_p = 0\%$	135	140	145	160
$\varepsilon_p = 2\%$	140	145	150	160
$\varepsilon_p = 5\%$	160	160	165	185
$\varepsilon_p = 8\%$	175	175	180	200
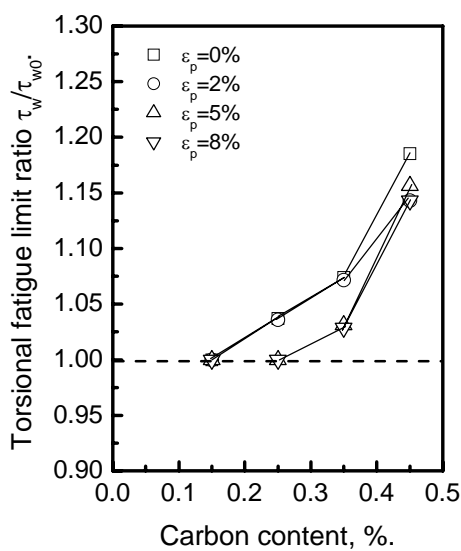
Fig.5.13 Relationship between torsioanl fatigue limits and carbon content
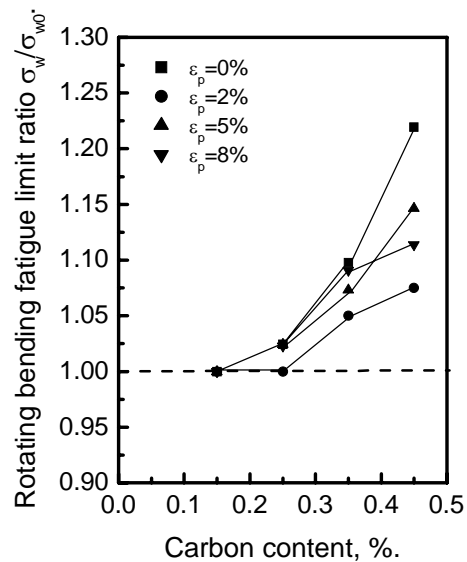
Fig. 5.14 Relationship between bending fatigue limits and carbon content

These phenomena could be due to the cooperation of carbon content and tensile pre-strain effect.

The effect of carbon content could be reflected in the stress-strain curves. Figure 5.15 shows the curves of the four kinds of test materials. The flow stresses of every material increased with the increasing of tensile pre-strain ratio from 2% to 8%, and the 2% pre-strained flow stresses are higher or almost equal to the non-pre-strained ones, as the specific values listed in Table 5. 2.

Tensile strength is mainly determined by the average strength of the grains, and the fatigue limit depends on the weakest strength of grains. When 2% pre-strain is applied on specimens, tensile slip lines firstly initiate in the weakest ferrite grains, therefore all of the fatigue limit increase. On the other hand, when 5% and 8% pre-strained are applied on specimens, for S15C and S25C, since the ferrite content is high, though there are tensile slip lines in ferrite grains, the density is very low and the work hardening effect is not so obvious. However for S35C and S45C, almost all of the grains are tensile slipped and the density of slip
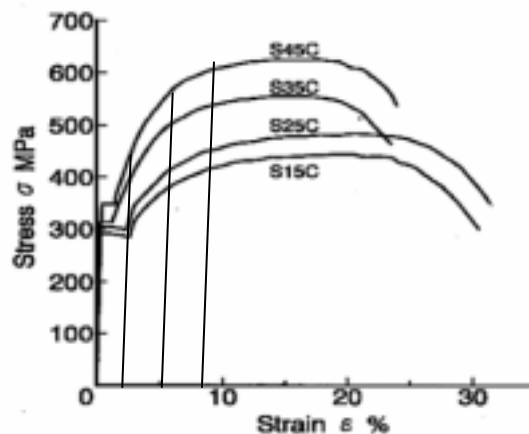
Fig.5.15 Stress-strain curves of structural carbon steels

Table 5.2. Flow stresses of test materials at
different pre-strain ratios, MPa

	$\varepsilon_p = 0\%$	$\varepsilon_p = 2\%$	$\varepsilon_p = 5\%$	$\varepsilon_p = 8\%$
S15C	285(100%)	290(102%)	380(133%)	405(142%)
S25C	300(100%)	310(103%)	410(137%)	450(150%)
S35C	305(100%)	400(131%)	500(164%)	540(177%)
S45C	350(100%)	455(130%)	560(160%)	600(171%)

lines increase with the increasing of tensile pre-strain ratio, which is much higher than that in S15C and S25C. Therefore, the fatigue limits of S35C and S45C increase more obvious compare to that of S25C.

Moreover, it is known that carbon is the primary hardening element in steel. When carbon content is lower, the soft ferrite grains are the most structural components in the material. With the increasing of carbon content, ferrite grains decrease and on the other way, the hard component, pearlite increases. The average surface hardness of the test specimens in this study is shown in Fig. 5.16, the hardness almost linearly increases with the increasing of carbon content. Even the hardness of ferrite grains in the materials also increased with the increasing of carbon content, as shown in Fig.5.17.

On the other hand, it is much different for the effect of tensile pre-strain on the fatigue limits of bending fatigue and torsional fatigue. This is mainly due to the different slip systems of tensile slip and torsional slip. After tensile pre-strain, dislocations and tensile slip lines would initiated in the surface of specimens. Small tensile pre-strain could decrease the fatigue limits of bending fatigue a little bit, as reported by many researches. The fatigue limits of bending fatigue decreased for specimens with 2% tensile pre-strain, and then increased with the increasing of tensile pre-strain [12-15]. For S15C, S25C and S35C, the fatigue limit were even higher than that non-pre-strained ones, however all of the pre-strained fatigue limits of S45C were lower than that of the non-pre-strained one, as shown in Fig.5.18. On the other hand, the fatigue limits of pre-strained torsional fatigue test specimens were equal to or higher than those of the non-pre-strained ones, and the difference of fatigue limit ratios were also smaller than that in the rotating and bending fatigue test. In other words, tensile pre-strain affected more on the fatigue limits of bending fatigue test than on the torsional fatigue test. Consequently, the carbon content effect expressed more on the torsional fatigue specimens than on the bending fatigue ones.

Moreover, as it is discussed above that the surface hardness was increased by tensile pre-strain and carbon content, respectively. And the relation between fatigue limits and the surface hardness can be shown in Fig. 5.19. From the figure, when the surface hardness is almost the same, as the three points connected by the dashed line, the fatigue limits improvement caused by tensile pre-strain is more remarkable than that of the carbon content. That is to say, for the structural carbon steels, the tensile pre-strain effect is much better for the torsional fatigue limit improvement than that of the carbon content effect.
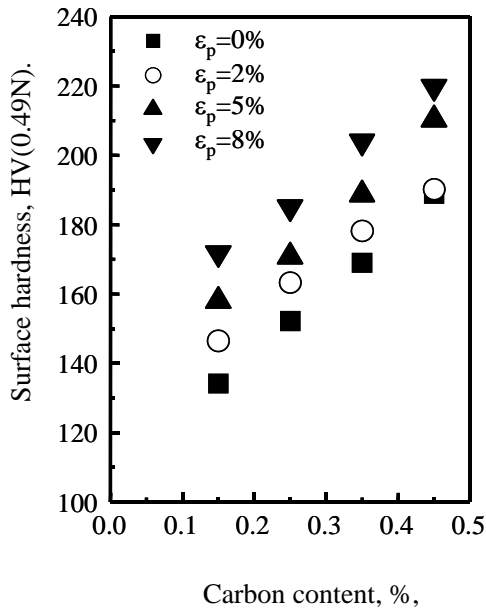
Fig.5.16 Relationship between surface hardness and carbon content
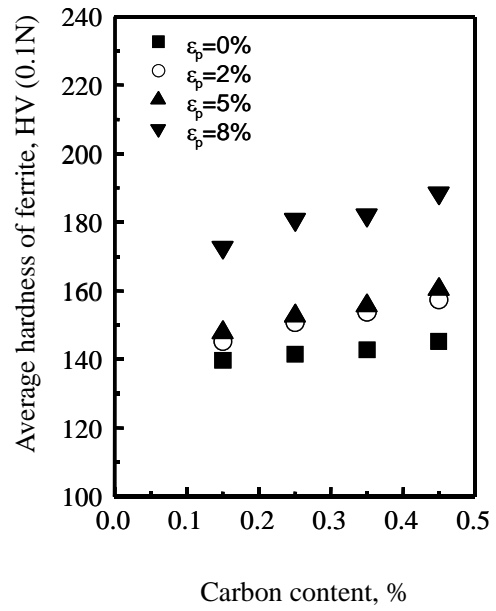
Fig.5.17 Relationship between hardness of ferrite grains and carbon content
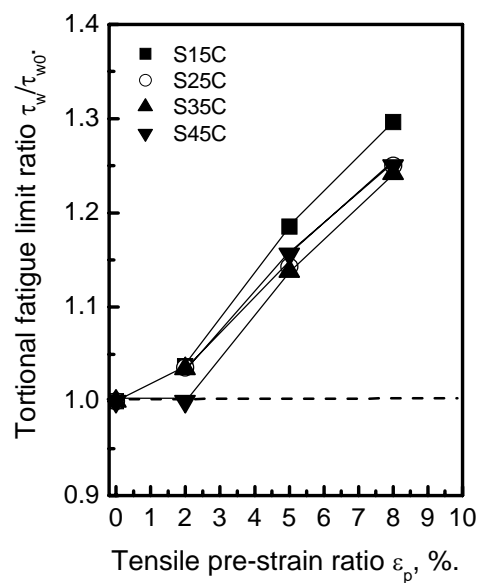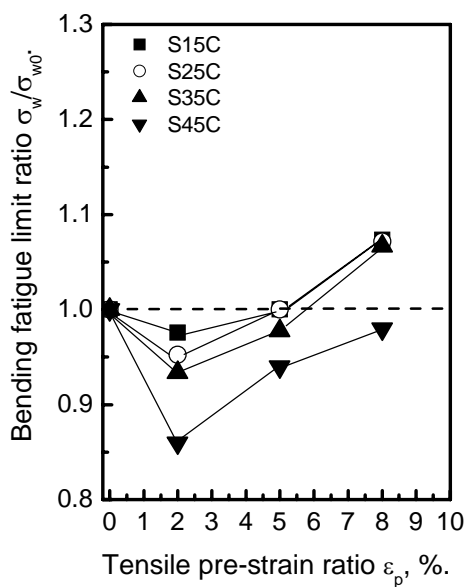
Fig.5.18 Relationship between bending and torsional fatigue limit ratios and tensile pre-strain ratios

113

S15C, 8% (175MPa)

S25C, 5% (160MPa)

S35C, 0% (145MPa)

S25C, 0% (140MPa)

S15C, 0% (135MPa)
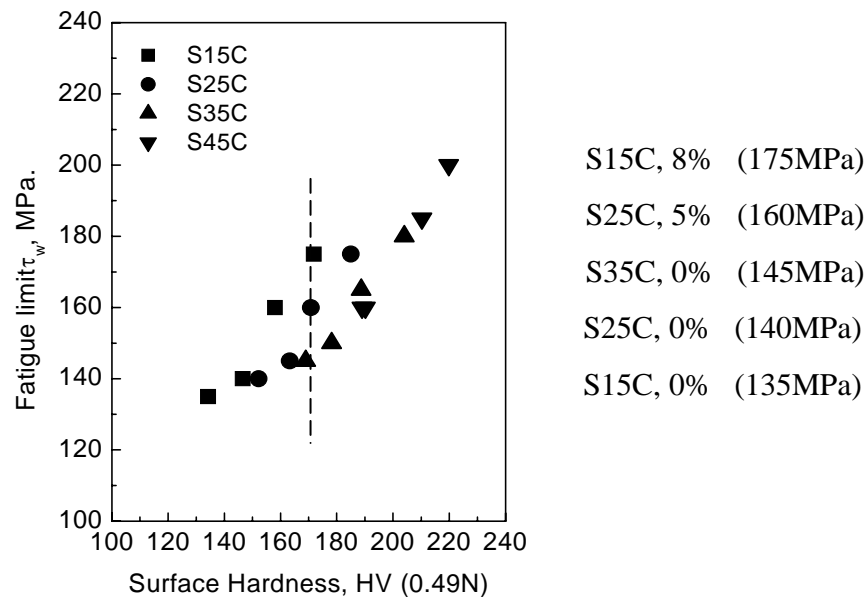
Fig. 5.19 Relation between torsional fatigue limits and
surface hardness

5.4 Conclusions

The main results of carbon content effect on the structural carbon steels obtained in this study are as follows:

For the structural carbon steels with almost same grain size,

(1). Torsional fatigue strength increases with the increasing of carbon content, both of the original specimens and tensile pre-strained specimens of structural carbon steels.

(2). The improvement of 5% and 8% pre-strained specimens were almost lower than that of the non-pre-strained specimens and 2% pre-strained one by a constant value.

(3). Fatigue crack initiation point, crack branch point and the branch direction are independent on the carbon content.

(4). There is no obvious difference on the crack growth rate on materials with the same tensile pre-strain ratio.

(5). For the length of non-propagating cracks, it decreases with the increasing of carbon content if they are with the same tensile pre-strain.

(6). The fatigue limit improvement is much more remarkable by the effect of tensile pre-strain than that of the carbon content.

114

References

[1]. William F. Smith, Foundations of material science and engineering (Second Edition), McGraw-Hill, Inc, Singapore, 1993, p. 419-433.

[2]. Kenneth G. Budinski, Michael K. Budinski. Engineering Materials - Properties and Selection, Prentice Hall International, Inc., New Jersey, USA, 1999, p.256-280.

[3]. J.J.F. Bonnen, T. H. Topper, The effect of bending overloads on torsional fatigue in normalized 1045 steel, International Journal of Fatigue, Vol. 21, 1999, p. 23-33.

[4]. M. Kawamoto, T. Shibata and Y. Yokoyama, Study on torsional fatigue strength of rectangular and circular cross sections of steel, Bulletin of JSME, Vol.9, 1966, p. 621-627.

[5]. S. Kitaoka, J. Chen and M. Seika, Dependence of the threshold stress of microcrack propagation on the stress ratio, JSME International Journal, Vol.31, 1998, p. 768-773.

[6]. Arthur J. McEvily, The growth of short cracks: a review. Material Science Research International, Vol.4, 1998, p.3-11.

[7]. H. Nisitani and T. Fukuda, Fatigue limit and small-crack growth law in rotating and torsional fatigue of Isotropic carbon steel plain specimen, JSME, Vol. 59, 1993, p.311-318.

[8]. Y. Nagase and M. Izumizawa, Effect of small pre-strain on the fatigue strength if low carbon steel, JSME, Vol.54, 1988, p.1474-1481.

[9]. H. Nisitani, M. Goto and H. Miyagawa, Effect of pre-strain on the fatigue life of 0.34%C steel plain specimens, JSME, Vol. 53, 1987, p. 378-386.

[10]. M. Goto, H. Nisitani, H. Miyagawa and A. Mimura, Effect of pre-strain on the fatigue strength of a heat treated 0.45% C steel, JSME, Vol.57, 1991, p. 1475-1480.

[11]. H. Nisitani, T. Teranishi, T. Takeno, S. Yamada and S. Tanaka, Effect of pre-strain on notched fatigue strength of 0.45% C steel, JSME, Vol. 64, 1998, p. 2502-2507.

[12]. W. Sun, S. Nishida and N. Hattori, Fatigue properties of pre-strained eutectoid steel, Material Science Research International, Vol.9, 2003, p. 210-215.

[13]. S. Nishida, W. Zhang and H. Kubota, Relationship between pre-strain and

fatigue properties of plain carbon steels, Proceeding of International Conference on Materials and Mechanics'97, 1997, p. 261-266.

[14]. D. Miao, S. Nishida and N. Hattori, Effect of strain aging on fatigue properties of pre-strained carbon steel, JSME, Vol. 67, 2001, p. 137-142.

[15]. D. Miao, S. Nishida and N. Hattori, Effect of carbon content on fatigue properties of pre-strained carbon steels, Fatigue'99, 1999, p.619-624.

CHAPTER 6

Summary and Recommendations for Future Researches

6.1 Summary

The present research consist of the study that assess the effects of pre-strain and carbon content on fatigue properties of structural carbon steels, to understand the torsional fatigue mechanism of the structural carbon steels. And the objectives of the study are to evaluate the effect on fatigue strength, crack initiation and propagation behaviors, and also on the behaviors of non-propagating cracks.

Chapter 1 reviewed the brief history of fatigue research, introduced the background of fatigue study and discussed the importance of fatigue study in industry and engineering. At the end of the chapter, various mechanisms were introduced involving in fatigue crack initiation and propagation in material and the subsequent behavior of fatigue strength.

In chapter 2, it listed the test materials and the experimental procedure of this study in detail. At the same time, the aim of the procedure and the mechanism of torsional fatigue test were introduced.

In chapter 3, the relationship between tensile strain ratios and the surface plastic deformation were investigated. According to the results, the tensile strength and yielding strength increase with the increasing of carbon content, the yielding strength of S35C is very near with that of S15C and S25C, and they are much lower than that of S45C. However the translation strain ratios from slip lines to short cracks decrease with the increasing of carbon content, and all of them are lower than their yielding strain ratios, respectively.

Chapter 4 was focused on the effect of tensile pre-strain on the torsional fatigue properties was studied. In this study, the influence of tensile pre-strain on fatigue strength, crack initiation and propagation behavior, together with the non-propagating crack behaviors were investigated. The mechanisms for the

modification of fatigue properties were explained by slip system difference and work hardening. The main results obtained from this test are as follows:

(1). Tensile pre-strain improves the torsional fatigue properties of structural carbon steels with same grain size.

(2). Torsional fatigue limits of tensile pre-strained specimens with different pre-strain ratios (ε_p=2%, 5% and 8%) are equal to or higher than that of the non-pre-strained specimens (ε_p=0%).

(3). For tensile pre-strained specimens of the same material, fatigue limits increase with the increasing of pre-strain ratio, in the range of ε_p=2% to 8%.

(4). Torsional fatigue cracks initiate in the soft ferrite grains that are torsional slipped easily in the fatigue test. There is no obvious difference in crack initiation point between the pre-strained specimens and the non-pre-strained one. Under the same stress amplitude, the crack initiate later and propagated slower with the increasing of tensile pre-strain ratio; while under the stress amplitude of $\tau_w=\tau_{wo}+10MPa$ (τ_{wo}, the fatigue limit of the specific material with certain pre-strain ratio), the torsional fatigue crack initiated a little earlier with the increasing of tensile pre-strain ratio from 2% to 8%.

(5). Under the same stress amplitude, there is no obvious different in the cracks crack growth rate of specimens with different tensile pre-strain ratio. In the case of stress amplitude of $\tau_w=\tau_{wo}+10MPa$, the growth rate gets a little larger with the changing of pre-strain ratio from 2% to 8%.

(6). Non-propagating cracks are observed in some specimens. In the checked specimens, the length of non-propagating crack of the same material decreases from low tensile pre-strain ratio to the higher ones.

The effects of carbon content on the torsional fatigue properties were investigated in chapter 5, and the following conclusions can be derived from the results of this study:

(1). Torsional fatigue strength increases with increasing of carbon content for structural carbon steels with same grain size, both for non-pre-strained specimens and the tensile pre-strained ones.

(2). The improvement of 5% and 8% pre-strained specimens were almost lower than that of the non-pre-strained specimens and 2% pre-strained one by a constant value.

(3). Fatigue crack initiation point, crack branch point and the branch direction are independent on the carbon content.

(4). There is no obvious difference on the crack growth rate on materials with

same tensile pre-strain ratio.

(5). The length of non-propagating cracks decreases with the increasing of carbon content if they are with same tensile pre-strain.

(6). The fatigue limit improvement is much more remarkable by the effect of tensile pre-strain than that of the carbon content.

6.2 Recommendations for the Future Study

In this study, it was focused on the torsional fatigue properties of plain specimens, mainly studied the tensile pre-strain and carbon content. Tensile pre-strain improved the torsional fatigue strength mainly because of the different directions of tensile slip liens and the torsional stress. In the previous studies, it was shown that low tensile pre-strain ratio decreased the rotating and bending fatigue strength, and then with the increasing of tensile pre-strain ratio, the rotating and bending fatigue strength increased. It is supposed that torsional pre-strain would affect the rotating and bending fatigue strength and torsioanl fatigue strength and other fatigue properties, it is recommended to obtain a compressive understanding of the mechanism of torsional pre-strain influences on the torsional fatigue properties of plain specimens in the further.

In the practical engineering, more than 90% of the fatigue failures are initiated from the stress concentration parts and the notched on the specimen is one of the most main reasons causing stress concentration. Therefore it is very important to investigate the tensile and torsional pre-strain effects on the torsional fatigue behaviors of notched specimens of structural carbon steels.

Since fatigue failures are mostly initiated in the surface of specimens, the surface modification is very important method to improve the surface condition. Cold rolling is one of the good methods in this way to improve the fatigue properties, some researches have been carried out, mostly concentrated to the roller working influences on the rotating and bending fatigue properties. Therefore the researches of roller working effects on the torsional fatigue properties are also recommended.

On the other way, it is well known that fatigue test is very costly both in term of time and the cost. FEM is a very helpful method to do some quantitative analysis, it is suggested to co-operate the FEM method with the experimental fatigue test to save cost and improve the research efficiency.